Jury

Chairman: Prof. Dr. J. Manca
UHasselt, IMO

Promotor: Prof. Dr. P. Wagner
UHasselt, IMO-IMOMEC

Co-promotor: Prof. Dr. L. Michiels
UHasselt, Biomed

Prof. Dr.-Ing M.J. Schöning
FH Aachen, INB

Members of the jury: Prof. Dr. L. Lagae
K.U. Leuven, IMEC

Prof. Dr. W. De Ceuninck
UHasselt, IMO-IMOMEC

Prof. Dr. K. Haenen
UHasselt, IMO-IMOMEC

Dr. A. Ethirajan
UHasselt, IMO

Dr. R. Thoelen
XIOS, EMAP

Preface

It is March 18th 2012 early in the morning. Together with my wife Debbie I am enjoying a cup of coffee in the kitchen while we look outside the window to the garden. We are both a little bit quiet because in few minutes my colleague and good friend Thijs will pick me up. We are going to Dresden for two weeks to give a talk and we are asked to work on some readout systems. Somehow I have succeeded to convince Thijs that it is best to take the car, instead of taking an airplane to go to former Eastern–Germany. We get in the university car and start our 790 kilometre long journey over the German autobahn. As I am listening to the low growl of the car engine I suddenly realize that I am almost at the end of my PhD. I have always been so busy with working towards this moment that I did not realize that the moment was approaching so rapidly. This realization made me take a trip down to memory lane and took me back to 2007. I just finished my bachelor degree and decided to go to the Hasselt University to obtain my masters degree in bioelectronics and nanotechnology. During our first class I got introduced to Lars, Jan, Tine, Tim and a fellow Dutchman called Cyril. Our first class was taught by Prof. Dr. Wagner. A German name in combination with a professor-title did install some nervosity. However, this nervosity washed out extremely fast once he walked through the door. With a broad smile, while wearing a Mickey Mouse T-shirt and short trousers he introduced himself to us. At the time I did not realise that this highly informal professor would become my mentor for several years, and that three of my fellow students would become my direct colleagues within months. After obtaining my masters degree and a short time of working in the Netherlands, I was contacted by Patrick and informed that there was an opportunity to start working on a PhD project in Hasselt, thus I started my intellectual adventure as a PhD student in Hasselt in October 2008. In retrospect I have gained much more then knowledge during my PhD period. I have learned the true meaning of team–work. When working as a technical person on a more biological project you´re not only working with people who own a different kind of knowledge, but also a different kind of thinking. These fundamental differences have led to some.........memorable discussions, but in the end I think it is safe to say that we did achieve some important milestones within the world of genomic research and I have enjoyed every minute of this scientific rollercoaster.

Acknowledgements

An experience is only as special as the persons you are experiencing it with. So before entering the more formal part of this thesis I would like to take the time and thank some of the people who shared this experience with me.

Prof. Dr. Patrick Wagner, a.k.a. paddy. Thank you for providing me with the opportunity to perform this research. I realize that it takes guts for a German professor to have confidence in a starting Dutch researcher, but despite the fact that I proposed some really strange ideas, sometimes even without any arguments to back it up you trusted me all the way. Thank you for being my tutor.

Prof. Dr. Luc Michiels. Being a technical person in a non technical project can lead to some strange misunderstandings. At the start of my PhD I did not have a clue about the biological problem which needed solving. You provided me with the understanding of the problem. I have to admit that I suffered a minor nervous breakdown when I first realized what I was hired to do, but you kept me on the right track.

Prof. Dr. Ward De Ceuninck. Thank you for being my technical sparring partner. It was great to have your enthusiasm when I was building the setup. You had the ability to put the technological part of this project in perspective and taught me that the simplest explanation often is the best one. By now I share your slogan: ´If you do not see it in the raw data, it simply isn´t there.`

Prof. Dr. Ken Haenen en Dr. Stoffel Janssens. Diamond has been indispensable in my research and you guys have provided me with the best samples available under the sun. Thank you for your cooperation and discussions. It has provided me with the necessary insight into my own topic.

Prof. Dr. Hans–Gerhard Boyen and Dr. Anitha Ethirajan. I consider you to be the scientific power couple. You have taught me the true definition of a discussion and taught me what it means to come up with convincing arguments. Thank you for taking the time to read my manuscripts and help me to formulate sentences and coverletters in a way that they become irresistible to editors. I consider this to be an art which I hope to acquire one day.

Veronique and Natalie. You have been my biological alliance for the past few years. I have enjoyed the many hours that we spent at the confocal microscope and the results that came out of it. I think it is safe to say that we had our ups and downs and it hasn´t always been easy, but I think that we can be proud of the achievements that are accomplished.

Johnny Baccus, Lieven De Winter, Jan Mertens, and Johan Soogen. Thank you for bearing with me for the past years and having an incredible amount of patience with me when I plunged into your offices, while spitting out ideas, ´asking` for your time and loaning tools on a .....somewhat permanent base. Your craftsmanship has been indispensable in my research. P.S. You might want to have a look in the basement, last desk, right side, bottom drawer.

Andreas ´Riesenbaby`Gaulke, Benno ´Berliner Mauer´Schneider. Thank you for being my imported German efficiency. You guys worked with me on the set up and never once complained about the working hours. Hannelore, Tanya, Bram. Thank you for collecting 7.65 Gb of .txt data for me. It has been a lot of work for all you guys and I might have been a little demanding from time to time, but I am proud to say that I have been your mentor.

My office buddies: Lars, Jan, Bert, Marloes, Mo, Thijs, Linny, Rob, Kasper, Matthi and Kathia. Sharing an office with you guys has been a true ´Big Bang Theory` experience. There simply are too many memories to write down here, ranging from fear of flying, elastic-band wars, orange balloons and enormous Egyptians to € 3500 fines and wrecked cars. Thanks for being my colleagues, but most of all for becoming my friends. Bert and Linny: Thank you for helping me fight Microsoft word in the last painful stages of my PhD.

José and Lefried. Ten years ago I became your daughters´ boyfriend and four years ago I became your daughters´ husband. Besides physical proportions we are very different people and this has led to some turbulent times. You have taught me (and are still teaching me) a fundamental principle in life which is unnatural and at the same time a necessity to me: accept that ´It is what it is.` I have to learn to accept certain things in life and not to plan everything. I admire your entrepreneurial spirit and want to thank you for stimulating both me and Debbie to live a little!

Mom, Dad In 1982 you decided that you wanted a third child. At the time it must have seemed like a good idea......... but I bet you guys have considered a post-natal abortion a couple of times since then. However, despite of all my peculiarities you supported me every step of the way and provided me with a rock solid fundament. Even now, when I am a married man, with a house and a job I can feel your safety net. Off course I am too stubborn to admit it, but it makes me feel really comfortable to know that I can always come home and be ´Bartje` again. I couldn´t have wished for better parents!

Debbie. When we met ten years ago I just finished high school. You then had to endure four years of exam stress during my bachelor degree and 1 year of exam stress during my master degree. Magically, after these five years you still had the strength to support me through 4 years of nervous breakdowns. You kept me calm if I had to leave to the other side of the world to give a presentation and picked up the pieces when I came back. Now it is time for me to turn the tables and make sure that I am there for you. I am a lucky man to have girl like you! Thank you for being my wife.

The most exciting phrase to hear in science, the one that heralds new discoveries, is not 'Eureka!' but 'mmm that's funny ...'

Isaac Asimov

Table of Contents

Abstract

One of the central challenges in genomics is the detection and identification of single nucleotide polymorphisms (SNPs). This importance stems from several reasons: first, SNPs are involved in hundreds of genetic disorders such as Alzheimer, mucoviscidosis, phenylketonuria, and several types of breast and colon cancer. Second, SNPs in the so called ADME (absorption, distribution, metabolism, excretion) genes significantly influence the effectiveness of treatment and this is a major topic in the field of theranostics. Established technologies exist to identify these SNPs, but several disadvantages need consideration. Nearly all technologies need a lab environment, lack in speed (reaction times at the scale of at least 16 hours), are unable to provide dynamic information on the DNA binding kinetics (end point measurement) and need fluorescent labelling of the target DNA, which induces the necessity of sophisticated optical readout techniques. Due to these reasons a general interest in fast, label-free, low-cost and user-friendly DNA sensors has emerged. This thesis reports on the development of DNA sensors that respond to these specifications.

In order to integrate DNA in a sensor one needs to develop specific immobilization protocols to tether DNA preferably covalently and in head-on configuration onto a transducer surface. The platform of the developed DNA sensors is based on nano-crystalline diamond (NCD). In a first step, the diamond is hydrogenated. After hydrogenation, fatty acid is attached to surface covalently. Once the fatty acid is attached, it is functionalized with a probe DNA sequence by means of an 1–ethyl–3-[3-dimethylaminopropyl]-carbodiimide (EDC) reaction and in a last step this probe DNA sequence is hybridized with either a full matching target sequence or a sequence containing a mutation at one or several base pairs.

Two readout technologies were developed to distinguish between these full matching and mutated sequences. The first technology is based on impedance spectroscopy. But before starting genomic experiments we have first build an impedance spectroscopy unit, fully customized to be an essential part of this label-free, diamond based DNA sensor. We investigated if we could distinguish between different buffer solutions at different molarities and temperatures, commonly used in genomic research. After it was clear that we could regulate

and understand these environmental variables we introduced the setup to genomic research and used the findings as preconditions for the experiments.

At this point we started the first experiments where we monitored the chemical denaturation of DNA (by inducing 0.1 M NaOH) electronically in combination with fluorescence spectroscopy. We found that the impedimetrical results could be separated into a time constant for NaOH exposure and a time constant for denaturation. This denaturation time can be used as a measure for the stability of the DNA duplex. When inducing a single mutation into a 29 base pair duplex, the denaturation time is almost halved. It is even possible to give an indication of the position of the mutation as we can distinguish between denaturation times of identical mutations, located elsewhere in the sequence. This electronic method requires minimal instrumentation, is label-free and fast (within a time scale of minutes). These elements suggest that the monitoring of chemically induced denaturation is an interesting method to measure DNA duplex stability and might be used as a tool in SNP analysis.

The mentioned method does produce results within the wanted SNP regime, but the raw data still needs mathematical processing. For automation purposes this is a drawback. Therefore, we started thermal denaturation experiments with an electronic readout. We considered it a possibility to make use of thresholds when denaturing thermally. This process would eliminate the need for a medium exchange. Impedance would be measured as a function of temperature instead of function of time and medium. However, when conducting first experiments a new finding surfaced. This new finding was in line, but not related to the impedimetrical data. A temperature anomaly occurred at the solid-to-liquid interface upon denaturation. We found that DNA in its double-stranded form has a lower thermal resistance than in its single-stranded form. This transfer from low to high thermal resistance could be linked to the denaturation process by confocal fluorescence spectroscopy. The transition occurred at a lower temperature when denaturing a mutated sequence when compared to a full matching sequence, meaning that this method allows identifying melting temperatures by using an adjustable heat source in combination with two thermocouples.

This project has led to the development of two label–free strategies to detect SNPs in DNA sequences. The first strategy is based on impedance; the second strategy is based on heat-transfer resistance. Both techniques show a high specificity and sensitivity. These findings should be addressed as high potential proof–of–principle technologies. To transcend to world of academic research and enter the competitive industrial market of medical devices some extra research and development steps are still a necessity:

i)   Deliver proof that this technology works on longer DNA strands.
ii)   Implementation of the technology in an array format, enabling multiple detections in real time.

Once these critical hurdles have been overcome, miniaturization can be considered and perhaps a first step outside the comfort and safety of the academic world.

Nederlandse samenvatting

Een van de grootste uitdagingen in genetisch onderzoek is de detectie en identificatie van puntmutaties in DNA sequenties. Opsporing en detectie van deze mutaties is enerzijds belangrijk omdat zij correleren met enkele honderden genetische aandoeningen zoals Alzheimer, mucoviscidose, fenylketonurie, en verschillende vormen van borst en darmkanker. Daarnaast kunnen mutaties in de ADME genen (absorptie, distributie, metabolisme, uitscheiding) een nadelige invloed hebben op de behandeling van ziekten.

Er zijn reeds methoden ontwikkeld om deze mutaties op te sporen, maar de meeste methodieken hebben één of meer van de volgende nadelen: Noodzaak aan een laboratorium, gebrek aan snelheid (orde grootte 16 uur), missen van dynamische informatie op het gebied van bindingskinetiek en het DNA moet voorzien worden van een fluorescent molecuul waardoor een geavanceerde optische set-up onmisbaar wordt. Dit heeft geleid tot een vraag naar snelle, goedkope en gebruiksvriendelijke DNA sensoren welke niet staven op aanwezigheid van fluorescente moleculen. Dit proefschrift is een uiteenzetting van de ontwikkeling van DNA sensoren welke tegemoet komen aan deze specificaties.

Om DNA te integreren in een sensor moet het gehecht worden aan een oppervlak (bij voorkeur covalent). De ontwikkelde DNA sensoren besproken in deze thesis hebben een nano-kristallijn diamant oppervlak (NCD) als basis. Eerst wordt het diamant gehydrogeneerd, daarna wordt vetzuur aan het oppervlak gehecht. Wanneer het vetzuur covalent gehecht is aan het oppervlak wordt het, met behulp van een EDC reactie, gefunctionaliseerd met enkelstrengig probe DNA. Als laatste stap wordt dit probe DNA gehybridiseerd met zijn tegen sequentie. Deze sequentie kan volledig passend zijn of een mutatie bevatten op een of meer posities.

Twee methoden zijn ontwikkeld om onderscheid te maken tussen deze volledige passende en gemuteerde sequenties. De eerste methode is gebaseerd op impedantie spectroscopie. Voordat gestart werd met het inzetten van deze technologie in genetisch onderzoek is een impedantiemeter gebouwd welke volledig is toegespitst om onderdeel te zijn van een label-vrije, op diamant gebaseerde DNA sensor. Onderzocht is of onderscheid gemaakt kon worden tussen verschillende buffer oplossingen zoals deze vaak gebruikt worden in

genetisch onderzoek. Deze oplossingen zijn gemeten met verschillende molariteiten en op verschillende temperaturen. Nadat bewezen was dat we deze omgevingsvariabelen volledig in de hand hadden is de impedantiemeter ingezet in genetisch onderzoek. De gevonden resultaten worden gebuikt als randvoorwaarden voor experimenten.

Dit is het startpunt geweest voor experimenten waar chemische denaturatie van het DNA (door het toevoegen van 0.1 M NaOH) elektronisch is gevolgd in combinatie met confocale fluorescentiespectroscopie. Hieruit leerden we dat de impedimetrische data gesplitst kunnen worden in een tijdsconstante voor het blootstaan aan NaOH (mediumwissel) en een tijdsconstante voor het denatureren van het DNA. Deze denaturatietijd bleek een goede maat te zijn voor de stabiliteit van een DNA duplex. Wanneer slechts één mutatie werd geïnduceerd in een 29 base-paar tellende sequentie werd de denaturatietijd bijna gehalveerd. Het bleek zelfs mogelijk onderscheid te maken tussen denaturatietijden, wanneer een identieke mutatie op een andere positie werd geplaatst in de duplex. Dit betekent dat we een indicatie kunnen geven van de positie van de mutatie. Deze elektronische methode is snel, vereist een minimum aan instrumentatie en het DNA hoeft niet voorzien te zijn van fluorescente moleculen. Dit alles suggereert dat het elektronisch volgen van chemische denaturatie een interessante methode is om de stabiliteit van een DNA duplex te bepalen en wellicht kan worden ingezet binnen genetisch onderzoek voor puntmutatie-analyse.

Met de genoemde methode is de gewenste puntmutatie-resolutie dan wel bereikt, maar de ruwe data moet grondig bewerkt worden. Dit is een nadeel wanneer we deze technologie volledig willen automatiseren. We zijn daarom gestart met experimenten waar thermische denaturatie impedimetrisch is gevolgd. Dit moest het gebruik van drempelwaarden mogelijk maken. Wanneer thermisch gedenatureerd wordt, is een mediumwissel niet langer nodig. De impedantie wordt dan gemeten als functie van temperatuur i.p.v. tijd en medium. Echter, tijdens de eerste experimenten werd een nieuw fenomeen ontdekt. Deze nieuwe bevinding was in overeenstemming met de impedimetrische data. We observeerden een abnormaliteit in de temperatuur op het grensvlak van vaste stof naar vloeistof en vonden dat DNA als dubbelstrengige duplex een lagere thermische weerstand bezit dan in haar

enkelstrengige vorm. De overgang van lage naar hoge thermische weerstand kon gecorreleerd worden aan het denatureren van DNA met behulp van confocale fluorescentiespectroscopie. In vergelijking met een volledig passende sequentie deed deze overgang van lage naar hoge thermische weerstand haar intrede op lagere temperatuur wanneer een gemuteerde sequentie gedenatureerd werd. Dit betekent dat deze methode het mogelijk maakt om smelttemperaturen van DNA op te meten door enkel gebruik te maken van een regelbare voeding in combinatie met twee thermokoppels.

Dit project heeft geleid tot de ontwikkeling van twee label–vrije methoden om puntmutaties in DNA te detecteren. De eerste methode is gebaseerd op impedantie, de tweede methode stoelt op de onverwachte thermische weerstand. Beide technieken bezitten een hoge sensitiviteit en specificiteit en moeten daarom worden gezien als een veelbelovende industriële mogelijkheid in kinderschoenen. Om deze technieken los te weken van zuiver fundamenteel onderzoek en binnen te dringen in de competitieve diagnostische sector zijn nog een aantal cruciale stappen nodig

i)   Het bewijs leveren dat deze technologie ook werkt met langere DNA sequenties.

ii)   De technologie implementeren in een array format wat het mogelijk maakt gelijktijdig meer mutatie detecties te doen.

Wanneer ook deze mijlpalen zijn bereikt kan gedacht worden aan miniaturisatie van het geheel en wellicht ook een eerste stap buiten de geboden veiligheid van de academische wereld.

Chapter 1

Introduction

This first chapter opens with the fundamentals of DNA as described by James D. Watson and Francis Crick. It discusses the concept and consequences of mutations in DNA sequences, evidencing the relevance of the scope in this thesis. It then describes the gold standards in mutation detection and follows through with the state–of-the-art DNA sensors and benchmarks these sensors to the chosen strategies in this work: impedance spectroscopy and thermal resistance.

1.1 DNA

When thinking of DNA, one immediately tends to think about its originators, James D. Watson and Francis Crick. These two visionaries suggested the first correct double–helix structure of DNA and published their findings in the journal Nature in 1953 [1]. Their model was based on a single X-ray diffraction image **(figure 1)**, taken by Rosalind Franklin and Raymond Gosling, together with the information provided by Erwin Chargaff that DNA bases were paired. Nearly 60 years later their model still stands and DNA is still considered one of the hottest research topics in the world. They established the common knowledge that DNA consists of a sequence of four bases, adenine (A), thymine (T), cytosine (C), and guanine (G), that can be paired as A=T, and the more stable C≡G pair, involving two and three hydrogen bonds respectively. **Figure 2** provides a schematic representation of DNA. The binding process between these pairs is called 'hybridization' and induces the secondary structure of the double-stranded helix. The destruction of the bonds between the strands is called 'denaturation' or 'melting.' This destruction can be caused by changing the chemical environment or by an increase in temperature. When looking at DNA sequences linked to specific functions in an organism, the sequences should be identical for all individuals for some of these functions. When denaturing a sequence one can use the probe sequence of "individual 1" and then hybridize it with the target sequence of "individual 2". One will not encounter any problems because hydrogen bonds can be formed at all base pairs as shown in **figure 3a**.
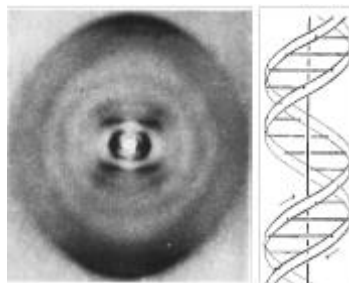

Figure 1: X-ray diffraction image, taken by Rosalin Franklin and Raymond Gosling, which led to the first correct double helix structure of DNA as proposed by James D. Watson and Francis Crick [1].

1.2 Single Nucleotide Polymorphism

Due to several reasons it can appear that a variation occurs in a DNA sequence. The smallest possible variation is called a single nucleotide polymorphism (SNP). A SNP is a DNA sequence variation occurring when a single nucleotide — A, T, C or G — in the genome differs between organisms of a biological species or paired chromosomes in an organism. When detaching the target from the probe in such a mutated sequence and subsequently hybridize it with a healthy probe sequence one will encounter the problem that no hydrogen bonds can be formed at a specific base pair as shown in **figure 3b.** The detection and identification of these SNPs in DNA are important in genomic research for several reasons. Many SNPs in many genes have been identified so far. Most of them are silent (without any effect), or cause harmless variations (*e.g.*, affecting eye or hair color), but some correlate to disorders such as Alzheimer, mucoviscidosis, phenylketonuria, and several types of breast and colon cancer [2, 3]. Furthermore, SNPs in the so called ADME (absorption, distribution, metabolism, excretion) genes significantly influence the effectiveness of treatment and this is a major topic in the field of theranostics [4]. Hence, the intended sensitivity of a DNA sensor is to distinguish between a fully complementary DNA sequence and a mutated sequence, mismatched at a single base pair.
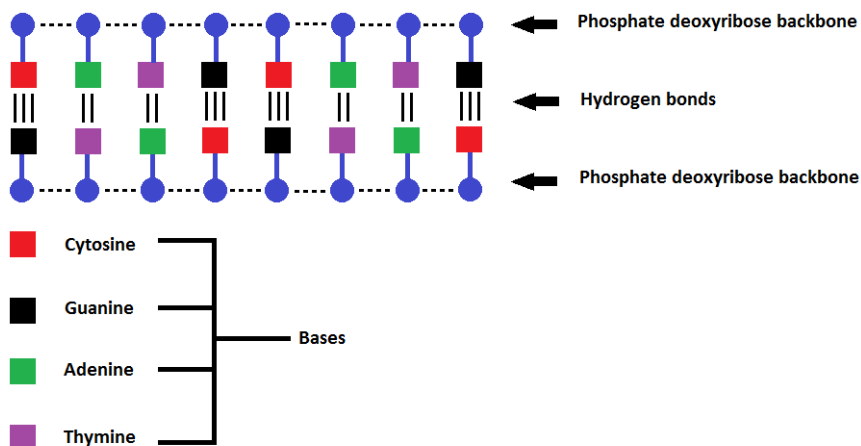

Figure 2: Schematic representation of DNA. The sequence consists of four bases, adenine (A), thymine (T), cytosine (C), and guanine (G), that can be paired as A=T, and the more stable C≡G pair.
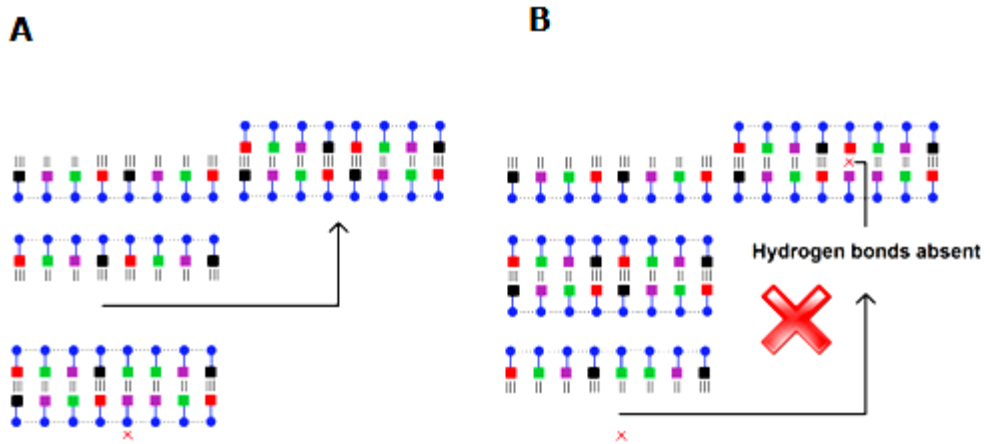
Figure 3: Principle of a SNP: When hybridizing a healthy probe sequence with a healthy target sequence, hydrogen bonds can be formed between all nucleotides (A). Hybridization between a healthy probe sequence and a mutated target sequence will lead to missing hydrogen bonds at the location of the mismatch (B).

1.3 "Gold standards" in DNA sensors
1.3.1 Microarrays
Most DNA sensors are based on the detection of hybridization such as microarrays: First a platform is functionalized with different sequences of single-stranded DNA (probe sequences). After this functionalization, counter sequences (target sequences) will be added to the hybridization buffer and are then allowed to hybridize with the probe sequences. These target sequences are tethered with a fluorescent molecule. A high number of complementary base pairs in a sequence means a tighter bond between the two strands (more hydrogen bonds). After washing off non-specific bonding sequences, only strongly paired strands will remain hybridized. The fluorescently labeled target sequences that bind to a probe sequence generate a signal that depends on the strength of the hybridization determined by the number of paired bases. The total strength of the signal, from a spot, depends upon the amount of target sample binding to the probes present on that spot. Two-color microarrays or two-channel microarrays are hybridized with target DNA from two samples (*e.g.*, diseased tissue versus healthy tissue). The two types of target DNA are labeled with two different fluorophores. The sample from the diseased tissue can be labeled with a fluorephore, emitting at a wavelength of *e.g.*, 570 nm (corresponding to the

green part of the light spectrum), and the sample from the healthy tissue with a fluorephore emitting at wavelength of 670 nm (corresponding to the red part of the light spectrum). The two labeled target DNA samples are then mixed and hybridized to a single microarray that is then scanned in a microarray scanner to visualize fluorescence of the two fluorophores after excitation with a laser beam of a defined wavelength. Relative intensities of each fluorophore may then be used in ratio-based analysis to identify the genes. The massive parallelized readout of this technique is an advantage, but the method requires fluorescent labelling, optical readout, and long hybridization times of ~ 16 hours at elevated temperatures. Furthermore, the method has an 'end-point' character without providing dynamic information on molecular recognition between probe and target fragments. The schematic of such a DNA microarray is shown in **figure 4.**
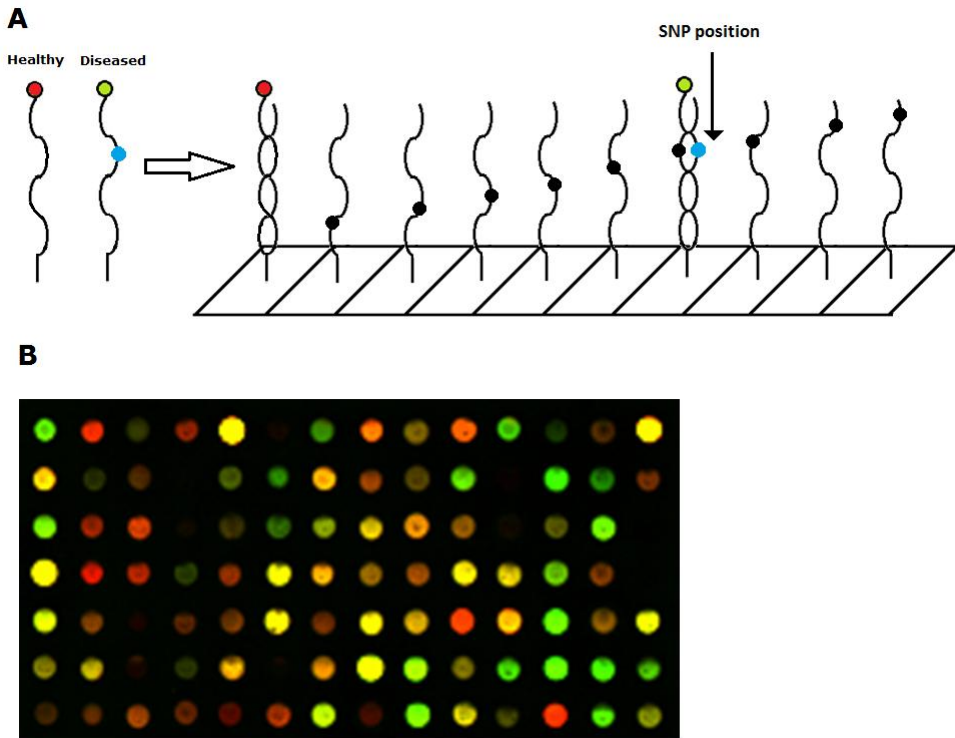

Figure 4: A collection of microscopic probe DNA spots is attached to a solid surface. Each DNA spot contains picomoles of a specific target DNA sequence that is used to hybridize under high-stringency conditions (A). Image of a DNA microarray, reflecting the gene expression differences between two different mouse tissues (B).

1.3.2 Denaturing-gradient gel electrophoresis and temperature-gradient gel electrophoresis

Due to these drawbacks, unknown mutations are frequently identified by denaturation based approaches. Widespread methods are denaturing-gradient gel electrophoresis (DGGE), temperature-gradient gel electrophoresis (TGGE) [5,6] and real-time PCR (polymerase chain reaction) with associated melting-curve analysis [7]. The core principle of DGGE can be found in the fact that DNA has a negative charge and so will move to the positive electrode in an electric field. The DNA is placed in a molecular mesh, with holes roughly the same size as the diameter of the DNA strand. When an electric field is applied, the DNA will begin to move through the gel, at a speed roughly proportional to the length of the DNA molecule. However, in TGGE, there is also a temperature gradient across the gel. At room temperature, the DNA will exist stably in a double-stranded form. As the temperature is increased, the strands begin to separate and the speed at which they move through the gel decreases drastically. The temperature at which melting occurs depends on the sequence (**figure 5**). TGGE not only separates molecules, but gives additional information about melting behaviour and stability [8].
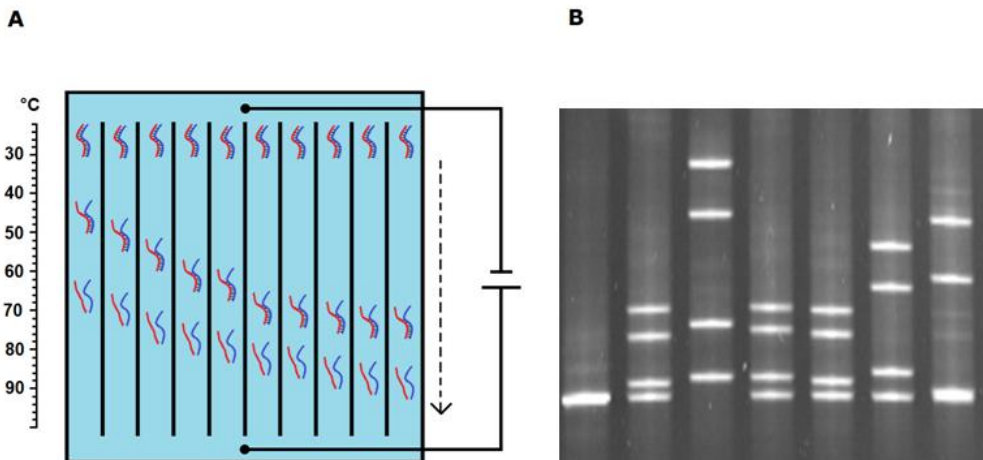

Figure 5: TGGE: DNA molecules are placed in a molecular mesh. A direct current (DC) voltage is applied over the molecular mesh and the DNA starts to travel towards the positive electrode, encountering a temperature gradient. Position of separation depends upon the sequence (A). Negative image of an ethidium bromide-stained DGGE gel (B).

1.3.3 The melting-curve analysis

The melting-curve analysis is comparable to the DNA microarray. Probe sequences are hybridized with a target sequence and the DNA is then functionalized with a DNA–intercalating fluorophore. The fluorescence intensity, generated by the DNA strands is then monitored as a function of temperature [9]. As long as the temperature will stay under the critical melting temperature at which the DNA sequence will denature, one will not observe a change in fluorescence intensity. However, when crossing the melting temperature the DNA will start to denature. This denaturation will lead to a decrease in fluorescence intensity because the fluorophore can only bind to the DNA in its double-stranded state and will have another (less fluorescing) conformation when floating freely in the fluid. The temperature at which 50% of the DNA is denatured is known as the melting point, though it is an inaccurate term as it has very little to do with a traditional melting point. At a certain temperature the fluorescence reaches a second stable platform. At this point every DNA strand is denatured. **Figure 6** provides a schematic representation of the melting curve analysis.
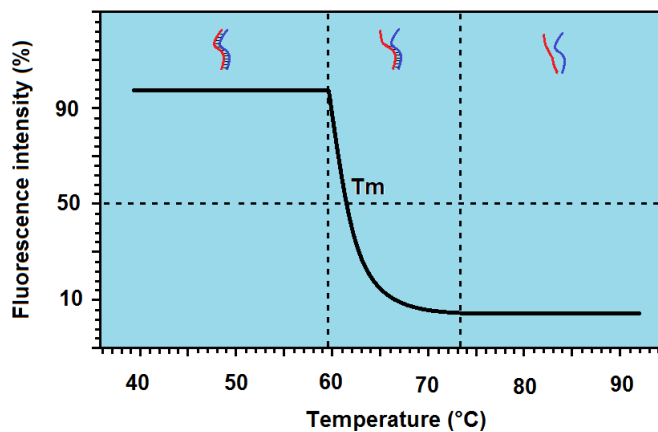

Figure 6: Melting-curve analysis. When DNA is present in the double-stranded state, fluorescence intensity is 100%. Upon denaturation the fluorescence intensity starts to decay. This deacy will stop when all DNA has entered the single-stranded state.

1.4 State of the art DNA sensors

The aforementioned technologies or derivatives thereof are considered to be the "gold standard" in common genomic research. However, there are several drawbacks that need consideration. They all need a lab environment and are time consuming. The typical duration for a microarray is approximately 16 hours and the DGGE and TGGE are less suitable for parallelized analyses. None of them provide any information on binding kinetics. The most important drawback is the fact they need fluorescent labelling, which implies the imperious need of a sophisticated and expensive optical readout technology. To overcome these general limitations, several DNA sensor concepts have been proposed in recent literature based on a wide range of strategies. Most promising strategies were based on the electrostatic switching effect of DNA, making use of the persistence length of DNA. A true label–free technology is to make use of the electric field-effect and the fact that current can be manipulated by applying an electric field, caused by DNA. A fourth method is to make use of the refraction index of light on a metal which can be influenced within a 100 nm vicinity by attaching DNA to the surface. A most elegant technology is to make use of the electronic properties of the DNA itself by measuring the DNA resistance at the single-molecule level. In the next section these strategies are explained in more detail.

1.4.1 The electrostatic switching effect

In 2007, Rant *et al.* reported on the electrostatic switching effect of DNA and the possibility to use this effect to distinguish between a full matching and mutated DNA sequences [10]. **Figure 7** represents the experiment with end-tethered probe sequences and illustrates the hybridization effect. A low-frequency (0.2 Hz) alternating current (AC) square wave is applied to a gold electrode (**figure 7A**) while the fluorescence emitted by the fluorescent-labeled DNA layer is observed simultaneously (**figure 7B**). Within each switching cycle, levels of high fluorescence intensity correspond to negative substrate potentials, whereas low intensities correspond to a positive bias. The difference between the upper and lower fluorescence levels is designated as 'switching amplitude.' It represents the electrically induced modulation of the layer thickness: during repulsive (negative) potentials the nucleic acids extend from the surface, whereas during attractive (positive) potentials they lie flat on the substrate.
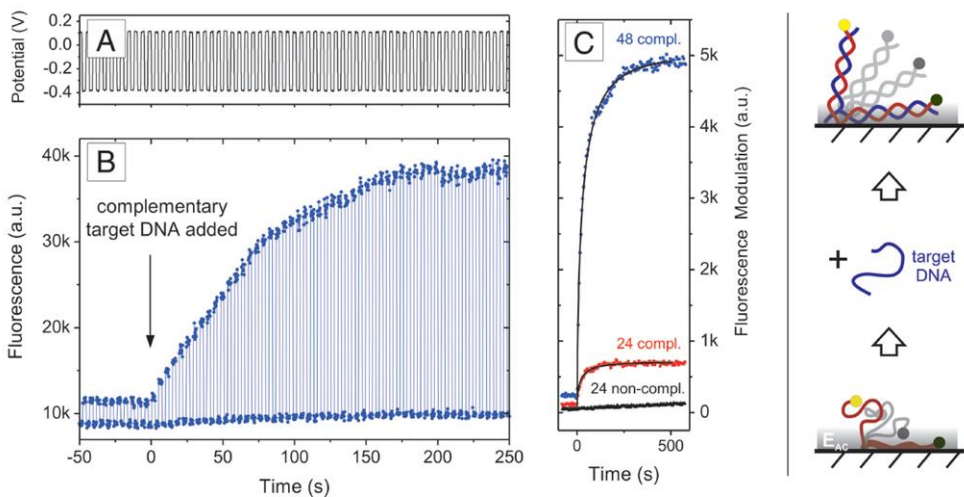

Figure 7: The schematic illustrates that flexible single strands are only partially aligned by the short-ranged electric field, emanating from the electrode surface, but double-stranded helices may be oriented efficiently because of their intrinsic rigidity, (*left*). A comparison is made between hybridization of complementary sequences comprised of 24 and 48 nucleotides and a non-complementary control (FMM) that exhibits negligible binding affinity, (*middle*). Long sequences give rise to strong signal enhancements. Picture adopted from [10].

1.4.2 The electric field-effect

A true label-free method to detect SNPs is to make use of the electric field-effect. In **figure 8,** the schematic drawing for the label-free detection of DNA using a field-effect transistor (FET) is shown. A FET is a transistor that relies on an electric field to control the shape and the conductivity of a channel of a charge carrier in a semiconductor material. All FETs have gate, drain, and source terminals. The FET controls the flow of electrons from source to drain by affecting the size and shape of a "conductive channel" created and influenced by a voltage (or lack of voltage) applied across the gate and source terminals. This conductive channel is the "stream" through which electrons flow from source to drain. When using a FET for DNA-sensing purposes, the gate of the FET is functionalized with a double-stranded DNA sequence. This layer influences the surface potential by its intrinsic molecular charge. This can be monitored by measuring the equivalent gate-voltage difference before and after attachment of the molecules to the surface in a potentiometric way. This principle was already established in 2002 by Fritz *et al*. [11], but it was Ingebrandt *et al.*, who presented a microarray-type DNA sensor by utilizing the differential transfer function (DTF) of silicon FET microarrays in an *ex situ* assay in 2007 [12]. They achieved the detection of SNPs in 20-base pair DNA sequences utilizing the DTF method with this *ex situ* readout.

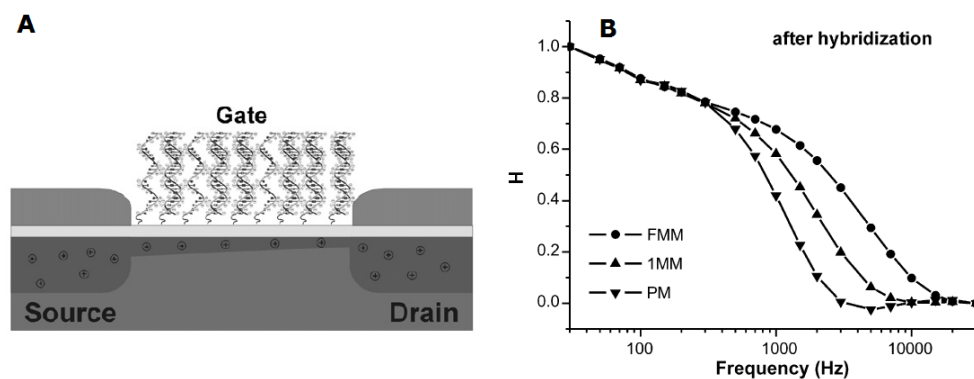**Figure 8:** Schematics of the readout circuit for the FET. The simplified gate input of the transistor with attached DNA layer is shown. The electric field, caused by the DNA which is functionalized on the gate will lead to a drop in current from source to drain (A). After hybridization, the differences between FMM, 1MM and FM can be clearly distinguished (B). Pictures are derived from [12].

1.4.3 Surface plasmon resonance

In 2010, Kick *et al.* reported on a DNA sensor, based on surface plasmon resonance (SPR) [13]. SPR can be described as the resonant, collective oscillation of conduction electrons in a metallic conductor stimulated by incident light. The resonance condition is established when the energy and the in-plane momentum component of the incoming photons match the energy and momentum of the plasma oscillations in the metal, preferably being an ultrathin (< 100 nm) gold coating on a glass prism.

SPR is the basis of many standard tools for measuring adsorption of material onto planar metal (typically gold and silver) surfaces (**figure 9A**). It is the fundamental principle behind many biosensor applications and various lab-on-a-chip sensors. Kick *et al.* accomplished an indirect detection of a genetic sequence using SPR. They spotted thiol-modified single-stranded probe DNA with different sequences onto a gold surface of a DNA chip (**figure 9B**). Their SPR spectrometer was able to detect hybridization on all spots of the sensor surface simultaneously. This approach is suitable for application with multiplex PCR and subsequent determination of products being specific for mutations in the genome.

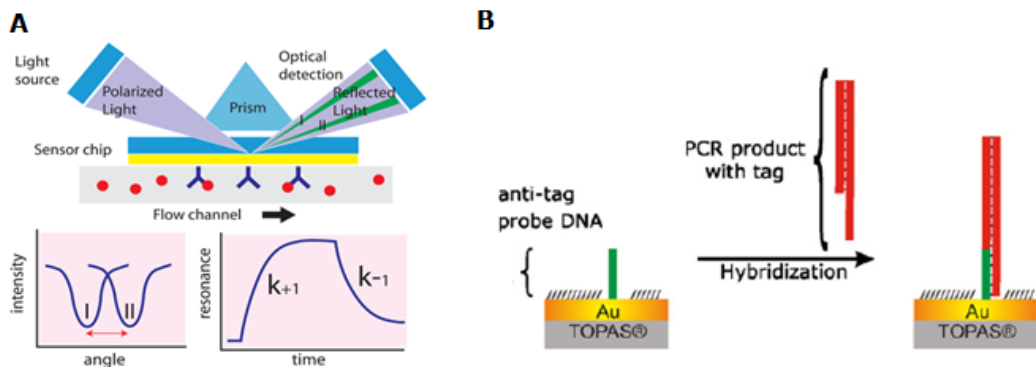

Figure 9: (A) Surface plasmon resonance (SPR) method for measuring kinetic and thermodynamic constants governing antigen-antibody interactions. (B) Schematic viewgraph of the hybridization principle adapted from [13]. PCR products (red) comprise a protruding single-stranded tag sequence and hybridize with a complementary anti-tag sequence (green) of probes immobilized on the gold surface.

1.4.4 Electronic properties of DNA at the single molecule level

In 2008, Guo *et al.* described a method to integrate DNA strands between single
-walled carbon nanotube (SWNT) electrodes and to measure their electrical
properties [14]. They modified DNA sequences with amines on either the 5´
terminus or both the 3´ and 5´ termini and coupled these to the single-walled
carbon nanotube electrodes through amide linkages, enabling the electrical
properties of complementary and mismatched strands to be measured. Full-
matching DNA in the gap between the electrodes exhibits a resistance on the
order of 1 MΩ. A single G-T or C-A mismatch in a 15-mer DNA strand increased
the resistance of the duplex 300-fold relative to a full-matched one. The
principle of this elegant technique is explained in **figure 10.**
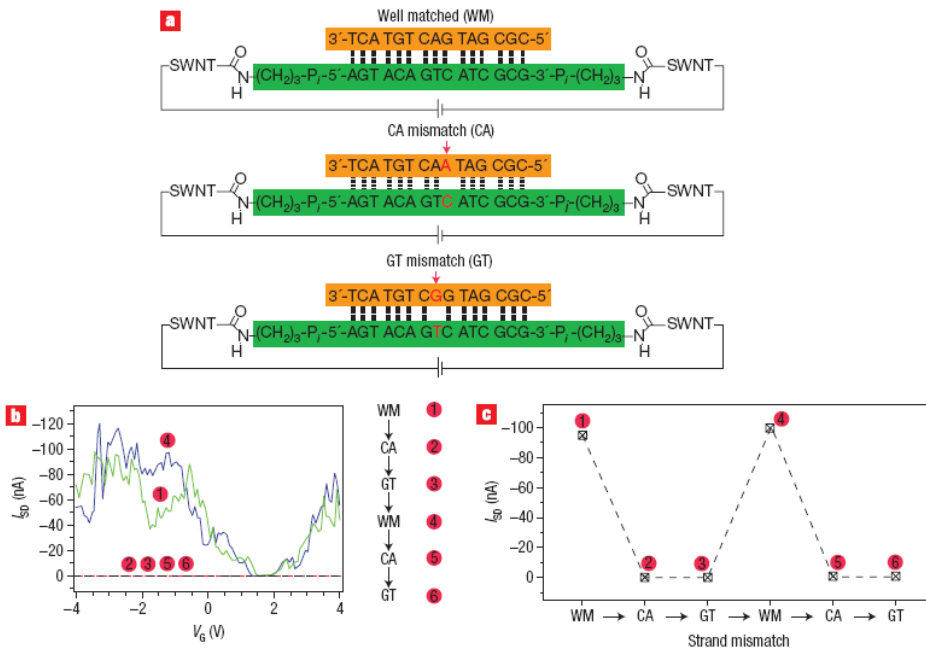

Figure 10: Mismatches have a large effect on DNA conductance. (a) Replacing well-
matched (WM) duplexes with CA and GT mismatches. (b) Source–drain current versus V_G
at a constant source–drain voltage (50 mV) for a SWNT device taken through the
sequence 1 through 6. The current levels for points 2, 3, 5 and 6 are 300 times lower. This
figure is adapted from [14].

1.4.5 Nanopores

In 2001, Howorka *et al*. reported on the application of engineered "DNA nanopores" to sense individual DNA strands with single-base resolution [15]. They built nanopores by covalently attaching an individual ssDNA oligomer within the lumen of an engineered version of the alpha-hemolysin pore from *Staphylococcus aureus.* The lumen measures 3 nm at the *cis* entrance, widens to 4.1 nm in the internal cavity, and narrows at the inner constriction to a diameter of 1.4 nm. In each DNA nanopore the ssDNA molecule was attached at the *cis* entrance, which permits duplex formation within the internal cavity. They demonstrated the ability of DNA nanopores to detect single-base mismatches in individual DNA strands. The pores were studied at an applied potential of +100 mV, which drives negatively charged DNA strands from the *cis* to the *trans* side of the pore. When a complementary target DNA strand was added to the *cis* side of the bilayer, negative current deflections were observed, interpreted as hybridization events **(figure 11A).** When inducing a target sequence carrying a single-base mismatch **(Figure 11B)**, only spikelike events were observed. It was concluded that the mismatched base of the target sequence abolishes the detectable formation of a duplex with the tethered DNA strand.
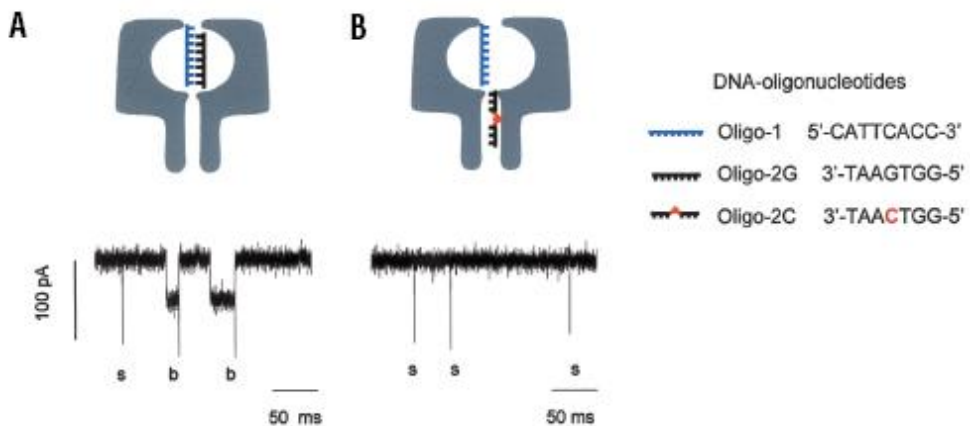
Figure 11: A single-base mismatch impedes the binding of an oligonucleotide to a tethered DNA strand within a DNA nanopore. (A) Representative single-channel current trace of a complementary sequence. Negative current deflections are individual binding events. (B) Representative trace of the same channel as in (A) after perfusion of the *cis* chamber and the addition of a mismatched target sequence; only short translocation events were observed [15].

1.5 Problem statement

The underlying principles of the mentioned methods for SNP detection are not yet explained in every detail, but they are linked to one or several of the following phenomena: change in mechanical rigidity of DNA, changes in the total charge of DNA, redistribution of counter ions, and changes of the dielectric properties near the surface onto which the probe DNA is attached. Given the limitations of the mentioned technologies there is a general interest in the development of fast, label-free, low-cost and user-friendly DNA biosensors. In order to integrate DNA in a sensor one needs to develop specific immobilization protocols to tether DNA preferably covalently and in head-on configuration onto the transducer surface [16]. Protocols are known for the attachment to *e.g.,* silicon, quartz, and gold surfaces [17-19], but it was shown by Yang *et al.* that these materials are not optimal: after several denaturation-rehybridization cycles the sensitivity and binding capacity deteriorate rapidly. They proposed synthetic diamond as a promising alternative [20]. Diamond can be prepared as thin films by chemical vapor deposition (CVD). Despite of its chemical inertness, there are photo- and electrochemical methods [20, 21] to ensure a covalent DNA binding and the sensitivity remains high even after 30 hybridization-denaturation cycles. In 2006, Christiaens *et al*. developed the so-called 'fatty acid & EDC' photochemical route, which requires only two surface-chemical steps and allows also for at least 33 regeneration cycles [22]. This two-step route for the DNA-functionalisation of diamond requires a hydrogen-terminated surface, obtained by a treatment with hydrogen plasma in a CVD reactor. In the first step, such a surface is reacted for 20 hours under 254 nm UV with omega-unsaturated fatty acid molecules (10-undecenoic acid), introducing COOH-groups for further reaction. In the second step, a zero-length cross-linker (1–ethyl–3-[3-dimethylaminopropyl]-carbodiimide, or EDC) is applied to establish a covalent bond between the COOH-groups on the diamond surface and amino-terminated DNA. This route is shown schematically in **figure 12**. Diamond has a wide electrochemical window, which makes it suitable as an electrode material for electrochemical bio-sensing techniques. As a proof-of-principle it was shown that sandwich electrodes (probe DNA sequences covalently bound to a diamond coating on silicon) in impedimetric sensor cells are indeed sensitive to DNA hybridization [23]. In conclusion, diamond based DNA electrodes as a

fundament for label-free readout technologies had a high potential, but the integration in sensor arrays was not yet demonstrated at the start of this project in October 2008.
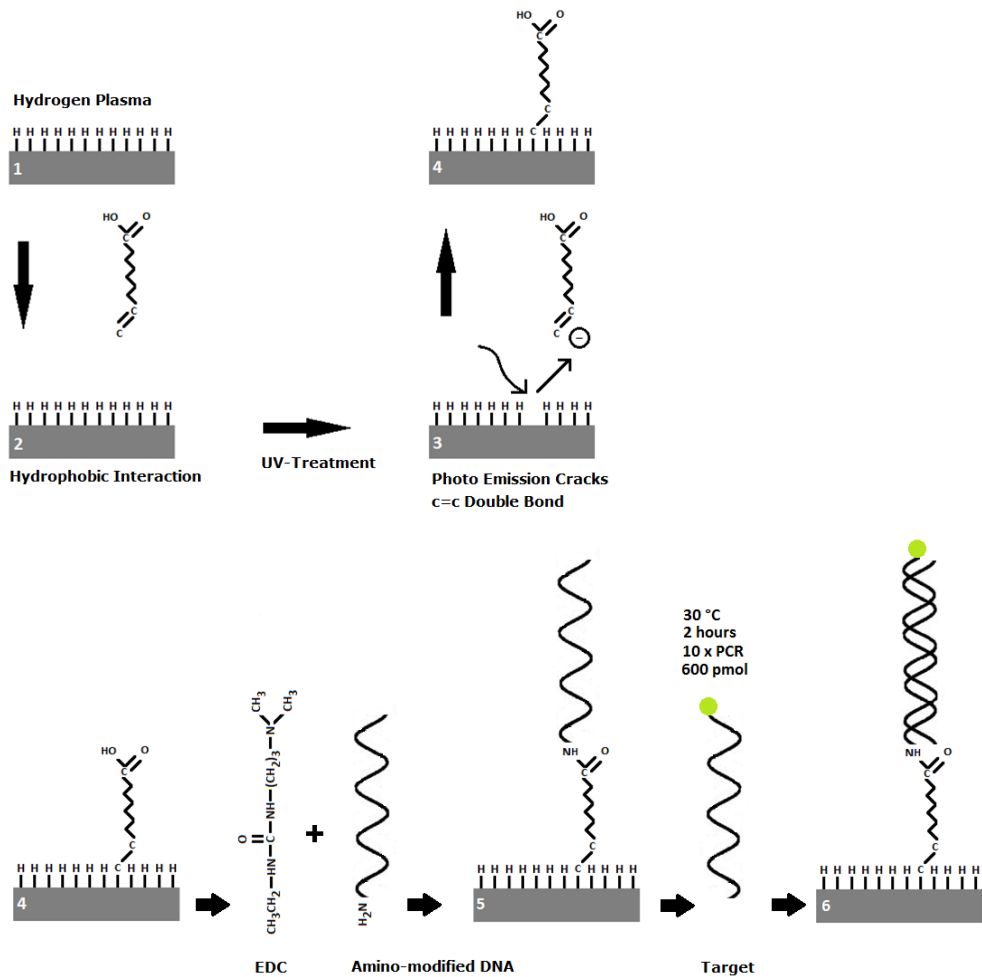

Figure 12: First an NCD surface is hydrogenated (1). After hydrogenation 10-undecenoic acid (fatty acid) is attached to the NCD surface through irradiation with 254 nm UV light (2). After the attachment of fatty acid (3,4), probe DNA is attached covalently to the fatty acid using an EDC mediated reaction (5). Now, the probe DNA sequence can be hybridized with its target (6).

Objectives

As a central objective, this project aimed at a comparative study on the performance of label-free readout strategies for the detection of SNPs in DNA sequences. 'Performance' is meant in the sense of a combination of three criteria:

i)   Fast response of the sensor at the minutes scale.

ii)   Clear distinction between complementary, mismatched, and single mismatched DNA fragments.

iii)   Low detection threshold, suitable for small concentrations of target DNA.

Various readout techniques can be considered, but keeping in mind that the sensitive spots should be miniaturized towards an array format the focus lies on relatively 'straightforward' but versatile perpendicular electrode configurations. The DNA activated diamond acts as bottom electrodes in a liquid cell with the counter electrode placed above in the hybridization / denaturation buffer. This setup was used for a detailed study on two specific sensing methods: the impedimetric and the thermal approach.

1.6 The impedimetric approach

The impedimetric approach is a well-known technique, which was already applied to immunosensors and sensors based on MIP-type synthetic receptors (MIP = molecularly imprinted polymer) [24, 25]. It is an efficient, fast and label-free technique for monitoring DNA hybridization and denaturation events in real time at the scale of a few minutes [23]. The impedance is measured by applying small AC potentials ($\sim$ 10 mV) in the frequency range from 100 Hz to 100 kHz between the DNA-functionalized working electrode (diamond layer on silicon substrate) and a counter electrode in the liquid. The electronic properties at the diamond surface change during denaturation, mainly due to the charge of the target DNA molecules, which induces a field-effect in the electrode material [23]. Since field-effect induced impedance changes are sensitive to the ion concentrations in buffer solutions and its temperature, see [26], we did not start immediately with impedance based SNP detection measurements. The starting

point for the practical work conducted in this project was the development of a new impedance spectroscopy unit, fully customized to be a vital part of a label-free, diamond based DNA sensor array, which was realized in 2009. Test measurements were conducted to investigate if one could distinguish between different solutions, like phosphate buffered saline (PBS) and NaOH at various temperatures and molarities [27]. After it was proven that this new developed measurement unit was able to distinguish between all these variables common in SNP detection measurements, the setup was implemented in SNP detection research. In retrospect it were these basic findings, which introduced the first SNP-success. In 2010 we reported on the electronic monitoring of DNA denaturation by NaOH using electrochemical impedance spectroscopy. The mathematical separation of the impedimetric signals into time constants for NaOH exposure and intrinsic denaturation-time constants provided strong evidence that the denaturation times reflect the intrinsic stability of the DNA duplexes [28].

1.7 The thermal denaturation method

After gaining the knowledge on how to interpret impedimetrical results upon denaturation, a second experiment was started. Now, the denaturation process was not done chemically, but by increasing the temperature. Chemical denaturation does provide results within SNP resolution, but the end result still needs to be fitted with exponential decay curves. This is considered to be a certain drawback when thinking of implementing such a system in the environment of a medical laboratory. It was considered to be a possibility to work with a threshold when denaturing thermally. A medium exchange is no longer present and one would measure impedance as a function of temperature instead of function of time and medium. This would eliminate the need for fitting because the temperature at which the impedimetrical anomaly occurs is the melting temperature. However, when conducting first experiments a new finding surfaced. This new finding was in line, but not related to the impedimetrical data. Upon denaturation a temperature anomaly was found at the solid-to-liquid interface. To gain more understanding of this phenomenon the temperature dependent heat-transfer properties were studied more in depth. It was found that DNA in its double-stranded form has a lower thermal resistance than in its

single-stranded form. As an explanation a geometrical model was provided. DNA fragments with a total length of 10 nm were used. This is far below the estimated persistence length of 50 nm [29, 30]. Therefore, these fragments can be considered as 'stiff rods' on the chip surface with a tilt angle in the range of 31° - 52° [31, 32]. After denaturation this persistence length drops to 1.5 nm [29]. This leads the single-stranded DNA to curl up, which increases the surface coverage. It was proposed that this increase in surface coverage density leads to an increase in heat-transfer resistance [33].

1.8 References

[1]   J. D. Watson and F. H. C. Crick, *Nature*, 1953, **171**, 737 – 738.

[2]   E. A. Schon, E. Bonilla and S. DiMauro, *J. Bioenerg. Biomembr.*, 1997, **29**, 131 – 149.

[3]   A. M. Dunning, C. S. Healey, P. D. P. Pharoah, M. D. Teare, B. Ponder and D. F. Easton, *CEBP,* 1999, **8**, 843 – 854.

[4]   J. W. Hooper, *Medical Laboratory Observer,* 2006, **38**, 22 – 35.

[5]   L. Lodewyckx, C. Vandevyver, C. Vandervorst, W. Van Steenbergen, J. Raus and L. Michiels, *Human Mutation,* 2001, **18**, 243 – 250.

[6]   E. A. Tindall, D. C. Petersen, P. Woodbridge, K. Schipany and V. M. Hayes, *Human Mutation,* 2009, **30**, 876 – 883.

[7]   R. Fodde and M. Losekoot, *Human Mutation,* 1994, **3**, 83 – 94.

[8]   P. Marten, K. Smalla and G. Berg, *J. Appl. Microbiol.,* 2000, **89**, 463 - 471.

[9]   E. A. Tindall, D. C. Petersen, P. Woodbridge, K. Schipany and V. M. Hayes, *Human Mutation,* 2009, **30**, 876 – 883.

[10]   U. Rant, K. Arinaga, S. Sherer, E. Pringsheim, S. Fujita, N. Yokoyama, M. Tornow and G. Abstreiter, *Proc. Natl. Acad. Sci. USA,* 2007, **104**, 17364 – 17369.

[11]   J. Fritz, J. E. B. Cooper, S. Gaudet, P. K. Sorger and S. R. Manalis, *Natl. Acad. Sci. USA,* 2002, **99**, 14142 – 14146.

[12]   S. Ingebrandt, Y. Han, F. Nakamura, A. Poghossian, M. J. Schöning and A. Offenhäusser, *Biosens. Bioelectron.*, 2007, **22**, 2834 – 2840.

[13]   A. Kick, M. Boensch, B. Katzschner, J. Voigt, A. Herr, W. Brabetz, M. Jung, F. Sonntag, U. Klotzbach, N. Danz, S. Howitz and M. Mertig, *Biosens. Bioelectron.,* 2010, **26**, 1543 – 1547.

[14]   X. F. Guo, A. A. Gorodetsky, J. Hone, J. K. Barton and C. Nuckolls, *Nat. Nanotechnol.,* 2008, **3**, 163 – 167.

[15]   S. Howorka, S. Cheley and H. Bayley, *Nat. Biotechnol.,* 2001, **19**, 636 – 639.

[16]   J. Wang, *Nucleic Acids Res.,* 2000, **28**, 3011 – 3016.

[17]   T. Strother, R. J. Hamers and L. M. Smith, *Nucleic Acids Res.,* 2000, **28**, 3535 – 3541.

[18]   M. Yang, R. Y. C. Kong, M. Kazmi and K. C. Leung, *Chem. Lett., 1998,*
        3, 257 – 258.

[19]   K. Hashimoto, K. Ito and Y. Ishimori, *Anal. Chem.,* 1994*,* **66**, 3830 –
        3833.

[20]   W. Yang, O. Auciello, J. E. Butler, W. Cai, J.A. Carlisle, J. E. Gerbi,
        D. M. Gruen, T. Knickerbocker, T. L. Lasseter, J. N. Russell jr.,
        L. M. Smith and R. J. Hamers, *Nat. Mater.,* 2002, **1**, 253 – 257.

[21]   H. Uetsuka, D. Shin, N. Tokuda, K. Saeki and C. E. Nebel, *Langmuir,*
        2007, **23**, 3466 – 3472.

[22]   P. Christiaens, V. Vermeeren, S. Wenmackers, M. Daenen, K. Haenen,
        M. Nesládek, M. vandeVen, M. Ameloot, L. Michiels and P. Wagner,
        Biosens. Bioelectron., 2006*,* **22**, 170 – 177.

[23]   V. Vermeeren, N. Bijnens, S. Wenmackers, M. Daenen, K. Haenen,
        O.A. Williams, M. Ameloot, M. vandeVen, P. Wagner and L. Michiels,
        Langmuir, 2007, **23**, 13193 – 13202.

[24]   P. Cooreman, R. Thoelen, J. Manca, M. vandeVen, V. Vermeeren,
        L. Michiels, M. Ameloot and P. Wagner, *Biosens. Bioelectron.,* 2005, **20**,
        2151 – 2156.

[25]   R. Thoelen, R. Vansweevelt, J. Duchateau, F. Horemans, J. D'Haen,
        L. Lutsen, D. Vanderzande, M. Ameloot, M. vandeVen, T. J. Cleij and
        P. Wagner, *Biosens. Bioelectron.,* 2008, **23**, 913-918.

[26]   A. Poghossian, A. Cherstvy, S. Ingebrandt, A. Offenhäusser and
        M. J. Schöning, *Sens. Actuators, B,* 2005, **111**, 470 – 480.

[27]   B. van Grinsven, T. Vandenryt, S. Duchateau, A. Gaulke, L. Grieten,
        R. Thoelen, S. Ingebrandt, W. De Ceuninck and P. Wagner, *Phys.Status
        Solidi A,* 2010, **9**, 2110 – 2113.

[28]   B. van Grinsven, N. Vanden Bon, L. Grieten, M. Murib, S. D. Janssens,
        K. Haenen, E. Schneider, S. Ingebrandt, M. J. Schöning, V. Vermeeren,
        M. Ameloot, L. Michiels, R. Thoelen, W. De Ceuninck and P. Wagner, *Lab
        Chip,* 2011, **11**, 1656 – 1663.

[29]   J. Ambia-Garrido, A. Vainrub and B. M. Pettitt, *Comput. Phys. Commun.,*
        2010, **181**, 2001 – 2007.

[30]   S. Wenmackers, V. Vermeeren, M. vandeVen, M. Ameloot, N. Bijnens, K. Haenen, L. Michiels and P. Wagner*, Phys. Status Solidi A,* 2009, **206**, 391 – 408.

[31]   B. Rezek, D. Shin and C. E. Nebel, *Langmuir,* 2007, **23**, 7626 – 7633.

[32]   S. Wenmackers, S. D. Pop, K. Roodenko, V. Vermeeren, O. A. Williams, M. Daenen, O. Douheret, J. D'Haen, A. Hardy, M.K. Van Bael, K. Hinrichs, C. Cobet, M. vandeVen, M. Ameloot, K. Haenen, L. Michiels, N. Esser and P. Wagner,*Langmuir,* 2008, **24**, 7269 – 7277.

[33]   B. van Grinsven, N. Vanden Bon, H. Strauven, L. Grieten, M. Murib, K. L. Jimenez Monroy, S. D. Janssens, K. Haenen, M. J. Schöning, V. Vermeeren, M. Ameloot, L. Michiels, R. Thoelen, W. De Ceuninck and P. Wagner, *ACS Nano*, 2012, **6**, 2712 – 2721.

Chapter 2

Customized Impedance Spectroscopy Unit for Label Free Affinity Biosensors

Bart van Grinsven[1], Thijs Vandenryt[1,2], Stijn Duchateau[1,2], Andreas Gaulke[3], Lars Grieten[1], Ronald Thoelen[1,2], Sven Ingebrandt[3], Ward De Ceuninck[1,4] and Patrick Wagner[1,4]

1) Hasselt University, Institute for Materials Research, Wetenschapspark 1, B-3590 Diepenbeek, Belgium

2) XIOS University College Limburg, Department of Electronic Engineering, Agoralaan Building H, B-3590 Diepenbeek, Belgium

3) University of Applied Sciences Kaiserslautern, Department of Informatics and Microsystems Technology, Amerikastrasse 1, D-66482 Zweibrücken, Germany

4) IMEC vzw – Division IMOMEC, Wetenschapspark 1, B-3590 Diepenbeek, Belgium

2.1 Abstract

A new impedance spectroscopy unit is developed, fully customized to be a vital part of a label-free, diamond based DNA sensor array. Test measurements are conducted to explore the accuracy and specificity of the system, both under electronic lab conditions and under wet cell conditions. The impedance of seven resistors was monitored for 17 hours and a maximum error < 0.2 % was found. Furthermore, the impedance of phosphate buffered saline (PBS) at different concentrations was monitored for 60 minutes per concentration and a different impedance for each concentration was detected. The impedance is also monitored for NaOH, PBS and nuclease-free water at different temperatures with a total duration of 60 minutes per fluid. Systematically different impedances for each temperature per fluid were found. All test measurements lead to results well within the required range.

2.2 Introduction

Impedance spectroscopy is an upcoming technique in the field of biomedical research [1]. This technique has already been used with success for monitoring DNA hybridization and the detection of single nucleotide polymorphisms [2], recognition of nicotine by means of molecular imprinted polymers [3] and the detection of C-reactive protein (CRP) [4]. The impedance based detection offers the possibility of device miniaturization and an electronic readout. After it was clear that it was possible to monitor hybridization and to detect single nucleotide polymorphisms it was time to explore the possibilities to increase measurement speed, allowing for semi-simultaneous detection of multiple types of receptors with their corresponding target molecules [5]. Therefore, a new unit is developed, based on a single chip developed by Analog Instruments [6]. When Analog Instruments presented a single chip solution for impedance measurements in 2005, it meant a revolution. Traditionally, it was an extreme design challenge to come up with a scheme to measure impedance. The only way it could be done was by using up to nine different integrated circuit chips, each with its own power provisions, separate resistors and capacitors. The design included an A/D converter, temperature sensors, different amplifiers etc. All these components had to be configured to operate at the same level and all the signal paths had to be investigated, not to influence the measurement by crosstalk effects. The integration in a single chip provides the possibility of miniaturizing the hardware, which is much better suited for point-of-care diagnostics (POC) and eventually lab-on chips. It also means a huge saving in surface area required for an impedance measurement setup and an enormous saving in design and testing time of the setup. Another note worth mentioning is that the cost of this device is 50 % less than the cost of a multichip solution. The impedance chip is able to measure frequencies between 100 Hz and 100 kHz, with an accuracy of at least 0.2 % [7]. The impedances measurable are in the range of 100 Ω and 10 MΩ. These overall numbers and facts are impressive, but when incorporating the chip in a design to measure the impedance of biological samples, one is stopped in their tracks. The Analog Devices AD5933 uses a direct current (DC) signal, with a superimposed alternating current signal, with a variable frequency [8]. This DC bias of 250 mV can ruin a measurement because the ions of the analyte are forced towards one electrode. This results in

deterioration of the electrodes due to corrosion or even destruction of the sensor surface because of hydrolysis occurring. In order to do the biological measurements, it was necessary to strip the DC voltage or at least make the bias user controllable [9]. The AD5933, unfortunately, did not provide the option to remove a bias voltage, as it is aimed primarily for automotive and fuel/battery cell monitoring purposes. So, a circuit had to be designed to remove the bias voltage in front of the sample under test and put it back on the signal behind the sample [10]. This circuit is schematically represented in **figure 1**. This work presents the new developed impedance spectroscopy unit based on this chip. Measurements have been conducted to proof the accuracy of the unit, not only on electrical resistors, but also on phosphate-buffered saline solution (PBS), NaOH and nuclease-free water, at different temperatures and concentrations. The measurements were successful; it was possible to distinguish even slight differences in concentration and temperature of the fluid and an accuracy of < 0.2 % is proven.
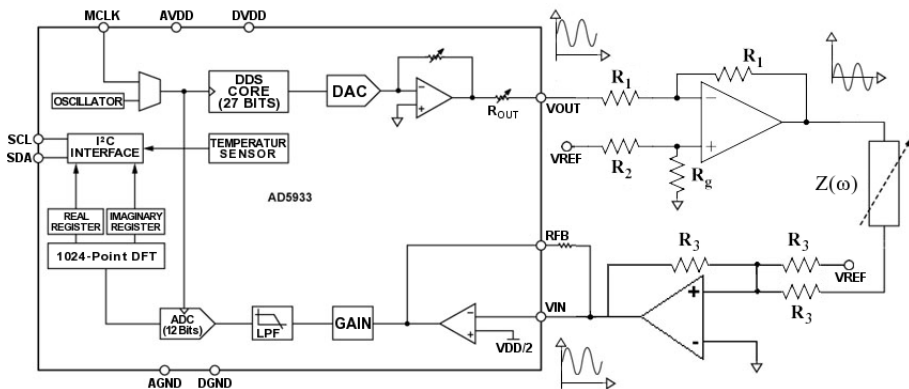

Figure 1: Circuit to remove the bias voltage in front of the sample under test and put it back on the signal behind the sample.

2.3 Experimental

To investigate whether or not the developed unit is applicable for the biological detection, test measurements were performed to prove the use of this chip for biosensor purposes.

2.3.1 Accuracy and durability test

The accuracy of the unit was tested by means of measuring the impedance of seven resistors with a value of 36 kΩ, 20 kΩ, 12 kΩ, 11 kΩ, 4.3 kΩ, 2.8 kΩ and 2.7 kΩ. The impedance was monitored for 17 hours at frequencies ranging from 100 Hz to 100 kHz, build up logarithmically with 10 frequencies per decade and a scanning speed of 5.3 seconds per frequency sweep. Because the impedance of an ideal resistor is purely real, the impedance of the chosen resistors should not change with increasing frequency and over time [11]. The maximum error is calculated with formula 1, shown below.

$$\text{maximum error} = \frac{|Z|_{max} - |Z|_{min}}{|Z|_{real}} \cdot 100 \quad (1)$$

The resistors had a common copper ground and were measured sequentially by means of a multiplexer mode, integrated in the impedance unit. In **figure 2**, the setup of this experiment is schematically represented.
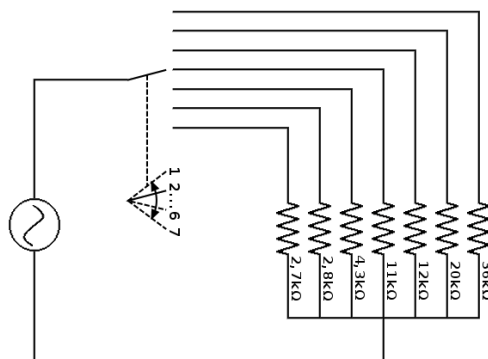

Figure 2: Schematic representation of the experimental setup to determine the durability and accuracy of the impedance unit.

2.3.2 Impedance of electrolytes at various concentrations and temperatures

Given the fact that the biosensor measurements are performed in a liquid cell, the influence of ionic solutions at different temperatures had to be investigated [12]. The solutions used in the protocol are PBS as a common buffer, NaOH, frequently used to denature DNA, and nuclease-free water to dissolve DNA [2]. For this study, a 1 liter stock of 10x PBS was prepared by dissolving 80 g NaCl, 2 g KCl, 14.4 g Na_2HPO_4 and 2.4 g KH_2PO_4 in 0.8 l of distilled water, and topping up to 1.0 l. Nuclease-free water, containing diethylpyrocarbonate (DEPC) to preserve DNA, was bought at Ambion Applied Biosystems (Japan) and 1M NaOH solution was purchased at VWR (Belgium). First, the impedance was measured for PBS at different concentrations (10x PBS, 1x PBS, 0.1x PBS and 0.01x PBS all with a volume of 140 µl), starting at the lowest concentration, in a frequency range of 100 Hz to 100 kHz built up logarithmically with 10 frequencies per decade and a scanning speed of 5.3 seconds per sweep. The conductivity and therefore, impedance should be linearly dependent on the concentration. However, this is only true in the lower concentration range where the tendency to form ion atmospheres and dipole states is negligible. The solutions are assumed to have a strong temperature coefficient, ranging from 1.4 % to 2 % per °C, because the viscosity of the liquid and the resulting frictional force on a migrating ion decreases with increasing temperature [13]. In **figure 3a** the setup is represented which was used to measure the impedance of PBS at different concentrations. A nanocrystalline diamond sample (NCD), functioning as a working electrode, was mounted on a copper back contact using silver paste. Diamond has a high thermal conductivity, is transparent in a wide region of wavelengths, is chemically inert, has a wide electrochemical window, and can be made semiconducting by chemical doping [14]. Diamond is biocompatible allowing eventually for in vivo applications and, moreover, it is suited for covalent attachment of biochemical receptors [15, 16, 17]. A rubber O-ring with an inner diameter of 7 mm and a teflon lid containing a circular opening of equal size was pressed onto the sample to create a reaction well above the NCD. The well was filled with 140 µl of reaction fluid. A gold wire, placed 1 mm above the NCD surface in contact with the reaction fluid, was used as a counter electrode. The working and counter electrode were connected to the impedance analyzer via 50 Ω coax cables. All concentrations were measured in the same well to

prevent crosstalk between different wells. This setup was put in an oven (Binder E28) at an ambient temperature of 37 °C and functioning as a Faraday cage. An identical setup, represented in **figure 3b**, was used to measure the impedance of all solutions at different temperatures with a frequency range of 100 Hz to 100 kHz, again with a volume of 140 µL. The setup was put in the oven but now it was exposed to different temperatures, ranging from 37 °C to 50 °C.
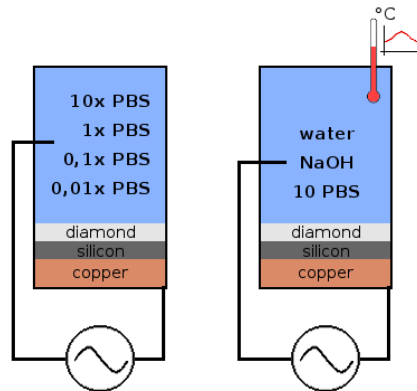

Figure 3: Experimental setup for impedemetrical differences at various concentrations of PBS (a), and various temperatures of nuclease-free water, NaOH and PBS (b).

2.4 Results

2.4.1 Accuracy and durability test

Sequential measurements were performed using seven electrical resistors. In accordance with the specifications from the AD5933 impedance chip the maximum error is < 0.2 % for all resistors at all frequencies [7]. In **figure 4**, the Bode plot is shown for the sequential measurements showing the impedance in the total frequency range for seven resistors, monitored for 17 hours. The absolute error, however (maximum measured value minus minimum measured value), does increase with increasing resistor value and was determined 6 Ω for the 36 kΩ resistor, 4 Ω for the 20 kΩ resistor, 2.3 Ω for the 12 kΩ resistor, 2.2 Ω for the 11 kΩ resistor, < 1 Ω for the 4.3 kΩ resistor, <1 Ω for the 2.8 kΩ resistor and < 1 Ω for the 2.7 kΩ resistor. It also became apparent that the impedance of all resistors decreased after 11 kHz, due to the capacitor effects in the electrical resistors.
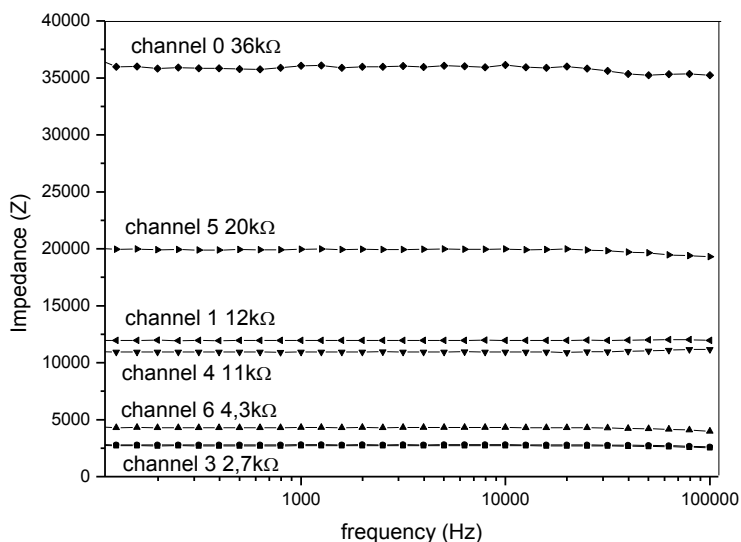
Figure 4: Bode plot of a sequential measurement showing the impedance in the total frequency range for seven resistors, monitored for 17 hours.

2.4.2 Impedance studies on electrolytes

The impedance is measured for PBS at different concentrations (10x PBS, 1x PBS, 0.1x PBS and 0.01x PBS all with a volume of 140 µl) in a frequency range of 100 Hz to 100 kHz and an ambient temperature of 37 °C. All concentrations were measured in the same well to prevent inter-well confounding. In **figure 5a,** the real and imaginary parts of the impedance are represented in a Nyquist plot. It can be observed that all concentrations show different plots and sequentially the lowest concentration shows the highest impedance and vice versa. Secondly, the temperature dependence of PBS, NaOH, and nuclease-free water was measured in a frequency range of 100 Hz to 100 kHz, with a volume of 140 µL; again the setup was put in an oven but now it was exposed to different temperatures ranging from 35 °C to 50 °C. In **figures 5b, 5c and 5d,** the real and imaginary parts of sequentially NaOH, 10x PBS and nuclease-free water are represented in Nyquist plots for three different temperatures. It can be seen for all solutions that the greatest difference occurs in the lower frequency ranges. Furthermore, it can be seen in **figures 5b and 5c** that for NaOH and 10x PBS the difference in impedance is the greatest in the temperature leap from 35 °C to 42 °C, both in

real and imaginary part, unlike nuclease-free water where the greatest difference is found between 42 °C and 49 °C, as shown in **figure 5d**. To investigate the linearity of this process, the impedance of NaOH, 10x PBS, and nuclease-free water, when increasing the temperature, was linearly fitted for 100 Hz, 1 kHz, 10 kHz and 100 kHz providing a Coefficient of determination (R^2) as a measure for linearity. In **table 1** it becomes apparent that the impedance decrease per increasing °C diminishes with rising frequency. However, a decrease in R^2 is observed above 11 kHz, probably caused by the capacitor effects described earlier.
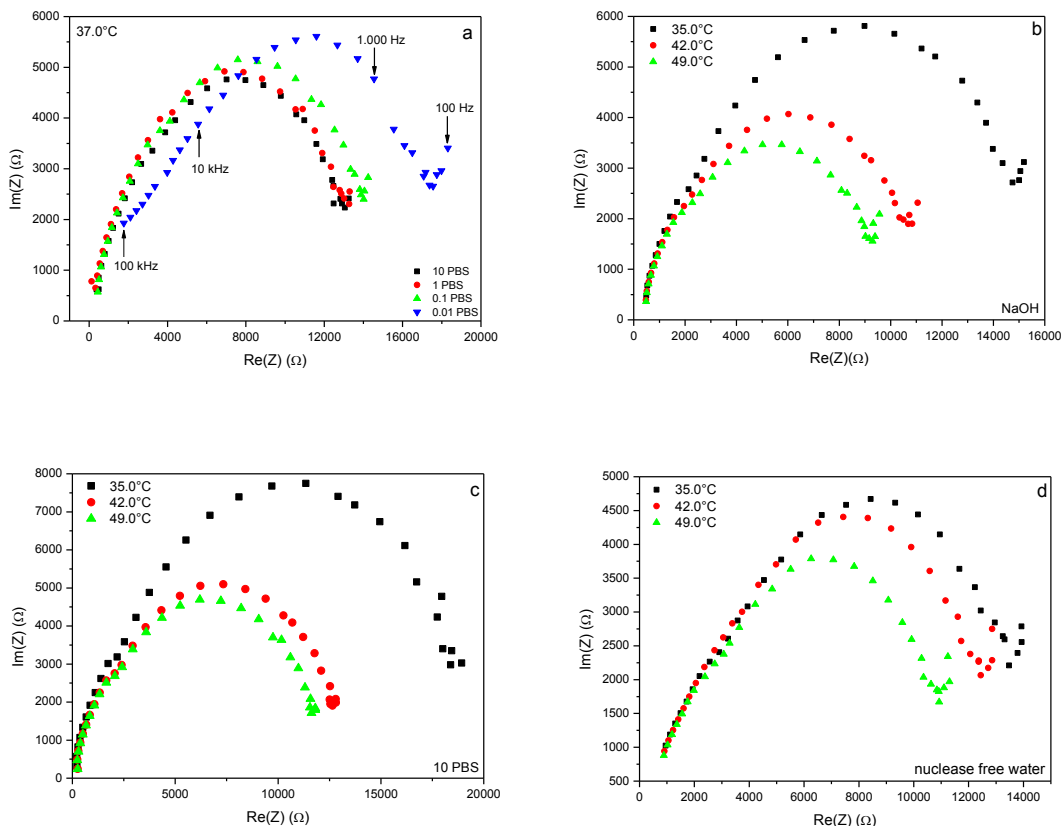

Figure 5: Nyquist plot showing the real and imaginary part of the impedance for 10x PBS, 1x PBS, 0.1x PBS and 0.01x PBS (a), for NaOH at 35.0 °C, 42.0 °C and 49.0 °C (b), for 10x PBS at 35.0 °C, 42.0 °C and 49.0 °C (c) and for nuclease-free water at 35.0 °C, 42.0 °C and 49.0 °C (d).

2.5 Discussion

The results demonstrate a newly developed impedance spectroscopy unit, customized to become part of a label-free, diamond-based DNA or protein sensor array. Accuracy and robustness of the system under electronic lab conditions as well as under wet cell conditions is shown. It is proven that the maximum error of the system is < 0.2 % under electronic lab conditions, but an increasing absolute error was monitored with increasing resistance. At frequencies below 11 kHz, the total impedance was equal to the resistor value. However, above these frequencies the impedance decreased below this resistor value. The impedance decrease at high resistor (Z_R) values (11 to 36 kΩ) is caused by a parallel parasitic capacitance of the sample. The impedance (Z_C) of this capacitor is inverse proportional to the frequency, as shown in formula 2.

$$Z_C = \frac{1}{2\pi f C} \qquad\qquad (2)$$

At lower frequencies this Z_C is too high to have an effect on the total impedance (Z), but at higher frequencies Z_C becomes low enough to cause a significant decrease in Z. This is illustrated in formula 3.

$$Z = \frac{Z_R \cdot Z_C}{Z_R + Z_C} \qquad\qquad (3)$$

Furthermore, if Z_R has a higher value, a decrease in Z_C is more apparent in proportion to the total Z than at lower Z_R values. This caused the slope of the graph to be much steeper at higher resistor values as is seen in figure 4. The calculated accuracy is high enough to recognize *e.g.,* DNA hybridization with an impedance drop of 20 % at a frequency of 1 kHz as described in [2]. The ability is shown to detect differences in concentration of PBS. The accuracy of this detection is also high enough to detect differences in concentrations, which may occur when (re)filling the wells with PBS or ssDNA dissolved in nuclease-free water. Also, the accuracy of detection of impedance changes due to temperature effects is sufficient. The fact that the impedance decrease per °C diminishes with rising frequency might be attributed to the fact that the impedance of a fluid is

Table 1: Impedance decrease (%) per increasing °C for NaOH, 10 x PBS and nuclease-free water for 100 Hz, 1 kHz, 10 kHz, 100 kHz.

Fluid	100 Hz	1 kHz	10 kHz	100 kHz
NaOH	3.1% (R^2=0.874)	2.6% (R^2=0.879)	0.7% (R^2=0.759)	0.6% (R^2=0.830)
10 x PBS	3.1% (R^2=0.780)	2.5% (R^2=0.789)	0.8% (R^2=0.790)	0.5% (R^2=0.691)
Nuclease-free water	3.1% (R^2=0.998)	1.3% (R^2=0.905)	1.0% (R^2=0.981)	0.7% (R^2=0.951)

more apparent in the higher frequency range in opposition to the impedance change of the solid parts of the setup (NCD, copper), which becomes less pronounced in the higher frequency range. In the future the frequency range will be extended from 10 Hz to at least 1 MHz, build up logarithmically with 10 frequencies per decade. Furthermore, the setup will be scaled down. Reaction wells, which need great volumes and are therefore more vulnerable to temperature bias, will no longer be a necessity.

2.6 Conclusion

According to the measurements described above, the developed impedance spectroscopy unit is considered to be robust and accurate. Long-term measurements give accurate results and it is proven that the unit not only functions under electronic lab conditions, but also under fluid cell conditions. It is expected that the system is employable as vital part of a label-free affinity biosensor system. However, the system still leaves room for improvement. In the future, the frequency range will be extended from 10 Hz to 1 MHz so that protein-antibody recognition is possible (at 10 Hz) [18] and DNA denaturation can be detected (at 1 MHz) [2]. Furthermore the setup as shown in **figure 3a and b** will be miniaturized. Reaction wells which need large volumes will no longer be present in the renewed setup. The developed system is already prepared for this down scaling and can directly be deployed for these measurements.

2.7 Acknowledgements

2.8 References

[1]   W. Cai, J. R. Peck, D.W. van der Weide and R. J. Hamers, *Biosens. Bioelectron.*, 2004, **19**, 1013 - 1019.

[2]   V. Vermeeren, N. Bijnens, S. Wenmackers, M. Daenen, K. Haenen, O. A. Williams, M. Ameloot, M. vandeVen, P. Wagner and L. Michiels, *Langmuir*, 2007, **23**, 13193 - 13202

[3]   R. Thoelen, R. Vansweevelt, J. Duchateau, F. Horemans, J. D´Haen, L. Lutsen, D. Vanderzande, M. Ameloot, M. vandeVen, T. J. Cleij and P. Wagner, *Biosens. Bioelectron.*, 2008, **23**, 913 - 918.

[4]   N. Bijnens, V. Vermeeren, M. Daenen, L. Grieten, K. Haenen, S. Wenmackers, O. Williams, M. Ameloot, M. vandeVen, L. Michiels and P. Wagner, *Phys. Status Solidi A,* 2009*,* **206**, 520 - 526.

[5]   S. Schwonbeck, A. Krause-Griep, N. Gajovic-Eichelmann, E. Ehrentreich-Förster, W. Meinl, H. Glatt and F. F. Bier, *Biosens. Bioelectron.*, 2004, **20**, 956 - 966.

[6]   Analog Devices, Datasheet AD5933, http://pdf1.alldatasheet.com/datasheetpdf/view/99319/AD/AD5933.html

[7]   L. Majer, V. Stopjaková and E. Vavrinský, *Measurement Science Review*, 2007, **7**, art. no. 3.

[8]   S. D. Keighley, P. Estrela, P. Li and P. Migliorato, *Biosens. Bioelectron.*, 2008, **24**, 912 - 917.

[9]   A. Malvino, Electronic Principles, Career Education, 6th edition, New York 1998**,** ISBN: 0028028333.

[10]   Agilent, Impedance Measurements Handbook, http://cp.literature.agilent.com/litweb/pdf/5950-3000.pdf.

[11]   B. M. Grafov, B. B. Damaskin, *Electrochim. Acta*, 1996, **41**, 2707 - 2714.

[12]   S. T. Lee, Z. Lin and X. Jiang, *Mater. Sci. Eng.*, 1999, **25**, 123 - 154.

[13]   S. Grimnes and G. Martinsen, *Bioimpedance and bioelectricity – Basics*, Academic Press, San Diego 2000, ISBN: 0-12-303260-1.

[14]   E. Gheeraert, S. Koizumi, T. Teraji, H. Kanda and M. Nesládek, *Diamond Relat. Mater.*, 2000, **9**, 948 - 951.

[15]   W. Yang, O. Auciello, J. E. Butler, W. Cai, J. A. Carlisle, J. E. Gerbi, D. M.
        Gruen, T. Knickerbocker, T. L. Lasseter, J. N. Russell Jr., L. M. Smith and
        R. J. Hamers, *Nat. Mater*., 2002, **1**, 253 - 257.

[16]   P. Christiaans, V. Vermeeren, S. Wenmackers, M. Daenen, K. Haenen,
        M. Nesládek, M. vandeVen, M. Ameloot, L. Michiels and P. Wagner,
        Biosens. Bioelectron., 2006, **22**, 170 - 177.

[17]   A. Härtl, E. Schmich, J. E. Garrido, J. Hernando, S. C. R. Catharino, S.
        Walter, P. Feulner, A. Kromka, D. Steinmüller and M. Stutzmann,
        Nat. Mater., 2004, **3**, 736 - 742.

[18]   A. Tlili, A. Abdelghani, S. Ameur and N. Jaffrezic-Renault, *Mater. Sci.
        Eng., C*, 2006, **26**, 546 – 550.

Chapter 3

Rapid Assessment of the Stability of DNA Duplexes by Impedimetric Real-time Monitoring of Chemically Induced Denaturation

Bart van Grinsven [1], Natalie Vanden Bon [2], Lars Grieten [1], Mohammed Murib [1], Stoffel D. Janssens [1], Ken Haenen [1,3], Eric Schneider [4], Sven Ingebrandt [4], Michael. J. Schöning [5], Veronique Vermeeren [2], Marcel Ameloot [2], Luc Michiels [2], Ronald Thoelen [1,6], Ward De Ceuninck [1,3] and Patrick Wagner [1,3]

1) Hasselt University, Institute for Materials Research, Wetenschapspark 1, B-3590 Diepenbeek, Belgium

2) Hasselt University, Biomedical Research Institute, Agoralaan, B- 3590 Diepenbeek, Belgium

3) IMEC vzw – Division IMOMEC, Wetenschapspark 1, B-3590 Diepenbeek, Belgium

4) University of Applied Sciences Kaiserslautern, Department of Informatics and Microsystems Technology, Amerikastrasse 1, D-66482 Zweibrücken, Germany

5) Aachen University of Applied Sciences, Institute for Nano- and Biotechnologies, Ginsterweg 1, D-52428 Jülich, Germany

6) XIOS University College Limburg, Department of Electronic Engineering, Agoralaan Building H, B-3590 Diepenbeek, Belgium

3.1 Abstract

In this article, we report on the electronic monitoring of DNA denaturation by NaOH using electrochemical impedance spectroscopy in combination with fluorescence imaging as a reference technique. The probe DNA, consisting of a 36-mer fragment was covalently immobilized on nanocrystalline-diamond electrodes and hybridized with different types of 29-mer target DNA (complementary, single-nucleotide defects at two different positions, and a non-complementary random sequence). The mathematical separation of the impedimetric signals into the time constant for NaOH exposure and the intrinsic denaturation-time constants gives clear evidence that the denaturation times reflect the intrinsic stability of the DNA duplexes. The intrinsic time constants correlate with calculated DNA-melting temperatures. The impedimetric method requires minimal instrumentation, is label-free and fast with a typical time scale of minutes and is highly reproducible. The sensor electrodes can be used repetitively. These elements suggest that the monitoring of *chemically induced denaturation* at room temperature is an interesting approach to measure DNA duplex stability as an alternative to thermal denaturation at elevated temperatures, used in DNA melting experiments and single nucleotide polymorphism (SNP) analysis.

3.2 Introduction

One of the central challenges in human genomics is the detection and identification of single nucleotide polymorphisms. Miniaturized assays such as microarrays play here an important role to allow for a massively parallelized readout in combination with small sample volumes [1, 2]. Disadvantages are the long reaction times at the scale of at least 16 hours, the complete lack of dynamic information on the DNA binding kinetics, the need for fluorescent labelling of the target DNA, and the sophisticated optical readout techniques. Also, microarrays are in principle limited to the detection of known mutations albeit there is recent progress to exploit the thermodynamic aspects of probe DNA – target DNA recognition to identify SNPs even in the presence of wild-type DNA [3]. Alternatively, mutation analysis can be performed using techniques that exploit the denaturation of double-stranded (ds) DNA rather than the hybridization process. The best known examples are real-time polymerase chain reaction (PCR) with associated melting-curve analysis [4] and denaturing gradient gel electrophoresis (DGGE) [5, 6]. Both techniques rely on the fact that DNA duplexes containing a SNP are less stable than complementary duplexes, resulting in lower denaturation (melting) temperatures. Nevertheless, both techniques require expensive instrumentation. Real-time PCR requires the use of fluorescent labels and DGGE is not suitable for high-throughput analysis.

Due to the inherent complexity of microarrays and the established denaturation-based approaches, strong efforts are put into the development of label-free detection techniques based on electronic readout principles. One of these electronic routes is the direct sequencing of DNA fragments with solid-state- or haemolysin nanopores, utilizing the current-blocking effect [7, 8, 9]. Alternatively, the DNA switching method on gold electrodes proposed by Rant *et al.* [10] allows for real-time monitoring of hybridization and denaturation with the possibility to distinguish between complementary and mismatched fragments. Although the method requires no fluorescent labelling of the target DNA, labels are involved on the probe DNA. A switching effect lies also at the basis of the E-DNA sensor [10], which employs an electrochemical redox reaction rather than fluorimetric detection and offers femtomolar detection limits. A method without any labelling and auxiliary chemistry is the solution-gate field-effect transistor (FET) device with the probe DNA directly immobilized on the

gate oxide [12, 13, 14]. Real-time monitoring of hybridization is in principle possible and FETs can discriminate between complementary and mismatched strands under *ex situ* conditions. The sensing effect of FETs is attributed to the intrinsic negative charge of ss- and ds-DNA fragments and to a redistribution of ionic charges at the proximity of the gate insulator during hybridization [15]. DNA-hybridization sensors based on impedance spectroscopy have been established with screen-printed carbon electrodes [16], mixed self-assembled monolayers on gold electrodes using a redox system, conjugated polymers, and GaN nanowires [17].

Despite of all recent progress, the aforementioned electronic- or opto-electronic methods for DNA sensing have in common that they suffer from at least two or more of the following drawbacks: i) need for high-end instrumentation and incompatibility with upgrading towards high-throughput assays; ii) need for additional chemicals such as fluorescent dyes or redox mediators; iii) lack of sensor-regeneration capacity; iv) missing proof that the sensor response is intrinsic and unaffected by conductivity effects related to temperature or ionic composition of the buffer liquids; v) insufficient statistics to demonstrate the reproducibility; vi) lack of dynamic information on the kinetics of hybridization- or denaturation events.

In this work, we will address these challenges by combining synthetic diamond electrodes, equipped with covalently immobilized probe DNA, with label-free, dynamic impedance readout and a stringent control on temperatures and medium composition using a miniaturized flow cell. Hereby, we will focus on the denaturation kinetics. One may expect a faster splitting of mismatched duplexes as compared to complementary duplexes, when they are exposed to a denaturation agent. Mismatch-related denaturation times have indeed been recently reported by Özkumur *et al.*, who employed label-free, optical interferometry on spotted microarrays, while the denaturation was induced by reducing the ionic strength of the buffer medium [18]. Besides of the intrinsic analogy with melting experiments, denaturation experiments offer the advantage to study duplex ensembles that are close to or at thermal equilibrium prior to the denaturation step. This starting condition is not necessarily fulfilled in the hybrization-based microarrays, where artefacts can occur due to metastable DNA-hybrid states formed between non-complementary strands [19].

3.3 Experimental

3.3.1 Design of the sensor cell and the impedimetric readout system

We use impedance spectroscopy, because this technique is especially versatile and can be employed not only for DNA hybridization, but also for protein detection and enzymatic reactions as shown in the review by Katz and Willner [20]. Moreover, impedimetric sensors are comparatively easy in fabrication since they are two-terminal devices without the need for specific semiconductor-doping profiles or advanced encapsulation techniques. From our prior impedimetric studies, there is indeed evidence that this method is suitable for monitoring DNA hybridization and denaturation under relevant buffer solution- and temperature conditions [21]. To measure the effect of denaturation of different DNA targets a sensor setup is constructed as shown in **figure 1**. This experimental setup consists of a homemade impedance spectroscopy unit as described in ref. [22] and a syringe system coupled to a Perspex flow cell with an inner volume of 110 µl. The working electrode is sealed with an O-ring, resulting in an effective area of 28 mm^2 exposed to the liquid. The counter electrode is a gold wire (diameter 500 µm, oriented perpendicular to the flow direction) at a distance of 1.7 mm from the surface of the working electrode. The working electrode is pressed on a copper lid, serving as back electrode and heat sink together. Miniaturized thermocouples are integrated in the copper lid and in the liquid. The cell is equipped with a quartz-glass bottom, enabling simultaneous fluorescence imaging with an inverted confocal fluorescence microscope. The syringe system comprises two identical programmable syringe pumps (ProSense, model NE-500, The Netherlands) enabling flow rates of 0.73 µl/hour to 1699 ml/hour. One syringe serves for administering 0.1 M NaOH solution, the other delivers 1 × Phosphate buffered saline (PBS) solution. Both are connected to a computer-controlled three-way valve. The impedance spectroscopy unit measures the impedance in a frequency range of 100 Hz to 100 kHz built up logarithmically with 10 frequencies per decade and a scanning speed of 5.7 s per sweep. All data discussed below refer to a frequency of 10 kHz, ensuring an optimal signal-to-noise ratio. The amplitude of the AC voltage was fixed to 10 mV. For Nyquist plots covering the full frequency range, we refer to the supporting material (paragraph 3.8).
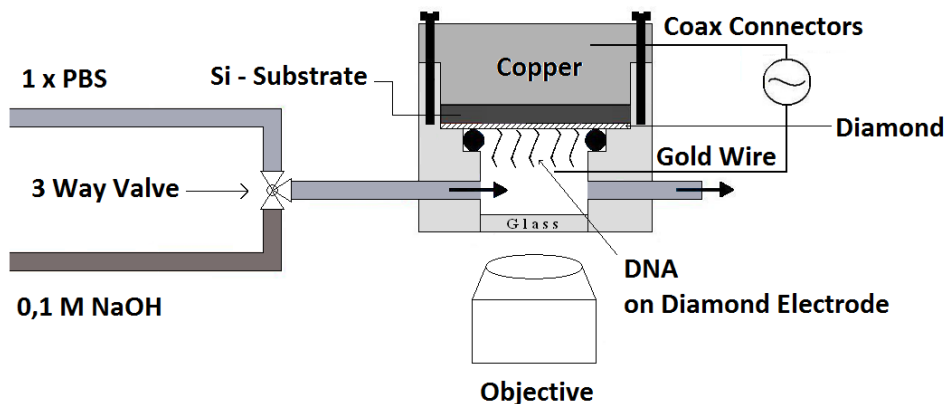
Figure 1: Schematic layout of the impedimetric flow cell. The working electrode (DNA on nanocrystalline diamond on highly-doped silicon) can be monitored with the fluorescence microscope while a gold wire serves as counter electrode. The liquids (1 × PBS buffer and 0.1 M NaOH) are sequentially administered by a syringe-driven pump system connected to a 3-way valve. The temperature of the liquid in the cell and of the copper back contact is measured by thermocouples (not shown). All connections to the impedance analyzer are done by mini-coax cables.

3.3.2 Preparation of the sensor electrodes and functionalization with DNA

3.3.2.1 Preparation of diamond-based sensor electrodes

Nanocrystalline diamond (NCD) electrodes were selected for their intrinsic biocompatibility [23, 24]. Moreover, they allow for the covalent immobilization of biochemical receptors by various techniques. Examples are the binding of proteins [25] and DNA fragments [26, 27], where a manifold of denaturation-rehybridization cycles has been demonstrated without loss of binding capacity. An overview of functionalization strategies, both on oxygen- and on hydrogen terminated diamond surfaces, can be found in the review articles by Wenmackers *et al.* [28] and Vermeeren *et al.* [29]. Furthermore, diamond offers a wide electrochemical window and it is chemically and physically stable at elevated temperatures, under extreme pH conditions, and in solutions with high ionic strengths. These elements make NCD a universal electrode material for monitoring biochemical reactions in real time. DNA-hybridization sensors based on diamond as a platform material have been reported in combination with impedance spectroscopy [21, 30], solution-gate FETs [31], and cyclic

voltammetry with a redox mediator on diamond nanowires [32]. Here, planar sensor electrodes were prepared by microwave plasma-enhanced chemical vapour deposition (MW PE-CVD) from methane / hydrogen mixtures in an ASTeX reactor as described in [33]. The substrates were 2-inch silicon wafers (thickness 500 – 550 µm, crystalline orientation (100), p-type doped with resistivities from 1 to 20 Ωcm), which were diced into samples of 10 mm by 10 mm after deposition. The diamond layers had a typical thickness of 100 nm with an average grain size of 50 nm as determined by X-ray diffraction. Due to the nanocrystalline character of the diamond coating, no preferential crystallographic orientation was detectable. To ensure a good electrical conductivity of the diamond layer (in the order of 1 Ωcm), the CVD deposition was done with an admixture of trimethyl borane ($B(CH_3)_3$) to the CH_4 gas with a concentration ratio of 200 ppm B/C. The as-prepared diamond electrodes were hydrogenated in H_2 plasma (50 Torr, 800 °C, power 4000 W, duration of 14 min) to facilitate the attachment of the fatty-acid linker molecules as described in the next paragraph. In total, 5 different diamond electrodes have been studied, denoted as # D1 to # D5.

3.3.2.2 Tethering of the probe DNA

First, 10-undecenoic fatty acid was photochemically attached to the H-terminated NCD electrodes by UV illumination (wavelength 254 nm, intensity 265 mW/cm^2) during 20 hours under a protective N_2 atmosphere. The reaction mechanism is presumably based on the fact that the hydrophobic C=C end of the fatty acid is oriented towards the H-terminated diamond surface and mediated by photoemission from the surface as proposed for the photochemical grafting of alkenes to silicon surfaces [34]. After this photochemical treatment, the samples were thoroughly rinsed in acidic acid at 100 °C to remove unbound fatty-acid fragments. In a second step, NH_2-modified ssDNA (36-mer with the sequence 5'-NH_2-C_6H_{12} AAA AAA ACC CCT GCA GCC CAT GTA TAC CCC CGA ACC-3') was covalently linked to the COOH group of the fatty acid using carbodiimide coupling. The details of this procedure and the final washing steps to remove non-reacted probe DNA have been described elsewhere [27, 35]. The origin and composition of chemical agents and buffer solutions is given in the supporting material, paragraph 3.8.2. The first 7 adenine bases at the 5' terminus of the

probe DNA serve as a spacer to avoid border effects at the proximity of the electrode surface. The total amount of probe ssDNA used to functionalize 1 cm^2 of the electrode surface was 300 pmol. This is in excess of the binding capacity of the surface, yielding a rapid functionalization.

3.3.2.3 Hybridization with target DNA

Hybridization of the probe ssDNA molecules (36 bp) attached to the NCD was performed by incubating ssDNA-modified NCD samples for 2 hours at 30 °C with 600 pmol of Alexa 488-labelled target ssDNA (29 bp) in 10 × polymerase chain reaction (PCR) buffer. Four different types of target DNA have been employed: a sequence, which was complementary to the probe ssDNA, a random sequence, and two sequences with a 1-base mismatch at base pair 7 or base pair 20 respectively (**table 1**). Note that for both 1-base mismatch sequences the mismatch is a 'CC' while the nearest neighbours are 'GC' and 'AT' in both cases. During hybridization, the samples were placed in a closed container under a saturated water vapour atmosphere to avoid evaporation of the reaction fluid. After hybridization, the samples were rinsed in 2 × saline-sodium citrate (SSC) buffer containing 0.5% sodium dodecyl sulfate (SDS) for 30 min at room temperature, followed by two 5 min rinsing steps in 0.2 × SSC buffer, once at 5 degrees below the hybridization temperature and once at room temperature. From previous studies based on fluorescence intensity and spectroscopic UV ellipsometry, it is known that the areal density of immobilized DNA duplexes is 10^{12} / cm^2 and their typical tilt angle with respect to the normal of the electrode surface is ≈ 50° [35, 36]. The areal density corresponds to an average distance of 10 nm between neighbouring DNA strands, which is slightly less than the length of the probe-DNA fragments (36 bases correspond to 12 nm), but still corresponding to a diluted molecular brush without sterical hindering.

Table 1: Compilation of the base sequences of the probe DNA and the four different types of target DNA employed in the hybridization and denaturation experiments. The probe DNA exhibits a spacer consisting of 7 A-bases while the target DNA fragments carry a fluorescent Alexa 488 label at the 5' end. The position of the mismatches with respect to the probe DNA is underlined and indicated by bold letters.

Name	Sequence
Probe DNA	3´-CCA AGC CCC CAT ATG TAC CCG ACG TCC CCA-α
Full match	5´-Alexa 488-C_6H_{12} GGT TCG GGG GTA TAC ATG GGC TGC AGG GG-3`
Mismatch at BP 7	5´-Alexa 488-C_6H_{12} GGT TCG GGG GTA TAC ATG GGC T**C**C AGG GG-3`
Mismatch at BP 20	5´-Alexa 488-C_6H_{12} GGT TCG GGG **C**TA TAC ATG GGC TGC AGG GG-3`
Random sequence	5´-Alexa 488-C_6H_{12} **TCA AAT T**G**C CAG A**AC A**AC TA**C TG**A CT**G **AA**-3`

3.3.2.4 Confocal fluorescence microscopy

The denaturation of DNA was evaluated by measuring the change in fluorescence intensity with a Zeiss LSM 510 META Axiovert 200 M laser scanning confocal fluorescence microscope using a 488 nm argon-ion laser excitation with a maximum intensity at the sample surface of 1.00 ± 0.05 mW. All images were collected with a 10x/0.3 Plan Neofluar air objective with a working distance of 5.6 mm. The image size was 128x128 with a pixel dwell time of 51.2 µs, corresponding to ~ 900 by 900 µm^2. The pinhole size was 150 µm and the laser intensity was set at 10%. The detector gain, being a measure for the photomultiplier voltage in arbitrary units, varied between 1000 and 1200 in different measurements. For photo bleaching experiments, the laser intensity was set at 100% for 3 minutes. Fluorescence images were processed and the average fluorescence intensities were retrieved using the AIM4.2. software package. After hybridization with the different types of target DNA, each of the NCD samples was studied by confocal microscopy to ensure the presence and homogeneous distribution of DNA. Bleaching experiments demonstrated clearly that the fluorescence intensity originated from the Alexa 488 dyes and not from the underlying diamond layer.
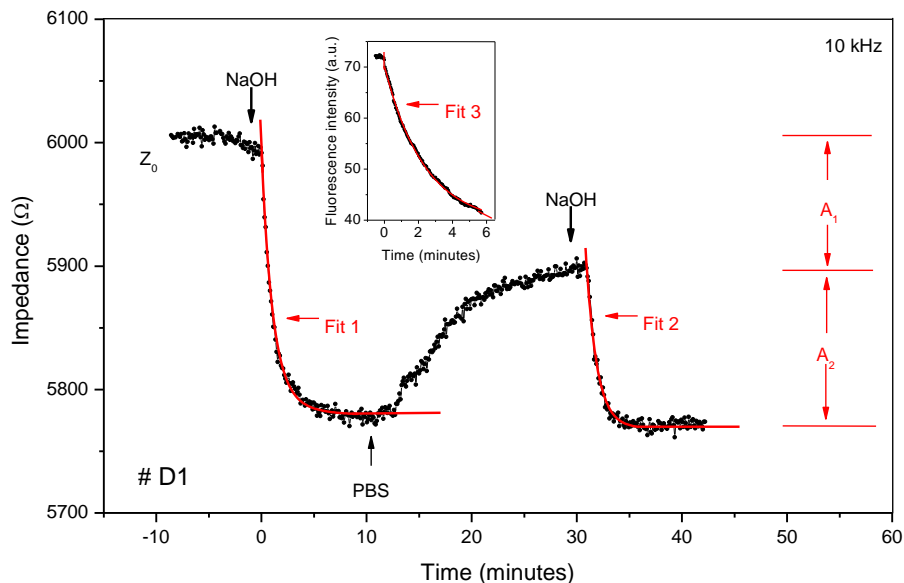
Figure 2: Impedance profile of the denaturation of full-match DNA on diamond sample # D1 with the time dependence of the fluorescence intensity in the insert. At t = 0, 0.1 M NaOH enters the cell and replaces the $1 \times$ PBS buffer. This causes a drop of the fluorescence intensity and the impedance. The impedance response emerges from the denaturation and the change of liquids, while the fluorescence drop stems from DNA denaturation only. The extraction of the time constants τ_1 (denaturation) and τ_2 (exchange of fluids) is based on the Fits 1 and 2, as described is the text. The time constant $\tau_1 = 2.24$ min $\pm$ 0.14 min from the impedimetric data is consistent with the fluorimetric result $\tau_3 \approx$ 2.41 min obtained from Fit 3. To determine $\tau_2 = 0.97 \pm 0.06$ min, the cell was refilled with $1 \times$ PBS at $t_1 = 12$ min and flushed with 0.1 M NaOH at $t_2 = 30$ min. The amplitudes A_1 and A_2 indicate the respective influence of denaturation and liquids exchange on the impedance changes.

3.4 Results and discussion

3.4.1 Comparative impedimetric and optical denaturation study

A real-time denaturation experiment on perfectly matched ds DNA (electrode # D1) is shown in **figure 2**. After mounting the functionalized electrode, the cell was filled with $1 \times$ PBS buffer and installed on the confocal fluorescence microscope. The cell was allowed to stabilize for 45 min to guarantee that drift effects were absent and the noise level was below 0.5 %. The moderate noise level in this measurement is related to the fact that the ambient temperature of about 25 °C could not be actively controlled. In all further measurements, not performed on the confocal microscope, the ambient temperature and temperature of all liquids were strictly stabilized to 19.3 °C, resulting in even lower noise levels. At $t_0 = 0$ min, 0.1 M NaOH at a flow rate of 250 µl per minute enters the cell and replaces the PBS filling. This results in an impedance drop, which consists of two separate contributions: i) the intrinsic effect of denaturation, which affects the electronic properties in the vicinity of the topmost diamond layer and ii) the medium exchange as the 0.1 M NaOH filling causes a higher conductivity than $1 \times$ PBS. To distinguish both contributions quantitatively, the 0.1 M NaOH was replaced by reintroducing $1 \times$ PBS at $t_1 = 12$ min (flow rate 250 µl/min). The impedance increases and stabilizes at a plateau with a lower value as compared to the starting condition. This demonstrates that the impedimetric properties of the electrode surface must have changed upon denaturation because the ionic properties of the PBS buffer are identical before and after the in between denaturation step. To analyze the typical time scale of introducing 0.1 M NaOH, at $t_2 = 30$ min the $1 \times$ PBS was finally replaced by 0.1 M NaOH at a flow rate of 250 µl/min. The superimposed processes of denaturation and the pure effect of medium exchange can mathematically be described as follows:

Fit 1: $Z(t) = Z(t = \infty) + A_1 \cdot \exp \left\{ -\dfrac{t}{\tau_1} \right\} + A_2 \cdot \exp \left\{ -\dfrac{t}{\tau_2} \right\}$ (Equation 1)

Fit 2: $Z(t) = Z(t = \infty) + A_2 \cdot \exp \left\{ -\dfrac{t - t_2}{\tau_2} \right\}$ (Equation 2)

The double-exponential **Fit function 1** for superimposed, independent decay processes is known *e.g.* from the decomposition of biomass (tomato leaves) and the mass loss of tomato DNA as a function of time [37]. The parameter A_1 represents the denaturation-related decay amplitude and τ_1 the associated time constant; the amplitude A_2 refers to the impedance drop by the medium exchange and τ_2 is the corresponding time constant. The **Fit function 2** describes solely the influence of the medium exchange from $1 \times$ PBS to 0.1 M NaOH after the denaturation has taken place and is therefore representative for the medium exchange as such. Note that there is no intrinsic reason for the exponential time dependence related to the medium exchange, but the agreement with experimental data is excellent with a coefficient of determination (R^2) of 0.97 for Fit 2. The exponential time dependence of the splitting of DNA duplexes is naturally inherent to decay processes of non-interacting ensembles. First, we applied **Fit 2** and extracted $\tau_2 = 0.97 \pm 0.06$ min together with $A_2 = 112 \pm 9$ Ω for the medium exchange effect. Inserting these values into **Fit 1** resulted in a denaturation-time constant $\tau_1 = 2.24 \pm 0.14$ min and an amplitude $A_1 = 115 \pm 13$ Ω. The R^2 of Fit 1 is 0.94, giving support to the concept of superimposed decay processes. All fits are performed with Origin 7.1.

To crosscheck the electronically determined τ_1, time-lapse fluorescence imaging was performed during the denaturation step (time interval of 1.4 seconds between subsequent images) and the intensity I(t) was averaged over an area of 900 by 900 μm^2. Selected images with intervals of 36 seconds, taken during the first 6 minutes of the dynamic imaging, are shown in **figure 3**. Note, that there is remnant background intensity I_0, which is not vanishing even long after this period, and therefore attributed to the reflected laser light. The area-averaged intensity values are shown as an insert in Figure 2 and described with **Fit 3**:

$$\textbf{Fit 3:} \quad I(t) = I_0 + I_{DNA} \cdot \exp\left\{ -\frac{t}{\tau_3} \right\} \quad\quad\quad \text{(Equation 3)}$$

The fluorescence decay time constant $\tau_3 = 2.41 \pm 0.05$ min is, within the error margins, perfectly consistent with the electronically determined τ_1. The determination of τ_3 is insensitive to the medium composition and truly reflects the progressing denaturation at the NCD-electrode surface. The Alexa 488 labeled target-DNA fragments, which are removed by NaOH exposure, do not contribute to the fluorescence intensity as they are transported away by the
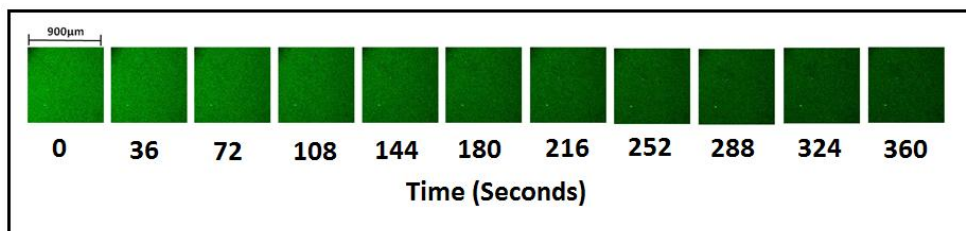
Figure 3: Series of confocal fluorescence images of the diamond electrode during the denaturation of perfectly complementary ds DNA at selected times. Note that the fluorescence-intensity curve in Figure 2 was derived from images with time intervals of 1.4 seconds. The depicted area is 900 by 900 μm^2.

constant NaOH flow, while the confocal volume is restricted to a distance of less than 4.5 µm from the surface of the NCD electrode. In conclusion, the electronically determined denaturation-time constant τ_1 is a reliable measure for the duration of the chemically induced denaturation process. It is important for the applicability of the approach that the time constant of the medium exchange is shorter than the duration of the denaturation process. In the opposite case (denaturation faster than medium exchange), the medium exchange would be the determining factor for the progressing DNA denaturation, making it more difficult to determine the time constant of the denaturation process. This is a useful aspect in the sense that the medium-exchange time constant can be adjusted in wide ranges by adapting the flow rate of the pumping system to meet conditions in which the medium exchange is considerable faster than the dynamics of biological recognition- or unbinding events.

Repeating the entire procedure on diamond sample # D1, re-hybridized with complementary target-DNA fragments, but measured in a temperature-stabilized environment of 19.3 °C and without laser illumination, gave $\tau_1 = 2.28 \pm 0.16$ min and $\tau_2 = 0.58 \pm 0.04$ min. The denaturation-time constant is clearly consistent with the measurement at 25 °C although the influence of the medium exchange levels off faster, due to a slight modification to the flow system. In a next step, the probe DNA was hybridized with target DNA with a single-nucleotide mismatch at base pair 7. This resulted in $\tau_1 = 1.21 \pm 0.10$ min and $\tau_2 = 0.48 \pm 0.02$ min. As expected, the time constant for the medium exchange is very similar under identical environmental- and flow conditions, but the DNA duplexes with the SNP mutation denature considerably faster than the

complementary duplexes. This strongly suggests that the monitoring of chemically-induced denaturation can give an indication for the presence of single-nucleotide polymorphisms.
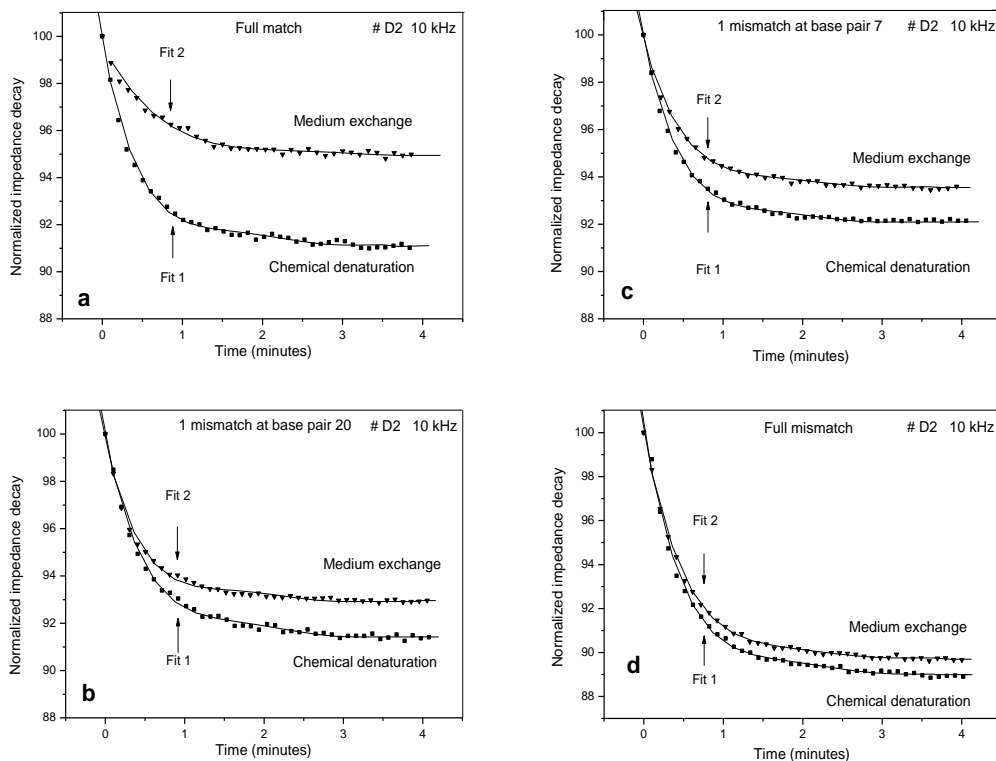

Figure 4: Overview of the denaturation steps performed on diamond sample # D2 with complementary target DNA **(panel a)**, mismatch at base pair 20 **(b)**, mismatch at base pair 7 **(c)**, and the random target sequence **(d)**. All data described as 'chemical denaturation' are normalized to the impedance value at the moment when 0.1 M NaOH enters the cell and fitted with the double exponential Equation 1 (Fit 1) as described in the text. The curves denoted as 'medium exchange' refer to the second replacement of $1 \times$ PBS by 0.1 M NaOH after the actual denaturation step. These data are normalized with respect to the equilibrium impedance value at time t_2 obtained after refilling the cell with $1 \times$ PBS buffer (Fit 2 according to Equation 2).
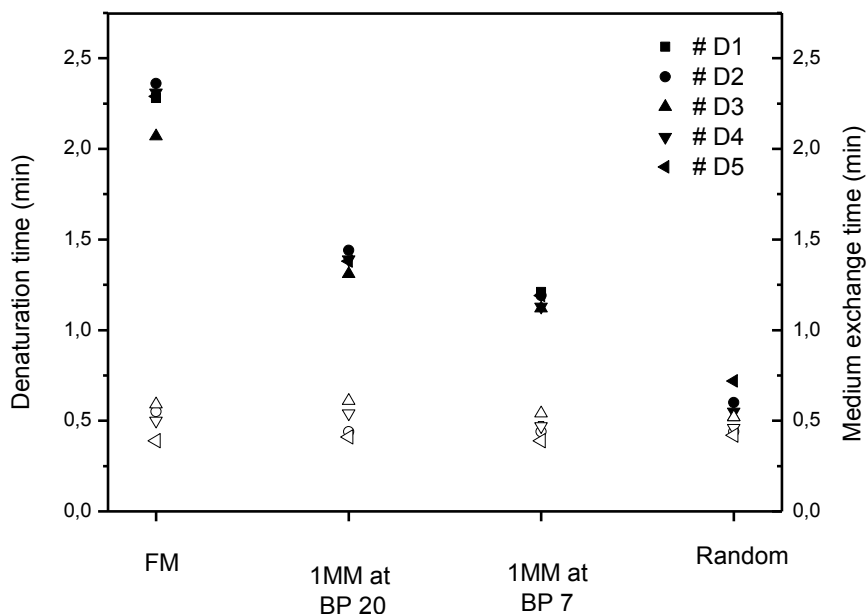
Figure 5: Compilation of the denaturation-time constants τ_1 (solid symbols) for the four different types of target DNA. Each time constant was measured on at least four different diamond electrodes and the scattering between the data is remarkably low. The time constants τ_2 for medium exchange from $1 \times$ PBS to 0.1 M NaOH are indicated by open symbols. Note that even in case of the random sequence there is still a slight difference between the denaturation time and the medium exchange.

3.4.2 Impedimetric denaturation monitoring with various types of target DNA

In order to evaluate the reproducibility of the method and whether in principal it allows to localize and to identify SNPs, we performed systematic studies on four additional diamond electrodes (# D2, # D3, # D4, and # D5). Each DNA-modified electrode was hybridized with four different types of target DNA: the perfect complement, the CC mismatch at base pair 7, the CC mismatch at base pair 20 (further away from the diamond electrode and closer to the distal end of the molecular brush), and a random-type target DNA. The random target can also form transient Watson-Crick pairs but this is limited to a few nucleotides as shown in **table 1**. Note that during the consecutive hybridizations with the different variants of target DNA, always the initial probe DNA has been used without any regeneration treatment. The results obtained with electrode # D2

are shown in **figure 4**. All measurements on # D2 (and on # D3, # D4, and # D5) were performed under temperature-stabilized conditions, which resulted in excellent R^2 values between 0.96 and 0.996 for the Fits 1 and 2. In **Figure 4**, the first impedance decay (additive effect of DNA denaturation and medium exchange) is normalized to the impedance at t = 0 min; the second impedance decay is normalized to the impedance value at the time t_2, when the bound DNA has already been denatured and $1 \times$ PBS is again replaced by 0.1 M NaOH. All data on the denaturation-time constant τ_1, obtained at 19.3 °C with the five different electrodes, are summarized in **figure 5**. The time constants τ_2 for the medium exchange are depicted for comparison. The averaged time-constants for denaturation and medium exchange and the averaged normalized amplitudes are summarized in **table 2** together with their respective standard deviation σ. Concerning $<\tau_1>$, we obtain 2.26 ± 0.11 min for complementary duplexes, 1.38 ± 0.05 min for the mismatch at base pair 20, 1.16 ± 0.04 min for the mismatch at base paire 7, and finally 0.59 ± 0.08 min for the random target. The time constant for denaturation of the random sequence is close to $<\tau_2>$ = 0.46 ± 0.04 min for the medium exchange, indicating that these fragments are at the most very loosely bound.

To ensure that the marked difference in time constants is not emerging from an electrode-aging effect during consecutive denaturation processes and exposure to 0.1 M NaOH, the order of hybridization and denaturation with the different types of target DNA was also considered. The samples # D2, # D3, and # D4 were first hybridized with the complementary sequence, second with the mismatch at base pair 7, third with the mismatch at base pair 20, and finally, with the random sequence. In case of sample # D5 the order was reversed, starting with the random sequence. As a result, all time constants determined with # D5 were found to be fully in line with the other electrodes.

Since the melting temperature T_m is the established measure for the stability of DNA duplexes and the key parameter in localization and identification of single-nucleotide polymorphisms, we employed two different algorithms to estimate T_m for the four different target-probe duplexes in our study. FractTM is available online [FractTM] and the underlying principles are described in ref. [38]. HyTher™ is also available online and allows taking into account that the 5′ end

Table 2: Comparison of the theoretical melting temperatures with the parameters deduced from the real-time denaturation experiments. The melting temperatures were calculated using the FractTM algorithm (values for filter hybrization in brackets) [38] and the HyTher™ algorithm. The denaturation-time constant $<\tau_1>$, the time constant of the medium exchange $<\tau_2>$, the normalized amplitude $<A_1/Z(0)>$ related to DNA denaturation, and the relative amplitude $<A_2/Z(t_2)>$ related to the medium exchange are averages of four to five independent measurements. The σ values are the respective standard deviations. Note that the $<\tau_2>$ values are almost indistinguishable and that $<A_1/Z(0)>$ can be considered as a measure of the quantity of bound target DNA.

Target DNA	Complement	Mismatch BP20	Mismatch BP 7	Random
T melting/ °C (FractTM)	91 (84)	85 (78)	88 (81)	-33 (-41)
T melting/ °C (HyTher)	79.5	75.0	76.7	-50.8
$<\tau_1>$/min	2.26	1.38	1.16	0.59
$\sigma<\tau_1>$/min	0.11	0.05	0.04	0.08
$<\tau_2>$/min	0.52	0.50	0.46	0.46
$\sigma<\tau_2>$/min	0.08	0.09	0.06	0.04
$<A_1/Z(0)>$/%	3.4	2.0	2.0	0.4
$\sigma<A_1/Z(0)>$/%	1.1	0.3	0.7	0.2
$<A_2/Z(t_2)>$/%	4.9	6.9	5.6	9.8
$\sigma <A_2/Z(t_2)>$/%	1.3	0.5	1.2	1.1

of the probe DNA is tethered to a solid support. Both algorithms calculate T_m on basis of the sequence of probe- and target DNA, nearest neighbor effects, the concentration of the probe DNA, and the Na^+ concentration of the surrounding electrolyte. The numerical results of both algorithms are summarized in **table 2**. Despite of minor differences in the absolute T_m values, the global trend is in agreement with the obtained denaturation-time constants: the complementary

duplexes have the highest melting temperature and the longest denaturation time, the duplexes with the random sequence have the lowest T_m and shortest τ_1. The melting temperature of the SNP duplexes is reduced by 3 to 6 °C as compared to their fully complementary counterparts, while we observe here a strongly decreased denaturation time. Interestingly enough, both algorithms predict a slightly higher stability for the duplex with the SNP at base pair 7 (T_m = 76.7 °C, calculated with HyTher) compared to the SNP at base pair 20 (HyTher: T_m = 75.0 °C). This difference is minimal, note that the type of the defect and its nearest neighbors are identical, but our data suggest reproducibly that the duplexes with the SNP at base pair 7 denature slightly faster than those with the SNP at base pair 20. This may be explained by the fact that the impedimetric signal is influenced by changes of the ion distribution close to the electrode surface at the scale of the Debye length [15], being in the order of 1 nm for 0.1 M NaOH. Assuming that chemically-induced denaturation starts preferentially at both ends of a DNA duplex and at the position of mismatches, a mismatch in proximity to the electrode surface may indeed cause a faster response than a more distant defect.

Furthermore, we studied also the *intra*-sample reproducibility by hybridizing and denaturating electrode # D1 six times with the complementary target-DNA sequence during a period of more than 4 months. The results are summarized in **table 3**. The averaged value of the denaturation-time constant $<\tau_1>$ is 2.25 min with a standard deviation $\sigma <\tau_1>$ = 0.18 min. This is comparable to the data obtained as an average over the same measurement (denaturation of complementary duplexes) performed with the five different electrodes # D1 to # D5. There, we obtained $<\tau_1>$ = 2.26 min with a standard deviation $\sigma <\tau_1>$ = 0.11 min as given in Table 2. The averaged values of this *intra*- versus *inter*-electrode comparison are practically identical. The slightly wider data scattering for the *intra*-electrode measurements can be attributed to the elongated time span in between these measurements with a possible influence on the biochemical reagents. The averaged time constant for the medium exchange $<\tau_2>$ and the corresponding standard deviation $\sigma <\tau_2>$ agree again nicely with the data in **Table 2** obtained with the five different electrodes.

Table 3: Time constants for denaturation (τ_1) and medium exchange (τ_2) for sample # D1, hybridized with complementary target DNA. The sample passed six hybridization-denaturation cycles over a period of 132 days. Note that all decay times, including the average values and standard deviations, are in close agreement with the results depicted in Table 2. This indicates a high *inter-* and *intra*-sample reproducibility.

# D1	τ_1/min	τ_2/min
Day 1	2.39 ± 0.08	0.49 ± 0.13
Day 44	2.21 ± 0.14	0.50 ± 0.07
Day 49	2.10 ± 0.16	0.55 ± 0.09
Day 50	2.02 ± 0.04	0.45 ± 0.08
Day 84	2.51 ± 0.02	0.46 ± 0.15
Day 132	2.28 ± 0.16	0.58 ± 0.04
$\langle\tau_{1,2}\rangle$	2.25	0.50
$\sigma\langle\tau_{1,2}\rangle$	0.18	0.05

Finally, also the amplitude parameter A_1 gives information on the amount of bound target DNA. There is a systematic decrease of the normalized value A_1/Z_0 from 3.4% (complementary target), to 2.0% (mismatch at base pair 20 or at base pair 7) and finally to 0.3% for the random sequence, which is close to a zero effect within the standard deviation. Keeping in mind that the hybridization was performed under standardized conditions it is evident that defected sequences bind to a lesser extent than the complementary fragments, which result in duplexes with the highest thermodynamic stability. Except for the random sequence, the normalized $A_2/Z(t_2)$ is identical for all samples and sequences within the error margins.

3.5 Conclusions

In summary, we have used impedance spectroscopy in combination with diamond-based sensor electrodes to monitor the kinetics of chemically induced DNA denaturation in real time. The probe DNA was covalently immobilized onto the electrodes and for four different types of target DNA (complementary, random, single mismatches at two different positions) we could reproducibly identify denaturation-time constants. All time constants are at the scale of minutes while the denaturation takes the longest for complementary DNA duplexes. Moreover, the time constants correlate well with calculated melting temperatures. This suggests that the novel approach may possibly allow for a fast localization and identification of SNPs similar to the established, but cumbersome DNA-melting techniques. In addition, the novel method is intrinsically label free (note that labels were only used to allow for fluorescence imaging as a reference technique) and as-prepared electrodes can be used repetitively thanks to the strong link between probe DNA and the diamond platform, and the chemical inertness of diamond as such. The required instrumentation is minimal, consisting of an impedance analyzer, which can simply operate at a fixed frequency, and a system to administer NaOH with defined temperature and flow rate. With practical applications in mind, we point out that it is not essential to do the full fitting and analyses of the impedance-decay curves. Any indication for the duration of the denaturation process, like a response-time criterium (95% of signal change), will presumably correlate with melting-temperature data. Finally, the proposed method has the potential to be downsized and parallelized towards a microarray-like format as illustrated by the diamond-based microelectrode arrays with spot sizes of just 50 µm as described in ref. [39]. Given the fact that the real-time denaturation method provides 'dynamic information', it can reduce the number of required spots considerably as compared to the 'end-point character' of classical microarrays with fluorimetric readout.

3.6 Acknowledgements

3.7 References

[1]   P. Y. Kwok, *Annual Review of Genomics and Human Genetics,* 2001, **2**, 235 - 258.

[2]   J. K. K. Ng and W. T. Liu, *Anal. Bioanal. Chem.,* 2006, **3**, 427 - 434.

[3]   J. Hooyberghs and E. Carlon*, Biosens. Bioelectron.,* 2010, **26**, 1692 – 1695.

[4]   E. A. Tindall, D. C. Petersen, P. Woodbridge, K. Schipany and V. M. Hayes, *Human Mutation,* 2009, **30**, 876 – 883.

[5]   R. Fodde and M. Losekoot, *Human Mutation,* 1994, **3**, 83 – 94.

[6]   L. Lodewyckx, C. Vandevyver, C. Vandervorst, W. Van Steenbergen, J. Raus and L. Michiels, *Human Mutation,* 2001, **18**, 243 – 250.

[7]   C. Dekker, *Nat. Nanotechnol.,* 2007, **2**, 209 – 215.

[8]   Y. Astier, O. Braha and H. Bayley, *J. Am. Chem. Soc.,* 2006*,* **128**, 10684 – 10685.

[9]   J. Clarke, H. C. Wu, L. Jayasinghe, A. Patel, S. Reid and H. Bayley, *Nat. Nanotechnol.*, 2009, **4**, 265 – 270.

[10]   U. Rant, K. Arinaga, S. Scherer, E. Pringsheim, S. Fujita, N. Yokoyama, M. Tornow and G. Abstreiter, *Proc. Natl. Acad. Sci. USA,* 2007*,* **104**, 17364 – 17369.

[11]   Y. Xiao, A. A. Lubin, B. R. Baker, K. W. Plaxco and A. J. Heeger, *Proc. Natl. Acad. Sci. USA,* 2006, **103**, 4017 – 4021.

[12]   F. Uslu, S. Ingebrandt, D. Mayer, S. Böcker-Meffert, M. Odenthal and A. Offenhäusser, *Biosens. Bioelectron.*, 2004, **19**, 1721 – 1731.

[13]   T. Sakata and Y. Miyahara, *ChemBioChem.*, 2005, **6**, 703 – 710.

[14]   S. Ingebrandt, Y. Han, F. Nakamura, A. Poghossian, M. J. Schöning and A. Offenhäusser, *Biosens. Bioelectron.*, 2007, **22**, 2834 – 2840.

[15]   A. Poghossian, A. Cherstvy, S. Ingebrandt, A. Offenhäuser and M. J. Schöning, *Sens. Actuators, B,* 2005, **111**, 470 – 480.

[16]   F. Davis, M. A. Hughes, A. R. Cossins and S. P. J. Higson, *Anal. Chem.*, 2007, **79**, 1153 – 1157, 2007.

[17]   J. Y. Park and S. M. Park, *Sensors,* 2009*,* **9**, 9513 – 9532.

[18]   E. Özkumur, S. Ahn, A. Yalcin, C. A. Lopez, E. Cevik, R. J. Irani, C. DeLisi, M. Chiari and M. S. Unlü, *Biosens. Bioelectron.*, 2010, **25**, 1789 – 1795.

[19]   J. Hooyberghs, M. Baiesi, A. Ferrantini and E. Carlon, *Phys. Rev. E*,
        2010, **81**, art. no. 012901.

[20]   E. Katz and I. Willner, *Electroanalysis,* 2003, **15**, 913 – 947.

[21]   V. Vermeeren, N. Bijnens, S. Wenmackers, M. Daenen, K. Haenen,
        O. A. Williams, M. Ameloot, M. vandeVen, P. Wagner and L. Michiels,
        Langmuir, 2007, **23**, 13193 - 13202.

[22]   B. van Grinsven, T. Vandenryt, S. Duchateau, A. Gaulke, L. Grieten,
        R. Thoelen, S. Ingebrandt, W. De Ceuninck and P. Wagner, *Phys. Status
        Solidi A,* 2010, **9**, 2110 – 2113.

[23]   L. Tang, C. Tsai, W.W. Gerberich, L. Kruckeberg and D. R. Kania,
        Biomaterials, 1995, **16**, 483 – 488.

[24]   N. Smisdom, I. Smets, O. A. Williams, M. Daenen, S. Wenmackers,
        K. Haenen, M. Nesládek, J. D'Haen, P. Wagner, J. M. Rigo, M. Ameloot
        and M. vandeVen, *Phys. Status Solidi A,* 2009, **9**, 2042 – 2046.

[25]   A. Härtl, E. Schmich, J. A. Garrido, J. Hernando, S. C. R. Catharino,
        S. Walter, P. Feulner, A. Kromka, D. Steinmüller and M. Stutzmann, *Nat.
        Mater.,* 2004, **3**, 736 - 742.

[26]   W. Yang, O. Auciello, J. E. Butler, W. Cai, J. A. Carlisle, J. E. Gerbi,
        D. M. Gruen, T. Knickerbocker, T. L. Lasseter, J. N. Russell, Jr.,
        L. M. Smith and R.J. Hamers, *Nat. Mater.,* 2002, **1**, 253 – 257.

[27]   P. Christiaens, V. Vermeeren, S. Wenmackers, M. Daenen, K. Haenen,
        M. Nesládek, M. vandeVen, M. Ameloot, L. Michiels and P. Wagner,
        Biosens. Bioelectron., 2006, **22**, 170 – 177, 2006.

[28]   S. Wenmackers, V. Vermeeren, M. vandeVen, M. Ameloot, N. Bijnens,
        K. Haenen, L. Michiels and P. Wagner, *Phys. Status Solidi A,* 2009, **206**,
        391 - 408.

[29]   V. Vermeeren, S. Wenmackers, P. Wagner and L. Michiels, *Sensors*,
        2009, **9**, 5600 – 5636.

[30]   H. Gu, X. Su and K. P. Loh*, J. Phys. Chem. B,* 2005, **109**, 13611 –
        13618,

[31]   S. Kuga, S. Tajima, J. H. Yang, K. Hirama and H. Kawarada, *IEEE
        International Electron Devices Meeting, Technical Digest*, 2008, **50**$_{th}$,
        483 – 486.

[32]   N. Yang, H. Uetsuka, E. Osawa and C.E. Nebel, *Angew. Chem. Int. Ed.*, 2008, **47**, 5183 – 5185.

[33]   O. A. Williams, M. Nesládek, M. Daenen, S. Michaelson, A. Hoffman, E. Osawa, K. Haenen and R. B. Jackman, *Diamond Relat. Mater.,* 2008, **17**, 1080 – 1088.

[34]   X. Y. Wang, R. E. Ruther, J. A. Streifer and R. J. Hamers, *J. Am. Chem. Soc.,* 2010, **132**, 4048 – 4049.

[35]   V. Vermeeren, S. Wenmackers, M. Daenen, K. Haenen, O. A. Williams, M. Ameloot, M. vandeVen, P. Wagner and L. Michiels, *Langmuir,* 2008, **24**, 13193 – 13202.

[36]   S. Wenmackers, S. D. Pop, K. Roodenko, V. Vermeeren, O. A. Williams, M. Daenen, O. Douheret, J. D'Haen, A. Hardy, M. K. Van Bael, K. Hinrichs, C. Cobet, M. vandeVen, M. Ameloot, K. Haenen, L. Michiels, N. Esser and P. Wagner*, Langmuir,* 2008, **24**, 7269 – 7299.

[37]   J. Poté, P. Rossé, W. Roselli, W. T. Van and W. Wildi, *Chemosphere,* 2005, **61**, 677 – 684.

[38]   M. Leber, L. Kaderali, A. Schönhuth and R. Schrader, *Bioinformatics*, 2005, **21**, 2375 – 2382.

[39]   M. Bonnauron, S. Saada, C. Mer, C. Gesset, O. A. Williams, L. Rousseau, E. Scorsone, P. Mailley, M. Nesládek, J. C. Arnault and P. Bergonzo, *Phys. Status Solidi A,* 2008, **205**, 2126 – 2129.

3.8 Supporting information
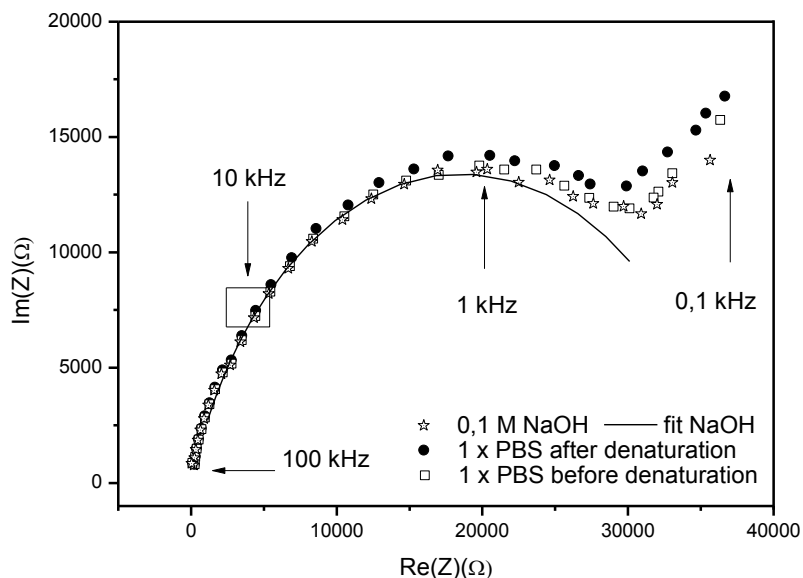3.8.1 Nyquist plots of the impedance spectra

Figure 6: This Nyquist plot shows the impedance data of # D1, see **Figure 2**, in the full frequency range from 100 Hz to 100 kHz before denaturation (sensor cell filled with $1 \times$ PBS), after denaturation (cell filled with 0.1 M NaOH), and after refilling with $1 \times$ PBS. The 10 kHz point, the frequency used to extract the denaturation dynamics, is indicated by an open box. The high frequency part of all plots can be simulated with a three-element circuit consisting of a solution resistance R_1 in series with a complex resistance describing the biological and the topmost DNA layer. This layer can be represented by a resistor R_2 and a constant-phase element CPE with an almost capacitive behaviour (n = 0.80). The Nyquist plot indicates that there is a second semi circle in the low-frequency domain, but the data, not extending below 100 Hz, do not allow for a reliable fitting. A complete scheme, taking into account also the space-charge region to model the second semi circle, is supposed to correspond to the circuit below.
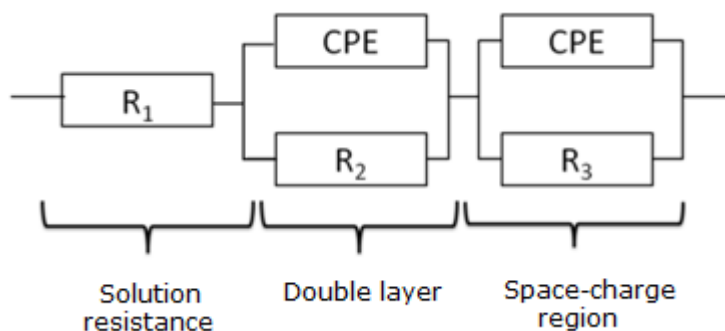
Figure 7: The fit parameters obtained for the three elements R_1, CPE and n, and R_2 are summarized in the following table. Only data points in the frequency range between 1 kHz and 100 kHz were taken into account. Although there is no marked difference for the situation in 1 × PBS buffer before and after denaturation, we suppose that the sensor effect is mainly related to the capacitive constant-phase properties of the electrode surface.

	1 x PBS before denaturation	1 x PBS after denaturation	0.1 M NaOH	Error (%)
R_1 (Ω)	142	142	140	2.5
CPE (nSs^n)	21.9	24.1	23.9	2.2
n	0.8	0.79	0.79	1.0
R_2 (kΩ)	39.3	38.0	37.1	1.2

3.8.2 Chemical agents and buffer solutions

The probe ssDNA molecules were purchased from Eurogentec (Seraing, Belgium), and were modified at the 5' end with a NH_2-modifier (36 bp: 5'-NH_2-C_6H_{12}-AAA-AAA-ACC-CCT-GCA-GCC-CAT-GTA-TAC-CCC-CGA-ACC-3'). The target ssDNA molecules, bought from Invitrogen (Merelbeke, Belgium), were modified at the 5'-end with an Alexa Fluor® 488 label. Target ssDNA contains a sequence that is either completely complementary to the probe ssDNA (29 bp: 5'-Alexa 488- C_6H_{12}-GGT-TCG-GGG-GTA-TAC-ATG-GGC-TGC-AGG-GG-3'), carries a 1-base mismatch to the probe ssDNA at bp 7 (29 bp: 5'-Alexa 488- C_6H_{12}-GGT-TCG-GGG-GTA-TAC-ATG-GGC-T**C**C-AGG-GG-3'), carries a 1-base mismatch to

the probe ssDNA at bp 20 (29 bp: 5'-Alexa 488- C_6H_{12}-GGT-TCG-GGG-**C**TA-TAC-ATG-GGC-TGC-AGG-GG-3') or is completely random (29 bp: 5'-Alexa 488-C_6H_{12}-TCA-AAT-TGC-CAG-AAC-AAC-TAC-TGA-CTG-AA-3'). Sodium dodecyl sulfate (SDS) was obtained from VWR International (Zaventem, Belgium). 10-Undecenoic acid (UDA) was bought from Sigma-Aldrich (Bornem, Belgium). EDC and 2-[N-morpholino]-ethanesulphonicacid (MES) were purchased from Perbio Science (Erembodegem, Belgium). Sodiumhydroxide (NaOH) was acquired from Merck (Overijse, Belgium). Phosphate buffered saline (PBS) (1.29 M NaCl, 0.05 M Na_2HPO_4*$2H_2O$, 0.015 M KH_2PO_4, pH 7.2) sodium chloride/ sodium citrate (SSC) buffer (3 M NaCl, 0.3 M $C_6H_8O_7$*3Na, pH7.5) and hybridization buffer (0.75 M NaCl, 0.075 M $C_6H_8O_7$*3Na, 0.1% BSA, 0.1% Ficoll, 0.1% C_6H_9NO, 5% dextran sulphate, 5 mM Na_2HPO_4, 0,1% SDS, 50µg/L herring sperm DNA) were homemade.

Chapter 4

Heat-Transfer Resistance at Solid-Liquid Interfaces: A Tool for the Detection of Single Nucleotide Polymorphisms in DNA

Bart van Grinsven [1], Natalie Vanden Bon [2], Hannelore Strauven [1], Lars Grieten [1], Mohammed Murib [1], Kathia L. Jiménez Monroy [1], Stoffel D. Janssens [1,3], Ken Haenen [1,3], Michael J. Schöning [4], Veronique Vermeeren [2], Marcel Ameloot [2], Luc Michiels [2], Ronald Thoelen [1,5], Ward De Ceuninck [1,3] and Patrick Wagner [1,3]

1) Hasselt University, Institute for Materials Research IMO, Wetenschapspark 1, B-3590 Diepenbeek, Belgium.

2) Hasselt University, Institute for Biomedical Research BIOMED, Agoralaan – Building B, B-3590 Diepenbeek, Belgium

3) IMEC vzw, IMOMEC, Wetenschapspark 1, B-3590 Diepenbeek, Belgium

4) Aachen University of Applied Sciences, Institute of Nano- and Biotechnologies INB, Heinrich-Mußmann-Straße 1, D-52428 Jülich, Germany

5) XIOS University College, Department of Applied Engineering, Agoralaan – Building H, B-3590 Diepenbeek, Belgium

4.1 Abstract

In this article, we report on the heat-transfer resistance at interfaces as a novel, denaturation-based method to detect single-nucleotide polymorphisms in DNA. We observed that a molecular brush of double-stranded DNA grafted onto synthetic-diamond surfaces does not notably affect the heat-transfer resistance at the solid-to-liquid interface. In contrast to this, molecular brushes of single stranded DNA cause, surprisingly, a substantially higher heat-transfer resistance and behave like a thermally insulating layer. This effect can be utilized to identify ds-DNA melting temperatures *via* the switching from low- to high heat-transfer resistance. The melting temperatures identified with this method for different DNA duplexes (29 base pairs without and with built-in mutations) correlate nicely with data calculated by modelling. The method is fast, label-free (without the need for fluorescent or radioactive markers), allows for repetitive measurements, and can also be extended towards array formats. Reference measurements by confocal fluorescence microscopy and impedance spectroscopy confirm that the switching of heat-transfer resistance upon denaturation is, indeed, related to the thermal on-chip denaturation of DNA.

The detection and identification of single-nucleotide polymorphisms (SNPs) in DNA is of central importance in genomic research for several reasons. First, SNPs are involved in hundreds of genetic disorders such as Alzheimer, mucoviscidosis, phenylketonuria, and several types of breast- and colon cancer [1,2]. Second, SNPs in the so-called ADME (absorption, distribution, metabolism, excretion) genes significantly influence the effectiveness of treatment and this is a major topic in the field of theranostics [3]. SNPs can be characterized by hybridization-based assays such as microarrays: the massive parallelized readout is an advantage, but the method requires fluorescent labelling, optical readout, and long hybridization times of ~ 16 hours at elevated temperatures. Furthermore, the method has an 'end-point' character without providing dynamic information on molecular recognition between probe- and target fragments. Finally, it is hard to unravel unknown mutations by microarrays although there is recent progress based on refined statistical analysis allowing detecting mutated fragments in the presence of wild-type DNA [4]. Due to these drawbacks, unknown mutations are frequently identified by denaturation-based approaches. Widespread methods are real-time PCR (polymerase chain reaction) with associated melting-curve analysis [5] and denaturing-gradient gel electrophoresis (DGGE) or temperature-gradient gel electrophoresis (TGGE) [6,7] However, real-time PCR requires fluorescent labelling and expensive instrumentation while DGGE is time-consuming, less suitable for parallelized analyses, and lacking information on denaturation kinetics.

To overcome these limitations, several label-free electronic and opto-electronic DNA-sensor concepts have been proposed in recent literature. All of them have in common that they can operate in principle under hybridization- and under denaturation conditions, while they can also be miniaturized and integrated in sensor arrays with a parallelized readout. Without being exhaustive, we mention electrostatic switching effects and associated fluorescence monitoring [8], impedance spectroscopy [9–12], electric field-effect based devices [13–15], surface plasmon resonance [16], and linear (electric) conductivity measurements through single DNA duplexes [17]. The underlying principles of these sensing effects are not yet clarified in all details, but they are presumably associated with one or several of the following phenomena, which occur upon hybridization or denaturation: change in mechanical rigidity of DNA, changes in the total charge

of DNA, redistribution of counter ions, and changes of the dielectric properties near the surface onto which the probe DNA is attached. Most straightforward, but especially hard to implement in a low-cost diagnostic instrument, are the conductivity measurements through single DNA molecules, which have been subject to extensive theoretical and experimental studies, see *e.g.* [17–20]. Very recently, Velizhanin *et al.* proposed in a theoretical study on nanoscale heat transport through individual DNA molecules that the thermal current should significantly increase upon denaturation [21]. This would offer, besides of the aforementioned (opto-) electronic approaches, an alternative access towards the detection of denaturation events and contribute to the understanding of the underlying vibrational dynamics.

In the present work, we study the temperature-dependent heat-transfer properties experimentally by using DNA brushes, in which the 5' terminus of the probe DNA is covalently tethered to planar, temperature-controlled diamond electrodes. Albeit this approach is not at the single-molecule level it offers distinct advantages: the DNA fragments are in contact with buffer medium at any time, the fragments are free to undergo conformational fluctuations, and the sensor device as such can be implemented with reasonable technological efforts. The methodology allows identifying melting temperatures by using only an adjustable heat source in combination with two temperature sensors. The sequence chosen exemplarily in this work is an exon-9 fragment of the phenylalanine hydroxylase (PAH) gene and mutations in this gene lead to the metabolic disorder phenylketonuria [22].

4.2 Results

4.2.1 General concept of the heat-transfer device for DNA chips

The principle of a heat-transfer measurement is illustrated in **figure 1A** and technical details are summarized in 'Methods', section 'Design of the sensor cell and the thermal- and impedimetric readout system'. The central element through which the thermal current will pass is a silicon chip (~ 10 by 10 mm^2) covered with a thin layer of boron-doped, nanocrystalline diamond [23], see 'Methods', section 'Preparation of the diamond-coated sensor electrodes'. This diamond layer serves as an immobilization platform onto which 29-mers of ds-DNA are covalently bound *via* the photochemical 'fatty acid & EDC' coupling
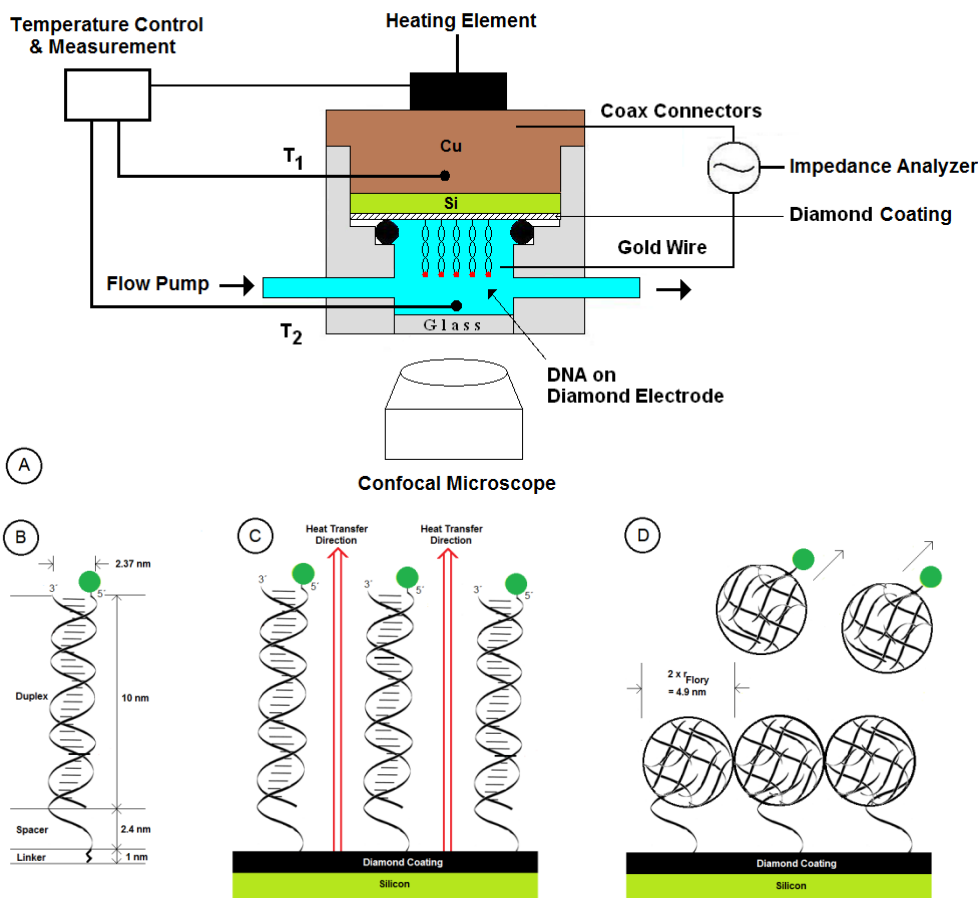
Figure 1: The upper **panel A** shows the schematic layout of the sensor cell, allowing for the thermal monitoring of DNA denaturation together with impedimetric and optical control experiments. The probe DNA is covalently immobilized on a diamond-coated silicon electrode while the cell is filled with PBS buffer. The temperature T_1 of the Cu backside contact is measured by a thermocouple and can be actively steered *via* a controller unit. The temperature T_2 inside the liquid is recorded by using a second thermocouple. The gold wire serves as a counter electrode for impedance measurements and the glass window provides optical access. The heat-transfer related parameters are the temperature difference $T_1 - T_2$ and the input power P provided by the heating element. **Panel B** sketches the DNA duplexes with labelled target strands and **panel C** illustrates the heat-transfer path through a molecular DNA brush. After denaturation, the probe DNA curls up in irregular structures characterized by the Flory radius, thus hindering the solid-to-liquid heat transfer (**panel D**).

route [24]. The length of 29-mers is in line with established, commercial microarray platforms, like the Affymetrix platform (25-mer oligonucleotide probes) or the Agilent system (60-mer probes), see: [25]. The 'fatty acid & EDC' route is applicable to various semiconductor surfaces including carbon nanotubes [26], while diamond has in addition an especially high thermal conductivity together with an outstanding chemical, electrochemical, and thermal stability. The probe ss-DNA is linked to the diamond surface *via* stable C-C bonds in 'head-on' configuration while the target ss-DNA is free to hybridize or to denature according to the experimental conditions without steric hindering, see **figures 1B** and **1C**. The sequence of the probe DNA is given in **table 1** together with the sequence of three different types of target DNA: the complement (full match), a sequence causing a CC mismatch at base pair 7, and a sequence resulting in a CC mismatch at base pair 20. The neighbouring base pairs of both defects are in both cases CG and AT. The hybridization conditions, see 'Methods' (section 'Functionalization of sensor electrodes with DNA') for details, were chosen in a way that also the defective duplexes will hybridize and be stable at room temperature. The areal density is in the order of $10^{12} - 10^{13}$ duplexes per cm^2, meaning that the average distance between duplexes is less than the total length of an individual duplex [27]. For optical reference purposes, unrelated to the heat-transfer measurement itself, the target DNA fragments were carrying Alexa 488 fluorescent labels at the 5' terminus. AFM micrographs of the chip surfaces in the subsequent stages (diamond surface, with attached fatty-acid linkers, with probe DNA and finally, after hybridization with target DNA) can be found in the 'Supporting Materials', section 'AFM images of NCD surfaces and the subsequent surface-functionalization steps'.

This 'DNA chip' was pressed mechanically with its backside onto a polished copper block, which served not only as an electrical contact, but also as heat provider (heating runs) or heat sink (cooling runs). The internal temperature of the copper block, T_1, was measured by a thermocouple and steered *via* a PID controller connected to a power resistor. Possible heat-transfer losses between copper and silicon were minimized by conductive silver paint. The front side of the DNA chip was exposed to $1 \times$ PBS buffer (phosphate-buffered saline solution) in a Perspex-made liquid cell: *via* an O-ring seal, a contact area of

Table 1: Compilation of the base sequences of the probe DNA and the three different types of target DNA employed in the hybridization and denaturation experiments. The probe DNA exhibits a spacer consisting of 7 A-bases while the target DNA fragments carry a fluorescent Alexa 488 label at the 5' end. The position of the mismatches with respect to the probe DNA is underlined and indicated by bold letters. The third column lists the calculated melting temperatures based on the HyTher™ algorithm, reflecting the relative stability of the complementary and the mismatched DNA duplexes.

Name	Sequence
Probe DNA	3´-CCA AGC CCC CAT ATG TAC CCG ACG TCC CCA-α
Full match	5´-Alexa 488-C_6H_{12} GGT TCG GGG GTA TAC ATG GGC TGC AGG GG-3`
Mismatch at BP 7	5´-Alexa 488-C_6H_{12} GGT TCG GGG GTA TAC ATG GGC T**C**C AGG GG-3`
Mismatch at BP 20	5´-Alexa 488-C_6H_{12} GGT TCG GGG **C**TA TAC ATG GGC TGC AGG GG-3`

28 mm^2 was defined between the chip and the liquid. Except for minor heat losses along the seal, heat will mainly be transferred from the chip to the liquid. The temperature in the liquid, T_2, was measured by a second thermocouple, positioned at a distance of 1.7 mm from the solid-liquid interface. In order to validate that a heat-transfer measurement can indeed give information on DNA binding or denaturation, the cell also featured a gold electrode in the liquid, which was connected, together with the copper backside contact, to a home-made impedance analyser [28]. Furthermore, a glass window allowed for optical monitoring with an inverted confocal fluorescence microscope (see 'Methods', section 'Confocal fluorescence microscopy'). Unless stated otherwise, the heat-transfer device was operated in a temperature-stabilized environment at 19.3 °C ± 0.1 °C.

4.2.2 Heat-transfer measurements with fluorimetric and impedimetric control

The first series of measurements, described in this section, refers to the most stable, fully complementary duplexes in combination with a diamond-coated silicon electrode denoted as # D1. During the measurement, T_1 was increased

with a heating rate of 1 °C/min from 35 °C to 90 °C and cooled back to 35 °C at the same rate by reducing the heating power. This was performed for three consecutive heating/cooling runs and the time dependence of T_1 and T_2 is shown in **figure 2**. Note that during the first heating, an anomalous behaviour of T_2 occurs, highlighted with a circle, which was absent during the second and the third run. This first-run temperature anomaly was also found with three other electrodes (# D2, # D3, and # D4), meaning that the effect appears to be intrinsic and most probably related to thermally induced DNA denaturation. In order to prove this assumption, the 'first and second heating run' experiment was repeated with simultaneously measuring also the impedance of the sensor cell and monitoring the fluorescence intensity on the electrode surface. These measurements were performed at non-regulated room temperature (about 22 °C) and we verified that there was no measurable heat input by the laser beam into the system.
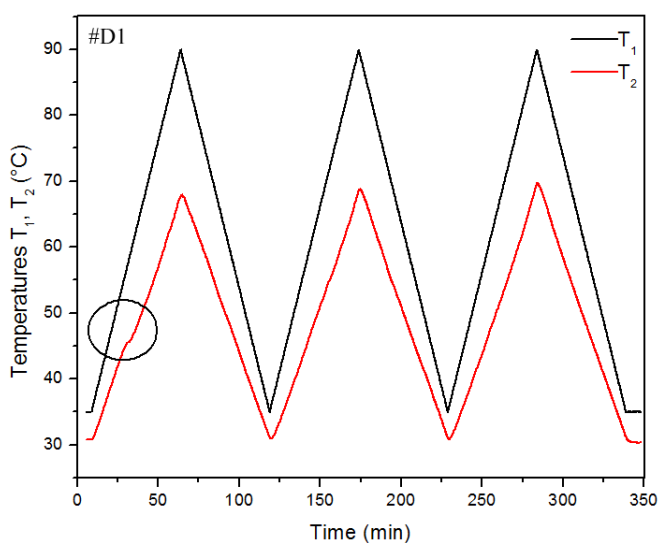

Figure 2: Three subsequent heating and cooling cycles performed with electrode # D1 with immobilized probe DNA. As a starting condition, the probe DNA was hybridized with the complementary target and the anomalous behaviour of the liquid temperature T_2 (indicated with a circle) during the first heating run is associated with the double-helix melting. The black, solid line is the temperature T_1 of the Cu backside contact, the liquid temperature T_2 is shown as a red, solid line. For heating and cooling, the temperature T_1 is increased or reduced at a rate of 1 °C per minute.

Figure 3 summarizes the data obtained with three independent methods, confirming the assumption that DNA denaturation has indeed an impact on the heat-transfer properties of the device. The temperature (T_1) dependence of the fluorescence-intensity signal from the electrode surface is shown in the top-left **panel 3A**: denaturation sets in at 47 °C and terminates at 55 °C, where the fluorescence intensity drops to its background value, which originates from strayed laser light. The denatured sample shows this background intensity at all temperatures. The midpoint temperature of the fluorescence-intensity decay is found at 49.7 °C ± 0.3 °C. Labelled target DNA, removed from the immobilized probe DNA during denaturation, cannot contribute to the signal anymore because the confocal volume is limited to a maximum of 5 μm above the chip surface, which is negligible as compared to the total cell volume. This fluorescence test is a stringent and independent control because it is electronically and physically decoupled from the rest of the setup, which is steering and monitoring T_1 and T_2 and measuring the impedance values. Therefore, the fluorescence data are definitely free of any hypothetical cross-talk effects. Confocal images of the denaturation process are included in the 'Supporting Materials', section 'Confocal fluorescence images during thermal DNA denaturation'. The lower-left **panel 3B** shows the T_1 dependence of the amplitude and the phase angle of the impedance signal at a frequency of 1058 Hz, avoiding possible noise input from the 50 Hz power grid. Below 47 °C, the double- and the single-stranded DNA electrode behave differently in impedance amplitude and in phase angle while they coincide for temperatures above 57 °C. The impedance amplitude of the first heating run (denaturation) clearly shows a local maximum at 49.5 °C ± 0.2 °C, which corresponds nicely to the midpoint temperature of the fluorescence-decay curve. We mention that the impedance results are a superposition of two effects: The surface impedance of electrodes with ds- *versus* ss-DNA are different as reported earlier [12], but also the impedance of the buffer solution depends sensitively on temperature. More details are given in the 'Supporting Materials', section 'Discussion of the impedance signal upon crossing the DNA-melting transition'.

The top-right **panel 3C** shows the temperature difference $\Delta T = T_1 - T_2$ as a function of T_1, with the black curve corresponding again to the first heating run while the red curve presents the second heating with only ss-DNA on the chip.

Both curves coincide at temperatures above 55 °C, where the melting transition is completed. **Panel 3C** also includes the temperature dependence of the electrical heating power P (T_1), which was required to achieve the linear raise of T_1 according to the heating rate of 1 °C/min. Also here there is a difference between the ds- and ss-DNA chip, which disappears above 55 °C. In order to extract the heat-transfer resistance R_{th} quantitatively, we analysed for all temperatures T_1 the ratio of the temperature difference $\Delta T = T_1 - T_2$ and the input power P according to $R_{th} = \Delta T / P$, see *e.g.* [29]. The resulting data are summarized in **panel 3D**. The somewhat noisy appearance is related to the fact that we show non-filtered, raw data obtained in an environment without active temperature control: while the temperature T_1 is strictly linear and smooth in time, the required heating power shows small fluctuations within short time periods. In case of the ds-DNA chip we find a low-temperature value of $R_{th} = 7.7$ °C/W, which starts to increase around 46°C and reaches a new equilibrium value of 8.9 °C/W at and above 55°C (black curve). The midpoint of the transition is found at $T_{midpoint} = 49.2$ °C ± 0.5 °C, that is again close to the midpoint temperature of the fluorescence-decay curve. Performing the same R_{th} analysis with the ss-DNA chip during the second heating run resulted in an almost temperature independent R_{th} of 8.9 °C/W (red curve). This increase of the absolute R_{th} value by ~ 1.2 °C/W (16 % increase) upon denaturation is a substantial effect, keeping in mind that the DNA brush is only a miniscule component (the fragment length corresponds to 10 nm) as compared to the total heat-transfer path with a distance of almost 3 mm between the two thermocouples. The effect size is also more than twice as strong as the denaturation-induced change of the impedance amplitude with an increase by about 7 %. From these observations together, we conclude that the temperature anomaly documented in **figure 2** (first heating run) is one-to-one related to the thermally induced denaturation of ds-DNA, which changes the heat transfer resistance at the solid-liquid interface.
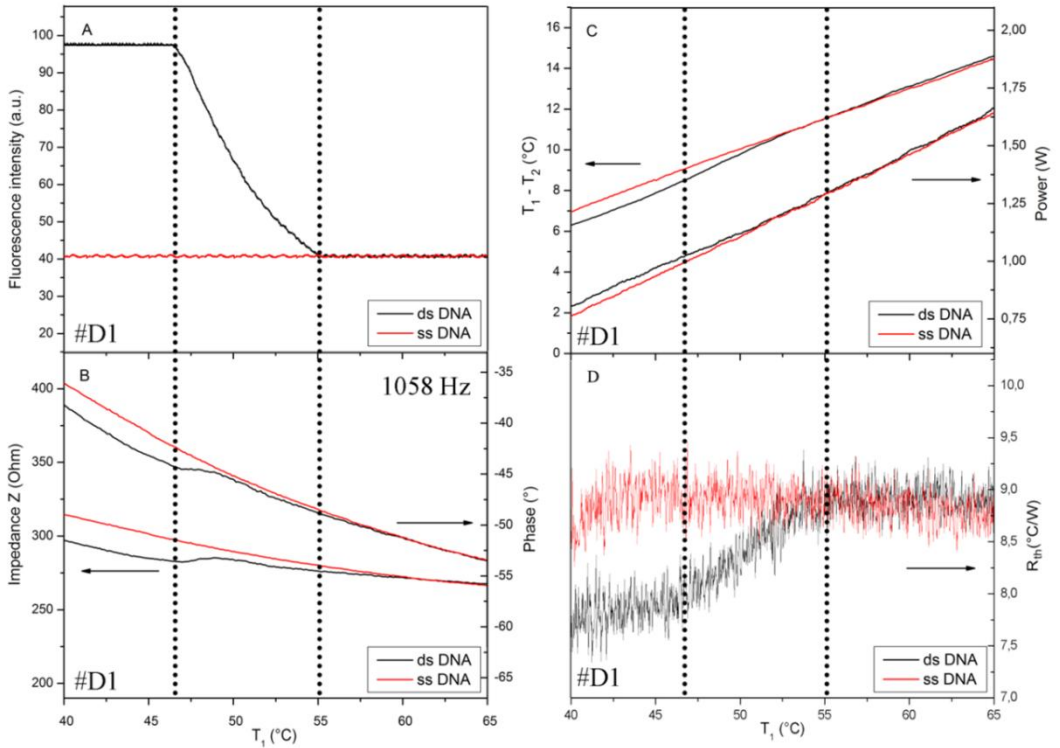
Figure 3: Compilation of simultaneously measured fluorescence-intensity data (**panel A**), impedance data (**panel B**) and heat-transfer related data (**C** and **D**) obtained for electrode # D1 with complementary ds-DNA (first heating run in black solid lines) and subsequently with ss-DNA (second heating run, red solid lines). Fluorescence indicates that denaturation starts at 47 °C and is completed at 55 °C. This is also the temperature range where the amplitude and phase of the impedance signals (here at 1058 Hz) converge. **Panel C** shows the temperature difference $\Delta T = T_1 - T_2$ as a function of T_1 (temperature of the copper back contact) together with the T_1 dependence of the heating power P at the right-hand axis. The heat-transfer resistance R_{th}, being the ratio $\Delta T/P$, is given in **panel D**. All data are raw data without further processing.

4.2.3 Studies on various chip surfaces and DNA with sequence defects

In the following, we will describe experiments performed with the diamond electrode # D2 in a temperature-stabilized environment, see **figure 4**. First, the as-grown diamond chip was oxidized with a UV-ozone treatment to obtain a hydrophilic surface termination, which is stable in aqueous solutions. The R_{th} value is about 6.7 °C/W – 7.0 °C/W and widely temperature-independent (red line). Attaching the fatty-acid crosslinker molecules (purple line) also resulted in a temperature-independent R_{th}, which can, within the experimental resolution, not be distinguished from the behaviour of the oxygen-terminated surface. In principle, this does not come as a surprise because the dense molecular brush of alkyl chains consisting of 10 carbon atoms is not longer than 1 nm. Attaching the single-stranded probe DNA made the R_{th} rise to 9.0 °C/W at 40 °C with a monotonous decrease to 8.4 °C/W at 80 °C. This sample was subsequently hybridized with complementary target DNA (black line), target DNA with a CC mismatch at base pair 7 (green line), and target DNA with the CC mismatch at base pair 20 (orange line). Note that the three hybridizations were performed with the original probe DNA on the sensor chip without any kind of surface regeneration. All curves exhibit the stepwise increase of R_{th} upon denaturation with midpoint temperatures of 63.0 °C ± 0.1 °C for the complement, 57.6 °C ± 0.1 °C for the mismatch at base pair 7, and 56.8 °C ± 0.1 °C for the mismatch at base pair 20. The relative order of stability agrees nicely with calculated melting-temperature values summarized within **table 1**. These calculations were based on the online HyTher[TM] algorithm (http://ozone3.chem.wayne.edu/), taking into account the lengths of fragments, the identity and orientation of neighbouring bases, the ionic strength of the buffer, and the fact that all fragments are tethered at one end. We point out that our denaturation temperatures are lower than the predicted values; however, the fluorescence control renders the experimental data unquestionable. Moreover, the same order of stability was confirmed with the three other DNA chips (# D1, # D3, and # D4).
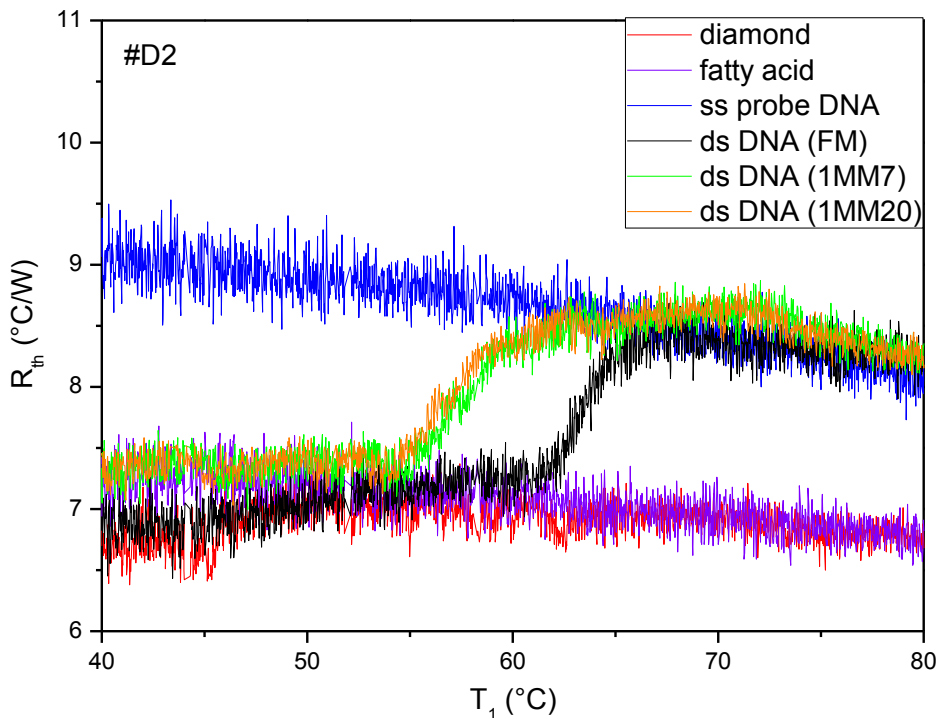
Figure 4: Heat-transfer resistance R_{th} as a function of temperature for electrode # D2 (data have not been filtered). The unmodified electrode (red line) and the electrode with covalently attached fatty-acid linkers (purple line) have a widely temperature independent R_{th} around 7 °C/W. In the configuration with attached probe DNA (blue line) the heat-transfer resistance has notably increased to 9 °C/W, indicating an efficient thermal insulation by the highly flexible ss-DNA fragments. The R_{th} of double-stranded DNA (black line for the complementary duplexes) is comparable to the non-modified surface at low temperatures and switches to the ss-DNA behaviour upon denaturation with a midpoint temperature $T_{midpoint}$ = 63.0 °C ± 0.1 °C. Repeating the experiment with defective DNA duplexes results in a clear shift of $T_{midpoint}$ to lower temperatures: for the duplex with CC-mismatch at BP 7 (green line) we obtain $T_{midpoint}$ = 57.6 °C ± 0.1 °C and for the same mismatch at BP 20 (orange line) this is 56.8 °C ± 0.1 °C. The relative order of stability corresponds to the calculated data given in table 1.

Finally, **table 2** summarizes all $T_{midpoint}$ – and R_{th} data for the four different DNA chips under study regarding the thermal denaturation of the most stable, complementary DNA duplexes. All data were obtained from measurements in the temperature-stabilized environment of 19.3 °C. In case of # D3, the measurement was performed in threefold (*run a*, *run b, and run c*) with a complete regeneration of the sensor surface between *run b and run c*, meaning that the fatty-acid and probe-DNA layers were etched off in oxygen plasma and built up for a second time. There is a certain sample-to-sample variation of the midpoint temperatures and we attribute this to the manual mounting of the DNA chip in the sensor device, possibly in combination with minor fluctuations in the precise size of the chips and the thickness- and grain-size of their diamond coatings. When looking at the intra-sample variability, it can be seen that the subsequent *runs a* and *b* performed with sample # D3 deliver practically identical results and only after the complete surface regeneration a certain shift of $T_{midpoint}$ occurs. Despite of this, the absolute change of R_{th} upon denaturation is remarkably constant and has for all DNA chips a value between 1.3 °C/W and 1.5 °C/W. To determine the 'jump height' ΔR_{th}, we calculated the difference between R_{th} measured at 10 °C above $T_{midpoint}$ and the corresponding value 10 °C below $T_{midpoint}$, in both cases clearly outside the regime of the melting transition. The universal amplitude of ΔR_{th} strongly supports the idea of a universal feature, which is independent of the employed sensor chip. Data obtained with heating rates of 0.5 °C/min and 2.0 °C/min are shown in the 'Supporting Material', section 'Heat-transfer resistance measured with different heating rates'.

Table 2: Compilation of the T-midpoint- and heat-transfer data of thermally induced denaturation of complementary DNA duplexes obtained with four different diamond electrodes. The data with electrode # D3 were measured in threefold (runs *a, b, c*) with a complete sensor regeneration between run *b* and run *c*. The R_{th} values of the single-stranded state were measured at 10 °C above $T_{midpoint}$ while the corresponding R_{th} in the double-stranded state was taken at 10 °C below $T_{midpoint}$. Note that the jump height ΔR_{th} is remarkably constant and independent of the electrode or the midpoint temperature, suggesting an intrinsic effect of the DNA brush on the total heat-transfer resistance of the device.

	# D1	# D2	# D3 run a	# D3 run b	# D3 run c	# D4
T midpoint °C	52.5 ± 0.2	63.0 ± 0.1	53.5 ± 0.2	53.5 ± 0.1	56.5 ± 0.1	52.0 ± 0.3
R_{th} (°C/W) ss- state	8.9 ± 0.2	8.6 ± 0.1	8.6 ± 0.1	8.7 ± 0.2	8.7 ± 0.1	8.7 ± 0.3
R_{th} (°C/W) ds- state	7.6 ± 0.2	7.1 ± 0.2	7.3 ± 0.2	7.3 ± 0.2	7.4 ± 0.2	7.2 ± 0.2
ΔR_{th} (°C/W)	1.3 ± 0.2	1.5 ± 0.1	1.3 ± 0.2	1.4 ± 0.2	1.3 ± 0.2	1.5 ± 0.2

4.3 Discussion

The increase of R_{th} upon denaturation has to our knowledge not been reported in prior literature and there is also no explanation yet based on first-principles calculations. The theoretical work of Velizhanin *et al.* predicts actually an enhanced heat transfer by single-stranded DNA, but the boundary conditions are different (DNA-molecule under dry conditions, clamped between two heat reservoirs with a fixed temperature difference) and modeling parameters come into play [21]. The experimental thermal- and electronic conductivity studies by Kodama *et al.* on individual ds-DNA fragments combined with gold nanoparticles is also not comparable to our approach: These measurements under vacuum conditions (temperature regime 100 K – 300 K) did not cross the melting transition and both fragment ends were tethered to gold contacts, limiting the mechanical freedom of the molecules [30].

However, we can clearly state that the observed impact of denaturation on the heat-transfer resistance cannot be explained by a calorimetric effect. Calorimeters measure interaction energies during a molecular-recognition- or unbinding process and have been employed in classical DNA studies [31, 32] and more recently in the context of synthetic receptors [33, 34]. Here, we find a persistent change of R_{th} from low values at all temperatures below the melting transition to higher values at all temperatures above this transition, an effect, which is not restricted to the melting transition itself. The fact that ds-DNA does not measurably increase the heat-transfer resistance can be understood on the following grounds: the fragments of 29 base pairs have a length of 10 nm, which is far below the estimated persistence length of 50 nm [35, 36]. Therefore, these fragments can be considered as 'stiff rods' on the chip surface with a tilt angle in the range of 31° - 52° [37, 38]. Most publications agree that the areal density of ds-DNA is, irrespective of the immobilization method, in the range from 10^{12} to 10^{13} duplexes per cm^2, see [27] and references therein. The most probable areal density in our case, as determined by x-ray photoemission spectroscopy, is $8 \cdot 10^{12}$/cm^2 [H. Yin and H.-G. Boyen, manuscript under preparation]. With a diameter of 2.37 nm for ds-DNA, we conclude that about 35% of the chip surface is dressed with ds-DNA while the remaining surface fraction of 65% still represents the unaltered solid-liquid interface, see **figure 1C** for a schematic illustration. The unaltered surface transfers thermal energy from the phonons in

the diamond lattice to the water molecules, while there is also recent evidence that the heat transfer along ds-DNA is based on molecular vibrations [30]. After denaturation, we are dealing with fragments with a total length of 36 nucleotides (L = 12.24 nm) while the persistence length drops to $l_p = 1.48$ nm [35]. Therefore, the ss-DNA curls up in irregular shapes and the typical Flory radius can be approximated according to $r_{Flory} = (l_p \cdot L/3)^{1/2}$ [36]. This results in $r_{Flory} = 2.46$ nm. Based on the presence of $8 \cdot 10^{12}$ ss-DNA fragments per cm^2, the surface coverage increases to nominally 150%, corresponding to a densely covered surface. Therefore, we suppose that denaturation brings about that major parts of the sample surface are covered with random coils of ss-DNA, which interrupts the heat-transfer channel from the phonons in the solid to the liquid. A visualization of the situation in the denatured state is given in **figure 1D**. From $\Delta R_{th} \sim 1.5$ °C/W, the size of the solid-liquid interface (28 mm^2), and an areal density of $8 \cdot 10^{12}/cm^2$ ss-DNA fragments, we conclude that each curled-up fragment can be considered as an individual thermal resistor R_{th}^*(ss-DNA) with a value of about $3.4 \cdot 10^{12}$ °C/W. Interestingly enough, Velizhanin *et al.* predict for individual ds-DNA fragments a thermal conductivity of $\sigma_{th} = 1.8 \cdot 10^{-3}$ W/(°C·m) at 300 K [21]. Considering the 29-mer fragments as stiff rods with a length of 10 nm and a nominal radius of 1.2 nm, this conductivity translates to a resistance R_{th}^*(ds-DNA) = $1.2 \cdot 10^{12}$ °C/W or roughly one third of the value we derived experimentally for the disordered, single-stranded state. Despite of the good agreement well within the same order of magnitude, this comparison is not yet stringent because in our case a substantial part of the thermal current in the ds-DNA state passes through the 65% surface fraction, where the sensor surface is in direct contact with the buffer solution.

Besides the considerations on the underlying principle of the heat-transfer effect, the method should of course be applicable in genetic research, where high-throughput analysis and parallelization are important aspects. The fact that DNA on diamond electrodes can be denatured and re-hybridized for at least 30 times without loss of binding capacity is already highly beneficial for serial analyses [39]. Moreover, the current hybridization time of 120 minutes (see 'Methods', section ´Functionalization of sensor electrodes with DNA`) can be shortened by employing higher concentrations of target fragments, by increasing the temperature to facilitate diffusion, or by a higher ionic strength of the

hybridization buffer. This way, hybridization times in the order of 20 minutes are reported in literature [14]. Whether a speeded-up hybridization would have an adverse influence on the precision of the heat-transfer technique is not yet clarified, however there is evidence that the current protocol guarantees a one-to-one correspondence between the numbers of probe-DNA- and target-DNA-fragments [27]. Comparing the $8 \cdot 10^{12}$ fragments per cm^2 to the cell volume of 110 µl results in a concentration of target molecules of 34 nM, corresponding in turn to $\Delta R_{th} \sim 1.5$ °C/W. Smoothening of the R_{th} data will easily allow to identify R_{th} changes in the order of 0.1 °C/W, meaning that the detection limit is about 2 nM. For comparison, the detection limit obtained for oligonucleotides with label-free surface plasmon imaging is 10 nM [40] and micromechanical sensors operate with target-DNA concentrations of 100 nM or higher [41].

The first step towards an array format would be the miniaturization of the sensing electrodes and diamond-based electrodes on glass substrates with a diameter below 100 µm have been documented in literature [42]. Also, diamond nanowires with a thickness even below 10 nm have been fabricated by reactive ion etching [43]. The functionalization of these micro- and nanostructures with selected probe- and target DNA can *e.g.,* be achieved by dip-pen nanolithography [44]. A bigger challenge would be the development of an array-type detection system, more specifically an array of planar thermocouples with a contact area comparable to the size of the sensor spots. Here, the present state-of-the-art are thermocouple arrays with an area of a few $µm^2$ of each junction [45], which looks most feasible to detect the heat flow through the individual sensor spots with sufficient spatial resolution to minimize crosstalk between neighboring spots.

In conclusion, we propose that label-free heat-transfer monitoring should be considered as a promising, inexpensive, and real-time alternative to the currently used denaturation-based techniques for DNA characterization and the identification of new point mutations. Moreover, the heat-transfer effect is certainly not limited to diamond surfaces alone and it may also be useful in monitoring other biomolecular interactions on solid supports. Finally, the method may serve as a characterization technique for the areal density and conformational aspects of molecular polymer brushes in general.

4.4 Methods

4.4.1 Design of the sensor cell and the thermal- and impedimetric read out system

The sensor setup shown in **figure 1** was described earlier in the context of chemical denaturation studies [12]. The flow cell has an inner volume of 110 µl and liquids can be exchanged with a syringe-driven flow system (ProSense, model NE-500, The Netherlands). All measurements described here were performed under static conditions. For heat-transfer measurements, the device was now equipped with two miniaturized thermocouples (type K, diameter 500 µm, TC Direct, The Netherlands) monitoring the temperature T_1 of the copper backside contact and the liquid temperature T_2 at a position in the center of the flow cell at 1.7 mm above the chip surface. The heat flow was generated with a power resistor (22 Ω, MPH 20, Farnell, Belgium) glued onto the copper block with heat-conductive paste and tightly fixed with a screw. To regulate T_1, the thermocouple signal was led to a data acquisition unit (Picolog TC08, Picotech, United Kingdom) and from there processed into a PID controller (parameters: P = 10, D = 5, I = 0.1). The calculated output voltage was sent *via* a second controller (NI USB 9263, National Instruments, USA) to a power operational amplifier (LM675, Farnell, Belgium) and fed into the power resistor. Sampling of the T_1- and T_2 values was done at a rate of one measurement per second. For impedance monitoring, the counter electrode was a gold wire (500 µm diameter), also at a distance of 1.7 mm from the surface of the diamond working electrode, but spanning the entire diameter of the liquid cell (5 mm). There was no measurable electronic crosstalk between the impedance spectroscopy- and the temperature regulation unit. The impedance unit, see [28] for circuitry details, measured the impedance in the frequency range of 100 Hz to 100 kHz with 10 frequencies per decade on a logarithmic scale and a scanning speed of 5.7 s per sweep. All data presented here refer to a frequency of 1058 Hz, ensuring an optimal signal-to-noise ratio. The amplitude of the AC voltage, applied under open circuit conditions, was fixed to 10 mV$_{rms}$.

4.4.2 Preparation of the diamond-coated sensor electrodes

The nanocrystalline-diamond coated sensor electrodes were prepared by plasma-enhanced chemical vapour deposition from methane/hydrogen mixtures (3% CH_4) in an ASTeX reactor [23]. The substrates were 2-inch silicon wafers (thickness 500 – 550 µm, crystalline orientation (100), p-type doped with resistivities from 1 to 20 Ωcm), which were diced into chips after deposition. The diamond layers had a thickness of 100 nm and an average grain size of 50 nm. To ensure a good electrical conductivity of the coating ($\sim$ 1 Ωcm), the deposition was done with an admixture of trimethyl borane gas to the CH_4 with a ratio of 200 ppm B/C. The as-prepared electrodes were hydrogenated in H_2 plasma (50 Torr, 800 °C, power 4000 W for 14 min) to obtain hydrophobic surfaces prior to the photochemical attachment of the fatty-acid linker molecules. Here, we employed 10-undecenoic fatty acid (purchased from Sigma-Aldrich), which was tethered with its hydrophobic C=C terminus to the electrodes by UV illumination (wavelength 254 nm, intensity 265 mW/cm^2) during 20 hours under N_2 atmosphere. A reaction mechanism for this covalent binding process was recently proposed by Wang *et al.* [46]. After this photochemical step, the samples were rinsed in acetic acid at 100 °C to release unbound fatty-acid fragments.

4.4.3 Functionalization of sensor electrodes with DNA

The probe ss-DNA (purchased from Invitrogen) was a 36-mer (see **table 1**) with a NH_2-modified 5' terminus allowing for a covalent linking to the COOH group of the fatty acid by using carbodiimide (EDC) coupling. EDC was purchased from Perbio Science and details of this procedure are published in [27]. The first 7 adenine bases at the 5' terminus served as a spacer to minimize steric hindering during hybridization due to the proximity of the solid surface. The total amount of probe ss-DNA used to functionalize 1 cm^2 of electrode surface was 300 pmol. This actually exceeds the binding capacity of the surface, but ensures a rapid functionalization. Non reacted probe DNA was rinsed off by washing the samples for 30 min in homemade 2 × SSC buffer (sodium chloride / sodium citrate) with 0.5% SDS (sodium dodecyl sulphate) at room temperature. Hybridization with the 29-mer target DNA (from Invitrogen) was performed by incubating these samples for 2 hours at 30 °C with 600 pmol of target fragments in 10 × PCR

buffer (homemade). During hybridization, the samples were kept under a saturated water vapour atmosphere to avoid evaporation of the reaction fluid. After hybridization, non-reacted target DNA was removed by rinsing again with 2 × SSC buffer with 0.5% SDS (30 min, room temperature), followed by two 5 min rinsing steps, once in 2 × SSC buffer and once in 0.2 × SSC buffer, both at room temperature. Reference tests with a hybridization temperature of 50 °C confirmed that the temperature of the melting transition is insensitive to the hybridization temperature.

4.4.4 Confocal fluorescence microscopy

For fluorescence intensity studies and photo-bleaching experiments, a Zeiss LSM 510 META Axiovert 200 M laser scanning confocal fluorescence microscope was used. Excitation of the Alexa Fluor® 488 labels was done with the 488 nm emission line of an argon-ion laser with a maximum intensity at the sample surface of 1.00 ± 0.05 mW. The settings of the filters and the confocal optics are documented in[26]; the confocal volume had a diameter of 0.44 µm and a height of 5 µm. All images were collected with a 10x/0.3 Plan Neofluar air objective with a working distance of 5.6 mm. The image size was 128 × 128 with a pixel dwell time of 51.2 µs, corresponding to a total scanned area of ~ 225 × 225 µm². The pinhole size was 150 µm and the laser intensity was set at 10%, corresponding to power input of 33 µW on the chip surface. The detector gain, a measure for the photomultiplier voltage, was set at 1000 for all measurements. After hybridization with the different types of labeled target DNA, the fluorescence of each DNA chip was studied to ensure the presence and homogeneous distribution of DNA. Moreover, bleaching experiments (laser intensity set to 100% for 15 min, bleached area of 20 × 200 µm^2) confirmed that the fluorescence intensity originated from the Alexa 488 dyes and not from the underlying diamond layer. The bleached areas served also to define the remnant background intensity due to strayed or reflected laser light. The fluorescence-intensity decay during denaturation was monitored at a frequency of one confocal image taken every 1.4 seconds and the area-averaged intensities were retrieved using the ImageJ 1.44 software package. All intensities measured after denaturation were in full agreement with the remnant intensities found before on bleached regions, meaning that the data are not affected by laser-intensity fluctuations.

4.5 Acknowledgements

4.6 References

[1]   E. A. Schon, E. Bonilla and S. DiMauro, *J. Bioenerg. Biomembr*., 1997,
        29, 131 – 149.

[2]   A. M. Dunning, C. S. Healey, P. D. P. Pharoah, M. D. Teare,
        B. A. J. Ponder and D. F. Easton, *CEBP,* 1999, **8**, 843 – 854.

[3]   J. W. Hooper, *Medical Laboratory Observer,* 2006, **38**, 22 – 35.

[4]   J. Hooyberghs and E. Carlon, *Biosens. Bioelectron.,* 2010, **26**,
        1692 – 1695.

[5]   E. A. Tindall, D. C. Petersen, P. Woodbridge, K. Schipany and
        V. M. Hayes, *Human Mutation,* 2009, **30**, 876 – 88.

[6]   R. Fodde and M. Losekoot, *Human Mutation,* 1994, **3**, 83 – 94.

[7]   G. Muyzer and K. Smalla, *Antonie van Leeuwenhoek*, 1998, **73**, 127 –
        141.

[8]   U. Rant, K. Arinaga, S. Sherer, E. Pringsheim, S. Fujita, N. Yokoyama,
        M. Tornow and G. Abstreiter, *Proc. Natl. Acad. Sci. USA,* 2007,
        104, 17364 – 17369.

[9]   E. Katz and I. Willner, *Electroanalysis,* 2003, **15**, 913 – 947.

[10]   V. Vermeeren, N. Bijnens, S. Wenmackers, M. Daenen, K. Haenen,
        O. A. Williams, M. Ameloot, M. vandeVen, P. Wagner and L. Michiels,
        Langmuir, 2007, **23**, 13193 – 13202.

[11]   J. Y. Park and S. M. Park, *Sensors,* 2009, **9**, 9513 – 9532.

[12]   B. van Grinsven, N. Vanden Bon, L. Grieten, M. Murib, S. D. Janssens,
        K. Haenen, E. Schneider, S. Ingebrandt, M. J. Schöning, V. Vermeeren,
        M. Ameloot, L. Michiels, R. Thoelen, W. De Ceuninck and P. Wagner,
        Lab Chip, 2011, **11**, 1656 – 1663.

[13]   A. Poghossian, A. Cherstvy, S. Ingebrandt, A. Offenhäusser and
        M. J. Schöning, *Sens. Actuators, B,* 2005, **111**, 70 – 480.

[14]   S. Ingebrandt, Y. Han, F. Nakamura, A. Poghossian, M. J. Schöning and
        A. Offenhäusser, *Biosens. Bioelectron.*, 2007, **22**, 2834 – 2840.

[15]   H. Kawarada and A. R. Ruslinda, *Phys. Status Solidi A,* 2011, **208**, 2005
        – 2016.

[16]   A. Kick, M. Boensch, B. Katzschner, J. Voigt, A. Herr, W. Brabetz,
        M. Jung, F. Sonntag, U. Klotzbach, N. Danz, S. Howitz and M. Mertig,
        Biosens. Bioelectron., 2010, **26**, 1543 – 1547.

[17]   X. F. Guo, A. A. Gorodetsky, J. Hone, J.K. Barton and C. Nuckolls,
        Nat. Nanotechnol., 2008, **3**, 163 – 167.

[18]   C. Dekker and M. Ratner, *Phys. World*, 2001, **14**, 29 – 33.

[19]   G. Cuniberti, L. Craco, D. Porath and C. Dekker, *Phys. Rev. B*,
        2002, **65**, art. no. 241314.

[20]   H. Cohen, C. Nogues, R. Naaman and D. Porath, *Proc. Natl. Acad. Sci.
        USA,* 2005, **102**, 11589 – 11593.

[21]   K. A. Velizhanin, C. C. Chien, Y. Dubi and M. Zwolak, *Phys. Rev. E,*
        2011, **83,** art. no. 050906.

[22]   P. Guldberg, F. Rey, J. Zschocke, V. Romano, B. Francois, L. Michiels,
        K. Ullrich, G.F. Hoffmann, P. Burgard, H. Schmidt, C. Meli, E. Riva,
        I. Dianzani, A. Ponzone, J. Rey and F. Guttler, *American Journal of
        Human Genetics,* 1998, **63**, 71 – 79.

[23]   S. D. Janssens, P. Pobedinskas, J. Vacik, V. Petráková, B. Ruttens,
        J. D'Haen, M. Nesládek, K. Haenen and P. Wagner, *New J. Phys.*, 2011,
        8, art. no. 083008.

[24]   P. Christiaens, V. Vermeeren, S. Wenmackers, M. Daenen, K. Haenen,
        M. Nesládek, M. vandeVen, M. Ameloot, L. Michiels and P. Wagner,
        Biosens. Bioelectron., 2006, **22**, 170 – 177.

[25]   http://corefacilities.systemsbiology.net/NucleicAcids/Microarrays/

[26]   M. F. L. De Volder, R. Vansweevelt, P. Wagner, D. Reynaerts,
        C. Van Hoof and A. John Hart, *ACS Nano,* 2011, **5**, 6593 – 6600.

[27]   V. Vermeeren, S. Wenmackers, M. Daenen, K. Haenen, O. A. Williams,
        M. Ameloot, M. vandeVen, P. Wagner and L. Michiels*, Langmuir,* 2008,
        24, 9125 – 9134.

[28]   B. van Grinsven, T. Vandenryt, S. Duchateau, A. Gaulke, L. Grieten,
        R. Thoelen, S. Ingebrandt, W. De Ceuninck and P. Wagner, *Phys.
        Status Solidi A,* 2010, **207**, 919 – 923.

[29]   M. Lenz, Thermal resistance, theory and practice, ed. G. Striedl and
        U. Fröhler, Special Subject Book January 2000: SMD Packages,
        released by Infineon Technologies AG, Munich, Germany (2000).

[30]   T. Kodama, A. Jain and K. E. Goodson, *Nano Lett.,* 2009, **9**, 2005 –
        2009.

[31]   P. L. Privalov, O. B. Ptitsyn and T. M. Birshtein, *Biopolymers*, 1969, **8**,
        559 – 571.

[32]   D. W. Gruenwedel**,** *Biochim. Biophys. Acta,* 1974, **340**, 16 – 30.

[33]   I. Smirnov and R. H. Shafer, *Biochemistry,* 2002, **39**, 1462 – 1468.

[34]   K. Lettau, A. Warsinke, M. Katterle, B. Danielsson and F. W. Scheller,
        Angew. Chem. Inte. Ed., 2006, **45**, 6986 – 6990.

[35]   J. Ambia-Garrido, A. Vainrub and B. M. Pettitt, *Comput. Phys. Commun.,*
        2010, **181**, 2001 – 2007.

[36]   S. Wenmackers, V. Vermeeren, M. vandeVen, M. Ameloot, N. Bijnens, K.
        Haenen, L. Michiels and P. Wagner*, Phys. Status Solidi A,* 2009,
        206, 391 – 408.

[37]   B. Rezek, D. Shin and C. E. Nebel, *Langmuir,* 2007, **23**, 7626 – 7633.

[38]   S. Wenmackers, S. D. Pop, K. Roodenko, V. Vermeeren, O. A. Williams,
        M. Daenen, O. Douheret, J. D'Haen, A. Hardy, M.K. Van Bael, K. Hinrichs,
        C. Cobet, M. vandeVen, M. Ameloot, K. Haenen, L. Michiels, N. Esser
        and P. Wagner,*Langmuir,* 2008, **24**, 7269 – 7277.

[39]   W. S. Yang, O. Auciello, J. E. Butler, W. Cai, J. A. Carlisle, J. Gerbi,
        D. M. Gruen, T. Knickerbocker, T. L. Lasseter, J. N. Russel, L. M. Smith
        and R. J. Hamers, *Nat. Mater.,* 2002, **1**, 253– 257.

[40]   T. Livache, E. Maillart, N. Lassalle, P. Mailley, B. Corso, P. Guedon,
        A. Roget and Y. Levy, *J. Pharm. Biomed. Anal*., 2003, **32**, 687-696.

[41]   M. Melli, G. Scoles and M. Lazzarino, *ACS Nano*, 2011, **5**, 7928–7935.

[42]   M. Bonnauron, S. Saada, C. Mer, C. Gesset, O. A. Williams, L. Rousseau,
        E. Scorsone, P. Mailley, M. Nesládek, J. C. Arbault and P. Bergonzo,
        Phys. Status Solidi A, 2008, **205**, 2126 – 2129.

[43]   N. Yang, H. Uetsuka, E. Osawa and C.E. Nebel, *Angew. Chem. Int. Ed.,*
        2008, **47**, 5183 – 5185.

[44]   L. M. Demers, D. S. Ginger, S. J. Park, Z. Li, S. W. Chung and
        C.A. Mirkin, *Science,* 2002, **296**, 1836 – 1838.

[45]   H. X. Liu, W. Q. Sun, Q. Chen and S. Y. Xu, *IEEE Electron Device
        Lett.,* 2011, **32**, 1606 – 1608.

[46]   X. Y. Wang, R. E. Ruther, J. A. Streifer and R. J. Hamers, *J. Am. Chem.*
        Soc., 2010, **132**, 4048 – 4049.

4.7 Supporting materials

4.7.1 AFM images of NCD surfaces and the subsequent surface-functionalization steps

Figure 5 shows AFM micrographs of the sensor surfaces representing the different phases of surface functionalization. All images were taken on a 10 × 10 µm^2 surface area under ambient conditions in dry state using a Park Systems NX10 instrument in tapping mode. The AFM tips were N-type silicon probes with a spring constant of 25 – 27 N/m and 5 – 10 nm tip radius. The image analysis was performed with Park Systems NXI software. The images 5) A, B, C, and D correspond to the electrodes # D1, # D2, # D3, # D4, all cut from the same NCD wafer. **Image 5A** shows the hydrogen terminated NCD surface with an average roughness Ra = 2.7 nm. After covalently attaching the fatty-acid linker layer (Image 5B), the average roughness drops to Ra = 2.2 nm. Grafting of the probe-DNA layer increases Ra to 3.2 nm (Image 5C) and hybridization with target DNA (Image 5D) finally results in a stiff molecular brush with Ra = 4.4 nm.
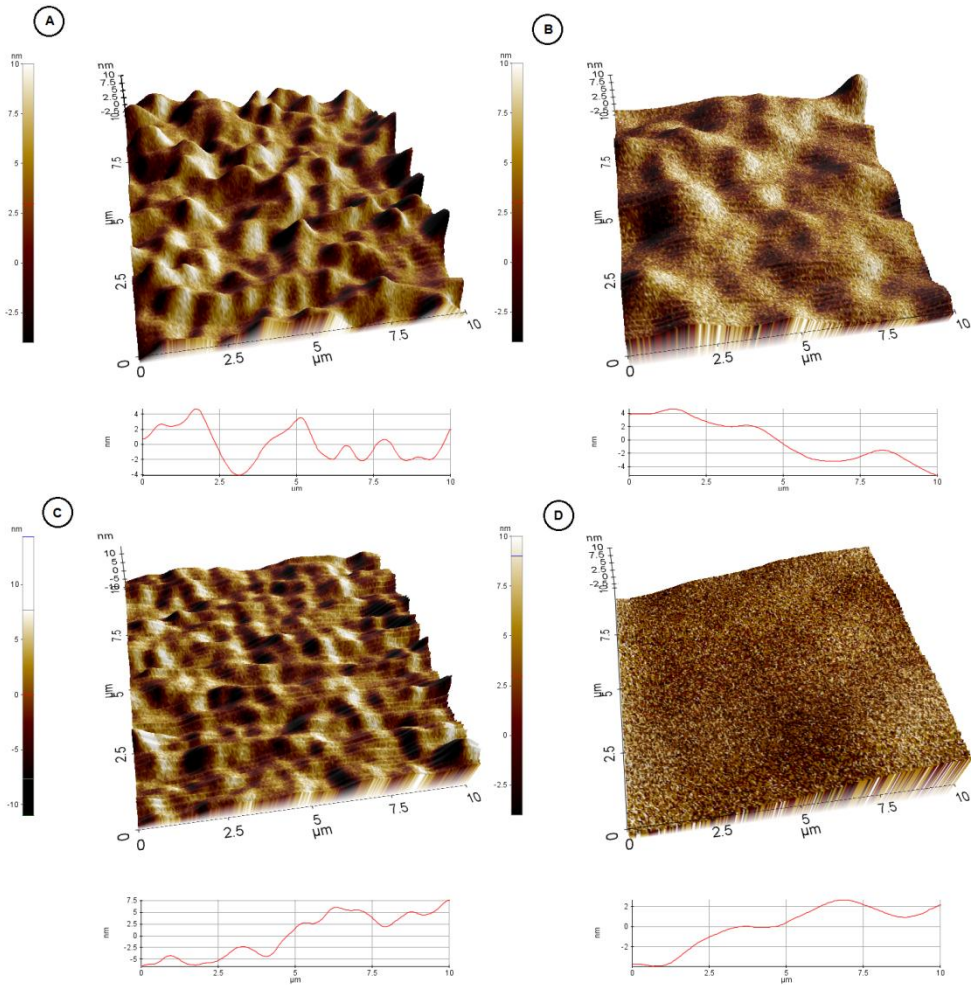
Figure 5: Non contact AFM images, combined with their line profiles of the surface of NCD (**A**), functionalized with fatty acid (**B**), ss-DNA (**C**) and hybridized with its target (**D**). The unmodified NCD shows an average roughness (Ra) of 2.7 nm. When functionalized with fatty acid the Ra decreases to 2.2 nm. After attaching the ss-DNA a Ra of 3.2 nm is measured and when hybridized with its complementary target the Ra is 4.4 nm. Image size 10 x 10 μm, scan rate 1 Hz.

4.7.2 Confocal fluorescence images during thermal DNA denaturation
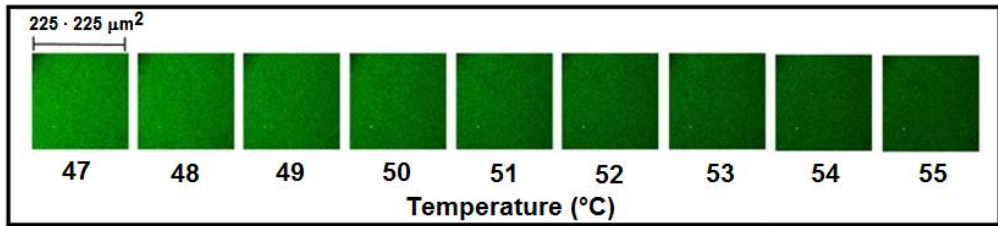
Figure 6: Series of confocal fluorescence images of the diamond electrode during the denaturation of complementary ds-DNA at selected temperatures. Note that the fluorescence-intensity curve in **figure 3A** was derived from images with time intervals of 1.4 seconds. The depicted area is 225 by 225 μm^2.

4.7.3 Discussion of the impedance signal upon crossing the DNA-melting transition

Within **figure 3B**, the impedance amplitudes show for ss- as well as for ds-DNA an overall decrease with rising temperature. This reflects the increase of ion mobilities due to decreasing viscosity of the liquid and has been investigated for various electrolytes [27]. Around 40°C, the impedance drops roughly by 2% - 3% for each additional °C, depending on the precise ionic composition and the considered frequency range. Within previous studies under isothermal conditions (room temperature), we observed that electrodes with ds-DNA in PBS buffer have slightly higher impedance than their denatured ss-counterparts, an effect in the order below 2% [12]. **Figure 3B** seems to contradict this; however, the actual temperature in the electrolyte is also different. When looking at a fixed temperature T_1 = 40.0 °C, the temperature of the liquid is T_2 = 33.8 °C for the electrode with ds-DNA, while T_2 = 33.0 °C in the denaturized state. The apparently higher impedance in the denatured state is therefore at least partly introduced by the temperature effect on the electrolyte.

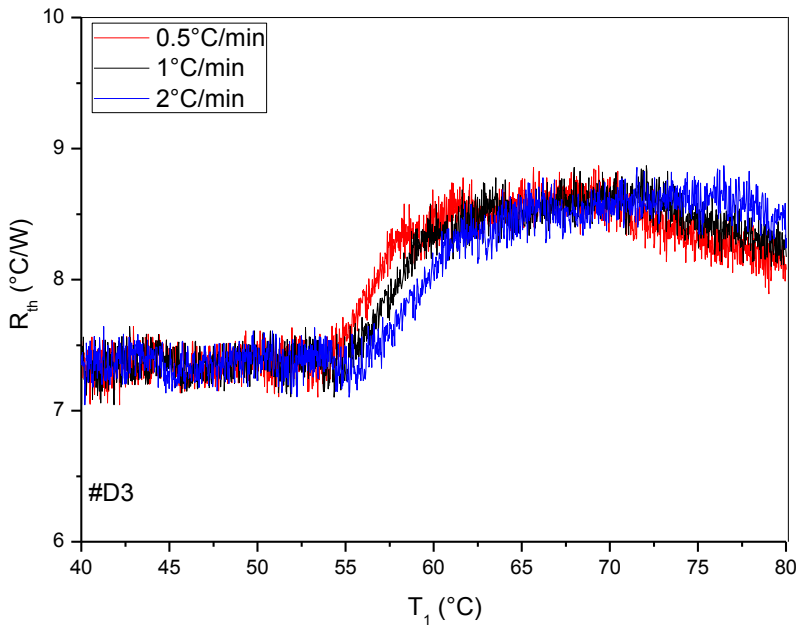4.7.4 Heat-transfer resistance measured with different heating rates

Figure 7: Temperature dependence of the heat-transfer resistance during the thermally induced denaturation of complementary DNA duplexes obtained with electrode # D3 (run *b*). The heating rate was 1 °C/min (black line) as in all other experiments while the red line represents heating with 0.5 °C/min. The blue line corresponds to heating with a rate of 2 °C/min. The moderate shift in midpoint temperature can be explained by the thermal inertia of the setup while the absolute values of R_{th} in the double-stranded and in the denatured state are fully consistent. The data have not been filtered.

Chapter 5

Conclusion and outlook

This chapter provides a brief summary of the results, obtained in this thesis. It discusses the strong points (SNP resolution, label–free, fast) but also highlights the remaining issues (extensive data processing, noise levels, detection limits). Some suggestions are made to overcome these last hurdles. Finally, a future outlook is provided.

This project aimed at the development of label–free strategies for the detection of SNPs in DNA sequences. These strategies had to fulfil three criteria before being considered successful:

i)   Fast response of the sensor at the minutes scale.
ii)   Clear distinction between complementary, mismatched, and single mismatched DNA fragments.
iii)   Low detection threshold, suitable for small concentrations of target DNA.

In the course of this PhD two technologies were developed, which satisfied these needs in greater or lesser extent. The first strategy was based on impedance spectroscopy where one could reproducibly identify denaturation-time constants associated with typical ds DNA structures. All time constants are at the scale of minutes while the denaturation takes the longest for complementary DNA duplexes as compared to mutated sequences. The second strategy is based on heat-transfer resistance. Here, a persistent change of R_{th} from low values at all temperatures below the melting transition to higher values at all temperatures above this transition was found. This change is probably caused by the difference in persistence length for ds DNA (50 nm) and ss DNA (1.5 nm). The persistence length of 1.5 nm leads the ss DNA to curl up upon denaturation which increases the surface coverage density. We proposed that this increase in surface coverage density leads to an increase in heat transfer resistance.

Both techniques show a high specificity and sensitivity, but there is still room for improvement. The readout is fast for both techniques but the sensor preparation time is too long. We might be able to decrease this time by employing higher concentrations of target fragments, but this is contradictive to the wanted low detection threshold. Less crude would be to increase the hybridization temperature to facilitate diffusion or by employing a hybridization buffer at higher ionic strength. This way, hybridization times in the order of 20 minutes are reported. The chemical denaturation method does produce results within the wanted SNP regime, but the raw data still needs mathematical analysis. This need is eliminated by the thermal approach. However, the thermal method infringes the rule for a low detection threshold. We calculated $8 \cdot 10^{12}$ fragments per cm^2 to the cell volume of 110 µl resulting in a concentration of target

molecules of 34 nM. This concentration has led to an effect size of $\Delta R_{th} \sim$ 1.5 °C/W. By decreasing the short–term noise of the R_{th} data, effect sizes in the order of 0.1 °C/W will become visible, putting target concentrations of ~ 2 nM in reach.

The developed technologies are capable of distinguishing between a healthy DNA sequence and a mutated DNA sequence and can provide an indication of the position of a mutation within the sequence. Both strategies do not need fluorescent labelling, eliminating the need for a highly sophisticated optical readout technology. Given the speed, minimal need of instrumentation and straightforward readout and processing, these findings are considered to be high-potential technologies. Last step is to transcend to the competitive industrial market of medical devices. Before making this transition some extra research and development steps are a necessity. First, we need to deliver proof that the technologies work on DNA strands, longer than 29 base pairs. Preliminary results already showed that the thermal approach works with DNA strands up to 50 nm (150 base pairs). The strategies will then be implemented in an array format, enabling multiple detections in real time. Once these last hurdles have been overcome, miniaturization can be considered and the first step outside the comfort and safety of the academic world can be taken with great confidence.

Appendix 1

Nomenclature

A	Adenine
A/D	Analogue/digital
A_1	Denaturation-related decay amplitude
A_2	Medium exchange-related decay amplitude
AC	Alternating current
ADME	Absorption, distribution, metabolism, excretion
AFM	Atomic force microscopy
bp	Base pair
C	Cytosine
CRP	C-reactive protein
CVD	Chemical vapor deposition
DC	Direct current
DEPC	Diethylpyrocarbonate
DEPC	Diethylpyrocarbonate
DGGE	Denaturing-gradient gel electrophoresis
DNA	Deoxyribonucleic acid
ds DNA	Double-stranded DNA
DTF	Differential transfer function
EDC	1 –ethyl –3-[3 -dimethylaminopropyl]-carbodiimide
FET	Field-effect transistor
FM DNA	Full match DNA
FMM DNA	Full mismatch DNA
G	Guanine
MES	2-[N-morpholino]-ethanesulphonicacid
MIP	Molecularly imprinted polymer
MM DNA	Mismatched DNA
MW PE-CVD	Plasma enhanced chemical vapour deposition
NaOH	Sodium hydroxide
NCD	Nano crystalline diamond
PAH	Phenylalanine hydroxylase
PBS	Phosphate buffred saline
PCR	Polymerase chain reaction

PCR	Polymerase chain reaction
PMMA	Poly(methyl methacrylate)
POC	Point-of-care diagnostics
Rth	Heat-transfer resistance
SDS	Sodium dodecyl sulfate
SNPs	Single nucleotide polymorphisms
SPR	Surface plasmon resonance
ss DNA	Single-stranded DNA
SSC	Saline-sodium citrate
SWNT	Single-walled carbon nanotube
T	Thymine
TGGE	Temperature-gradient gel electrophoresis
Tm	Melting temperature
UV	Ultra violet
XPS	X-ray photoelectron spectroscopy
τ_1	Denaturation time constant
τ_2	Medium exchange time constant
τ_3	Fluorescence decay time constant

Appendix 2

Publications, Patents and Conference contributions

<u>Publications</u>

[1]   M. Peeters, F.J. Troost, <u>B. van Grinsven</u>, F. Horemans, J. Alenus,
        M.S. Murib, D. Keszthelyi, A. Ethirajan, R. Thoelen, T.J. Cleij and
        P. Wagner, *Sens. Actuators, B*, 2012, **DOI** 10.1016/j.snb.2012.05.040.

[2]   <u>B. van Grinsven</u>, N. Vanden Bon, H. Strauven, L. Grieten, M. Murib,
        K. L. Jimenez Monroy, S. D. Janssens, K. Haenen, M. J. Schöning,
        V. Vermeeren, M. Ameloot, L. Michiels, R. Thoelen, W. De Ceuninck and
        P. Wagner, *ACS Nano*, 2012, **6**, 2712 – 2721.

[3]   <u>B. van Grinsven</u>, N. Vanden Bon, L. Grieten, M. Murib, S. D. Janssens,
        K. Haenen, E. Schneider, S. Ingebrandt, M. J. Schöning, V. Vermeeren,
        M. Ameloot, L. Michiels, R. Thoelen, W. De Ceuninck and P. Wagner,
        Lab Chip, 2011, **11**, 1656 – 1663.

[4]   T. Clukers, <u>B. van Grinsven</u>, T. Vandenryt, S.D. Janssens, P. Wagner,
        W. De Ceuninck, R. Thoelen, M. Daenen and K. Haenen, *MRS Symp.
        Proc.*, 2011, **1282**, 123 – 128.

[5]   J. Broeders, S. Duchateau, <u>B. van Grinsven</u>, W. Vanaken, M. Peeters,
        R. Thoelen, T. J. Cleij, P. Wagner and W. De Ceuninck. *Phys. Status
        Solidi A*, 2011, **208**, 1357 – 1363.

[6]   T. Clukers, <u>B. van Grinsven</u>, T. Vandenryt, S. D. Janssens, P. Wagner,
        W. De Ceuninck, R. Thoelen, M. Daenen and K. Haenen. *Phys. Status
        Solidi A*, 2010, **207**, 2110 – 2113.

[7]   <u>B. van Grinsven</u>, T. Vandenryt, S. Duchateau, A. Gaulke, L. Grieten,
        R. Thoelen, S. Ingebrandt, W. De Ceuninck and P. Wagner, *Phys. Status
        Solidi A,* 2010, **9**, 2110 – 2113.

[8]   F. Simon, J. P. Martinez, P. Laguna, <u>B. van Grinsven</u>, C. Rutten and
        R. Houben. *Conf. Proc. IEEE Eng. Med. Biol. Soc.*, 2007, **32**, 2587 -
        2590.

Patents

[1]   *Heat-transfer resistance based analysis of bioparticles.*
        <u>B. van Grinsven</u>, P. Wagner, W. De Ceuninck, L. Michiels
        WO2012/076349A1, (14 – 06 – 2012).

[2]   *A biosensor using impedimetric real-time monitoring.*
        <u>B. van Grinsven</u>, P. Wagner, W. De Ceuninck
        WO2012/076350A1, (14 – 06 – 2012).

[3]   *Electrode for medical applications.*
        <u>B. van Grinsven,</u> M. Hoppenbrouwers
        PCT/EP2008/0165956, (10 – 06 – 2008).

Invited lectures

[1]   Fraunhofer-Institut für Zerstörungsfreie Prüfverfahren,
        Dresden (23 – 03 – 2012)
        Label–Free Strategies for SNP Analysis in DNA.

[2]   2nd NanoSensEu Symposium on Biosensor Development,
        Hasselt (26 – 04 - 2012)
        Session: Trends and Technology.
        Label–Free Tools for The Detection of Single Nucleotide
        Polymorphisms in DNA.

Oral Presentations

[1]   Material Research Society, San Francisco (27 - 04 - 2011).
        Session: Carbon Functional Interfaces.
        Rapid Assessment of the Stability of DNA Duplexes by Impedimetric
        Real Time Monitoring of Chemically Induced Denaturation.
[2]   Belgian Physical Society, Namur (25 – 05 - 2011).
        Session: Biophysics and Medical Physics.
        Detecting Single Nucleotide Polymorphisms by Impedimetric Monitoring
        of Denaturation.
[3]   Material Research Society, Boston (30 - 11 - 2011)
        *Session: Diamond Electronics and Biotechnology: Fundamentals to
        Applications.*
        Heat-transfer Resistance at Solid-Liquid Interfaces: a New Tool for
        the Detection of Single Nucleotide Polymorphisms in DNA.
[4]   SBDD diamond workshop, Hasselt (15 - 03 - 2012).
        Session: Carbon Interfaces.
        Label-Free Tools for Mutation Detection in DNA.
[5]   Belgian Physical Society, Brussels (30 – 05 - 2012).
        Session: Biophysics and Medical Physics.
        Heat-transfer Resistance: a New Tool for the Detection of SNPs in DNA.
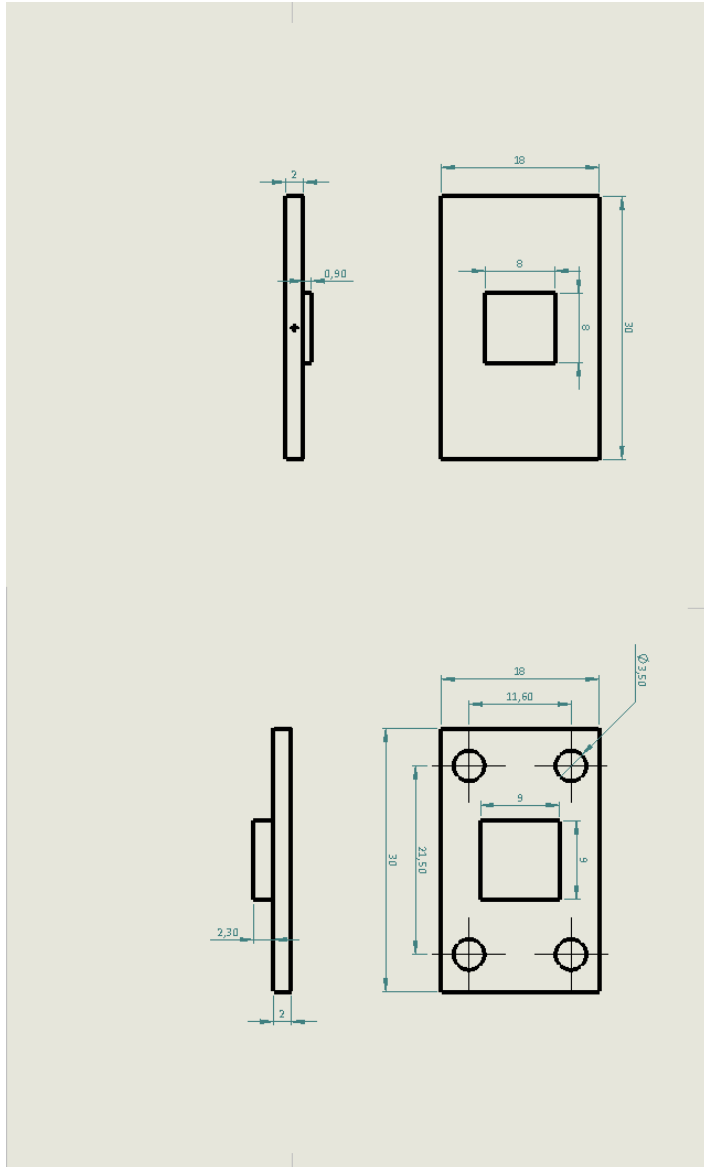
Appendix 3

List of Figures and Tables

Appendix 4

Blueprints and Schematics

Perspex flowcell

Copper lid

Pump system

TOP VIEW

BOTTOM VIEW

NE-500
Single Syringe Pump

Steppermotor

NE-500
Single Syringe Pump

Steppermotor

USB

Temperature control unit